# MICROSTRUCTURAL AND THERMOPHYSICAL PROPERTIES OF $UO_2$-Mo COMPOSITE REACTOR FUELS

A Thesis Submitted to the College of

Graduate and Postdoctoral Studies

In Partial Fulfillment of the Requirements

For the Degree of Master of Science

In the Department of Mechanical Engineering
University of Saskatchewan
Saskatoon

By

MURALI KRISHNA TUMMALAPALLI

# Permission to use

In presenting this thesis in partial fulfillment of the requirements for a postgraduate degree from the University of Saskatchewan, I agree that the Libraries of this University may make it freely available for inspection. I further agree that permission for copying of this thesis/dissertation in any manner, in whole or in part, for the scholarly purpose may be granted by the professor or professors who supervised my thesis work or, in their absence, by the Head of the Department or the Dean of the College in which my thesis work was done. It is understood that any copying or publication or use of this thesis/dissertation or parts thereof for financial gain shall not be allowed without my written permission. It is also understood that due recognition shall be given to me and to the University of Saskatchewan in any scholarly use, which may be made of any material in my thesis.

Request for permission to copy or to make other uses of materials in this thesis/dissertation in whole or part should be addressed to:

Head of the Department of Mechanical Engineering,
University of Saskatchewan,
57 Campus Drive,
Saskatoon, Saskatchewan S7N 5A9,
Canada.

OR

Dean
College of Graduate and Postdoctoral Studies,
University of Saskatchewan,
116 Thorvaldson Building, 110 Science Place,
Saskatoon, Saskatchewan S7N 5C9,
Canada.

# Abstract

Nuclear fuel performance under normal operating conditions and extreme accident conditions have studied using experimental procedures to investigate the microstructural and thermophysical properties of the fuel. Attention has been drawn to the catastrophic nuclear power station accident at the Fukushima Daiichi in Japan. After the reactor system's failure, efforts are focused on preventing the existing nuclear fuel, uranium dioxide ($UO_2$), and zirconium (Zr), system from melting. Research is required to replace the fuel and clad system with a more robust system that can withstand accidents. With the recognition of associated risks with the current fuel, hence, developing an accident-tolerant fuel (ATF) became a major motivation for research. In this work, Molybdenum (Mo) has been deployed as an additive material in $UO_2$ fuel due to its high thermal conductivity, high boiling point, high melting point, and low thermal neutron absorption cross-section.

The nuclear reactor safety analysis showed that thermal conductivity is an essential property of fuel because it regulates fuel operating temperature and therefore influences the safety of reactor operation. Low thermal conductivity leads to the rapid meltdown at the core of the fuel pellet during the loss of coolant scenario. Apart from thermal conductivity, pellet microstructure and density also played an essential role in fission gas buildup and release, the accumulation of the fission gas in form of voids in the center of fuel pellets. Therefore, three major critical areas of focus have been identified in this research: i) Enhanced thermal conductivity of $UO_2$-Mo composite fuel for high-temperature accident scenarios, ii) Evaluation of the pellet microstructure, grain size, texture, and grain boundary character distribution in $UO_2$-Mo composites, and iii) Optimizing the high densification of the $UO_2$-Mo composite fuel pellets.

One of the limitations of the accident-tolerant fuel has the difficulty of processing dense pellets by the conventional sintering methods. Hence the fabricating of $UO_2$-Mo composite fuels by spark plasma sintering (SPS) was proposed, and the effect of the sintering parameters on the density, microstructure, and thermal conductivity of $UO_2$-Mo composite fuel have established. Finally, a composite fuel of $UO_2$-Mo (micro and nano particles) has been manufactured with enhanced thermal conductivity.

# Acknowledgement

I take this opportunity with great delight to thank God Almighty, my parents, and all the people who have assisted me through the course of my journey towards creating this thesis. First, I would like to pay my sincere and heartful gratitude to my beloved supervisor Prof. Jerzy A Szpunar, for allowing me to carry out my dissertation under his esteemed guidance. I am also thankful for his unconditional support and valuable comments during the entire course of my master's journey.

I would also like to thank my advisory committee members: Prof. Chris Zhang (Committee chair), Prof. Duncan Cree, and Prof. Rob Pywell for their encouragement, comments, and productive discussions. Additionally, I appreciate the valuable support from my family, friends, teachers, and colleagues of the Advanced Materials and Renewable Energy (AMRE) group at the University of Saskatchewan. My sincere thanks to Dr. Ahmed Tiamiyu, Dr. Ericmoore Jossou, Dr. Jahidur Rahman, Dr. Linu Malakkal, and Jayangini Ranasinghe for their unconditional support during my MSc. I also thank the support provided by Prof. Lukas Bichler and Anil Prasad of the University of British Colombia for their assistance with the fabrication of the fuels. I also remember my previous supervisors Prof. A. Gopala Krishna (JNTU-Kakinada) and Prof. P. L. Nayak (PL Nayak Research Foundation), for their guidance and encouragement.

# Dedication

*I dedicate this thesis to my beloved parents, Rama Mohana Rao Tummalapalli and Savitri Tummalapalli, for the unconditional support and for always been my inspiration to be intense and persistent, no matter how significant the obstacles have been. Also, to my beloved brother, Dr. Kiran Srinivasa Satyanarayana Tummalapalli, the reason for all the achievements that I have accomplished. I am much delighted for your endless love, support, and encouragement.*

Some work of this thesis was also presented at the following conference.

**M. K. Tummalapalli,** L. Malakkal, J. Szpunar, A. Prasad and L. Bichler; *"*Microstructural and thermophysical characterization of pure and Mo-doped $UO_2$ pellets"; presented at 14$^{th}$ international conference on CANDU fuel, Mississauga, Ontario, Canada July 21-24 (2019).

# Table of contents

# List of tables

# List of figures

# List of abbreviations and symbols

| Abbreviation | Definition |
|---|---|
| ATF | Accident Tolerant Fuels |
| AGR | Advanced Gas-cooled Reactor |
| $Al_2O_3$ | Aluminium Oxide |
| BCC | Body Centered Cubic |
| BWR | Boiling Water Reactors |
| BSE | Back Scattered Electron |
| Ba | Barium |
| BeO | Beryllium Oxide |
| B | Boron |
| CANDU | CANada Deuterium Uranium |
| $CaF_2$ | Calcium Floride |
| CSL | Coincidence Site Lattice |
| $Cr_2O_3$ | Chromium Oxide |
| $CO_2$ | Carbon Dioxide |
| Cd | Cadmium |
| Ce | Cerium |

| | |
|---|---|
| Cs | Caesium |
| Cu | Copper |
| C | Graphite |
| DLF | Discovery Laser Flash |
| DSC | Differential Scanning Calorimetry |
| $D_2O$ | Heavy Water |
| EBSD | Electron Backscatter Diffraction |
| EDS | Energy Dispersive Spectroscopy |
| EBR | Experimental Breeder Reactor |
| FCC | Face Centered Cubic |
| FWHM | Full Width and Half Maximum |
| GBCD | Grain Boundary Character Distribution |
| HAGB | High Angle Grain Boundaries |
| He | Helium |
| Hf | Hafnium |
| $H_2O$ | Light Water |
| IPF | Inverse Pole Figure |
| I | Iodine |

| | |
|---|---|
| LAGB | Low Angle Grain Boundaries |
| La | Lanthanum |
| MgO | Magnesium Oxide |
| Mo | Molybdenum |
| Nb | Niobium |
| ND | Normal Direction |
| Nd | Neodymium |
| $N_2O_5$ | Dinitrogen Pentoxide |
| PWR | Pressurized Water Reactor |
| Pr | Praseodymium |
| RPM | Revolutions Per Minute |
| RD | Relative Density |
| SCWR | Super-Critical Water-Cooled Reactor |
| SEM | Scanning Electron Microscope |
| SFR | Sodium-cooled Fast Reactor |
| SPS | Spark Plasma Sintering |
| SiC | Silicon Carbide |
| Sb | Antimony |

| | |
|---|---|
| Sr | Strontium |
| TGA | Thermo Gravimetric Analysis |
| TD | Theoretical Density |
| Tc | Technetium |
| Te | Tellurium |
| Kr | Krypton |
| LFA | Laser Flash Apparatus |
| LWR | Light Water Reactor |
| PCA | Process Control Agent |
| PWR | Pressurized Water Reactor |
| Pu | Plutonium |
| Pd | Palladium |
| $PuO_2$ | Plutonium Oxide |
| Ru | Ruthenium |
| Rh | Rhodium |
| U | Uranium |
| UN | Uranium Mononitride |
| $UO_2$ | Uranium Dioxide |

| | |
|---|---|
| $UB_2$ | Uranium Diboride |
| U-Si | Uranium Silicide |
| $U_3O_8$ | Triuranium Octoxide |
| VHTR | Very High Temperature Reactor |
| XRD | X-ray Diffraction |
| Xe | Xenon |
| Y | Yttrium |
| Zr | Zirconium |

| Symbols | Definition |
|---|---|
| $R$ | Reaction Rate |
| $\Phi_0$ | Thermal Neutron Flux |
| $\sigma$ | Thermal Neutron Cross Section |
| $n$ | Number Density |
| $V$ | Volume |
| $\rho$ | Density of Material |
| $M$ | Molar Mass |
| $N_A$ | Avogadro's Number |
| K | Kelvin |
| MPa | Mega Pascal |
| psi | Pound-force Per Square Inch |
| $^{o}$C | Degree Celsius |
| W | Walt |
| m | Meter |
| T | Temperature |
| $t$ | Time |
| P | Pressure |
| $C_p$ | Heat Capacity |
| $\beta^-$ | Beta Decay |

| | |
|---|---|
| ϒ | Gamma Decay |
| Å | Angstrom |
| kV | Kilovolt |
| μm | Micrometer |
| nm | Nanometer |
| mm | Millimeter |
| cm | Centimeter |
| α | Thermal Diffusivity |
| λ | Thermal Conductivity |
| L | Thickness of the Sample |

# CHAPTER 1
# INTRODUCTION

## 1.1 Nuclear power

Due to climate change, there is an ever-growing need to produce large amounts of energy while avoiding harm to the environment that occurs through the generation of carbon dioxide ($CO_2$). Nuclear energy is a fully developed technology that can be reliably used as a source of clean energy on-demand, without $CO_2$ production. A nuclear power station is a thermal power plant in which a nuclear reactor (atomic pile) is a heat source that is used to produce steam, which moves a turbine connected to a generator to generate electricity [1]. After discovering the first neutron in 1932, the nuclear chain reaction concept was brought out by nuclear reactions based on neutrons. Shortly after that, scientists raised their ideas of a simple, standard reactor in 1933. Such concepts were realized in 1938 when the reactor was developed using uranium fuel, Subsequently, in 1939, the scientists "Szilard and Fermi," identified that several neutrons were also released during fission, creating the opportunity for nuclear chain reaction [2].

Nuclear fuel is the most important element of nuclear power plants; it is the substance that creates nuclear fission and heat. The atoms of the nuclear fuel hit by the slow neutrons, and they will split; by splitting, they emit energy, which creates heat. Similarly, they will release two or three neutrons to create a self-chain reaction to continue the process. Today's primary fuel in the nuclear industry was uranium dioxide ($UO_2$) this fuel can withstand complex thermo-mechanical and harsh irradiation environments. The fission reaction can create many different products like various oxide, gas bubbles, metallic precipitates, and solid solutions that can be identified in the fuel matrix [3]. The future nuclear reactors are classified as Generation IV in-designs, as shown in Figure 1.1. There are various types of nuclear reactors in operation today, all of which are classified as generation II and III type designs, as discussed in Section 1.2. Generation III+ reactors feature enhancements to the existing generation III reactors, and generation IV reactors are novel reactors still in the development stage designed to use different fuel materials [4].

## 1.2 Nuclear reactors

The first artificial nuclear plant called Chicago Pile-1 was created in late 1942 at the University of Chicago. The structure of this reactor contained wood, which supports the reactor graphite blocks, inserted in natural uranium oxide 'pseudospheres' or 'briquettes'[5]. "World's first nuclear power plant" named experimental breeder reactor (EBR-1) having an output of 200 kW electricity, has now be seen in the museum. Initially, it is called "Chicago Pile-4," and was operated by the U.S. Atomic Energy Commission [6,7]. The nuclear power plant's development continued, and various technological advances in terms of costs, safety, and performance. The Generation-I are the first commercial power plants they were gas-cooled and had graphite as a moderator or were water-cooled and moderated. Generation-II reactors are the standard light-water pressurized and boiling water reactors are in operation today. The Generation-III models are under construction in many countries, the design is based on the current light-water reactor (LWR) with enhanced performance and extended design lifetimes, which prevents core damage. Currently, nuclear research has been focused on Generation-IV reactors. These are aimed to improve safety, accident-tolerance, efficiency, and should have a lower cost.

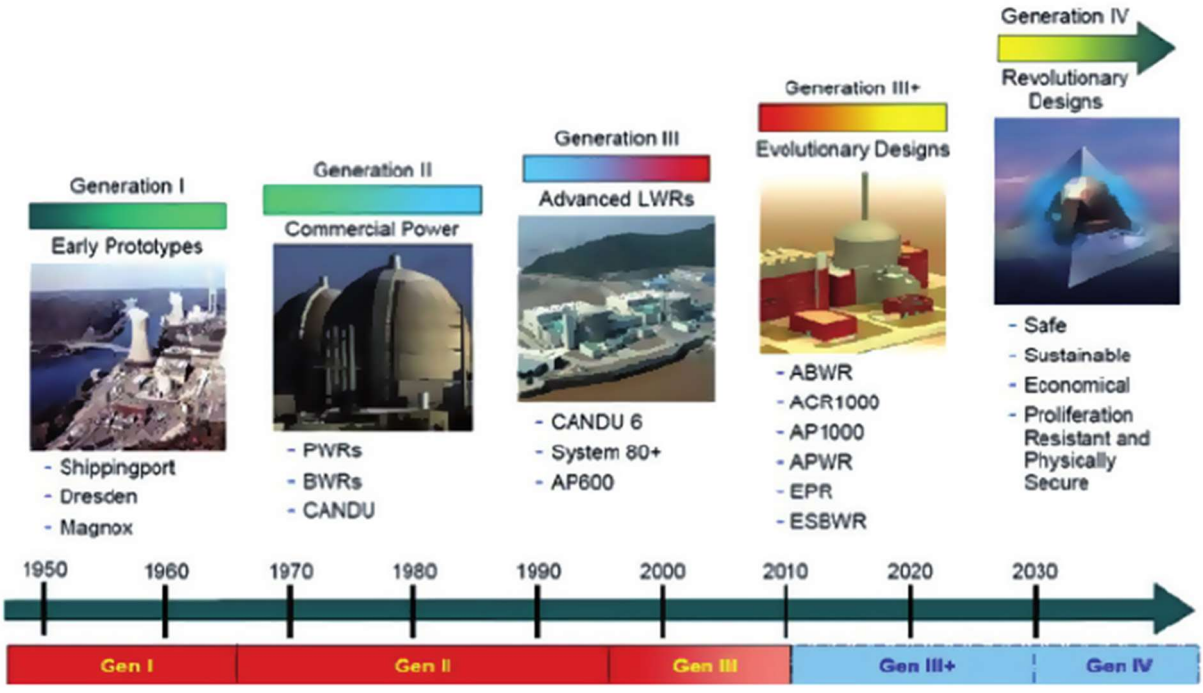


Figure 1.1: A simple illustrative diagram of various generations of nuclear power reactors [8].

### *1.2.1 Types of nuclear reactors*

Worldwide, there are four main types of reactors in operation today used to generate commercial electricity. Figure 1.2. shows various nuclear power reactor designs. Both the pressurized water reactor (PWR) and boiling-PWR use enriched $UO_2$ as fuel and light water ($H_2O$) as coolant and moderator. The pressurized heavy water reactor (PHWR)-Canada Deuterium Uranium (CANDU) uses natural $UO_2$ as fuel and heavy water ($D_2O$) as coolant and moderator. The advanced gas-cooled reactor (AGR) utilizes $UO_2$ as fuel, $CO_2$ as coolant, and graphite (C) as a moderator [9–11]. These various models use different enrichments of uranium dioxide for fuel, different moderators to slow neutrons, and different coolants to transfer the heat.

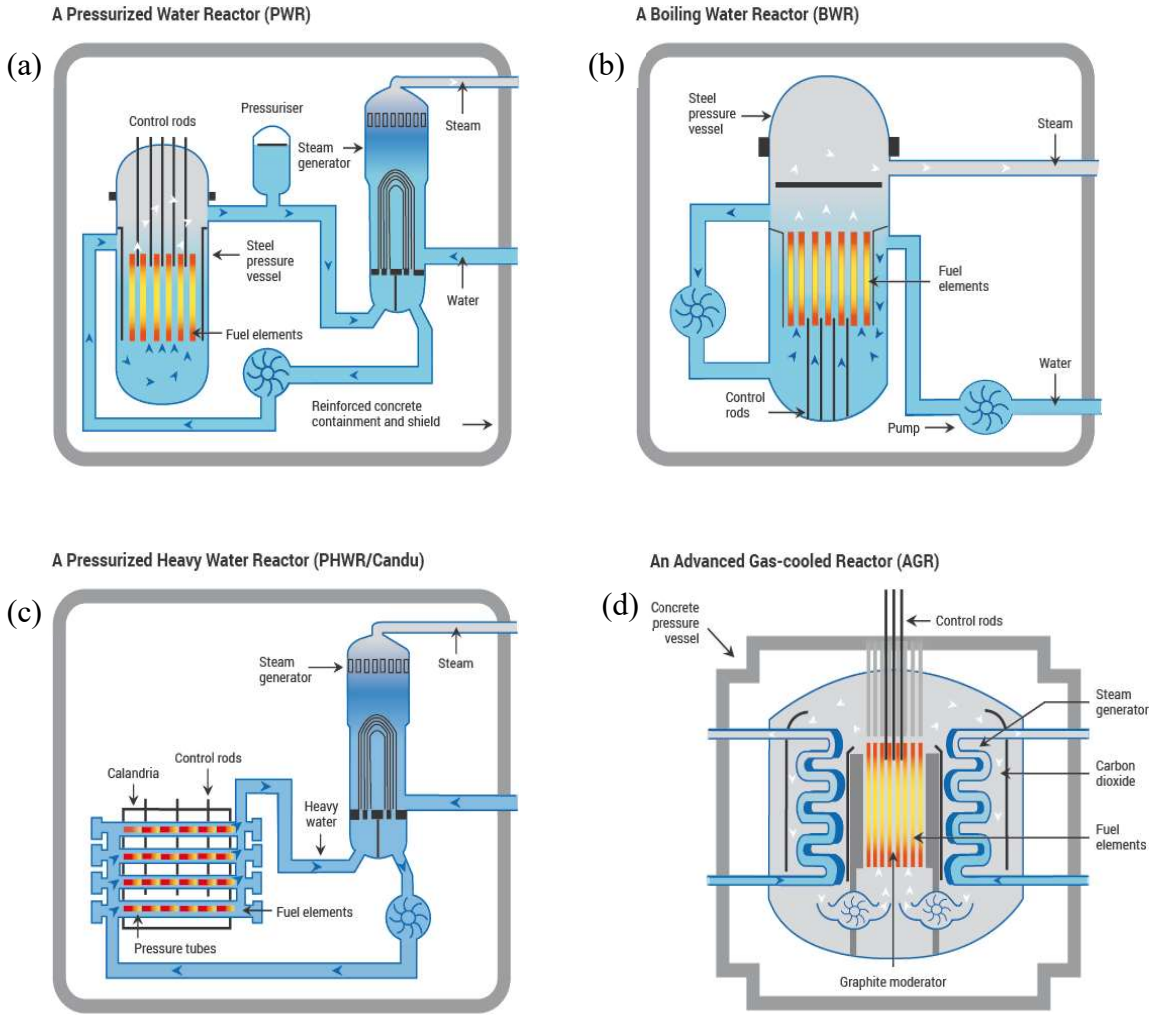


Figure 1.2: The four main types of nuclear power reactors in operation today [11].

***Example: A typical CANDU reactor***

The use of natural uranium fuel and utilizing heavy water is a fundamental concept in CANDU reactors. Heavy pressure tube water-moderated reactors were first developed in Canada but are now located in many other countries. The natural $UO_2$ is placed in a zircaloy-clad of 37 fuel pins, about 1.3 cm in diameter, and is 49 cm long. The twelve fuel bundles are loaded into each calandria tube and kept end to end in a pressure tube in which the pressure flows at about 10 MPa, 1450 psi, $D_2O$. The CANDU reactor core contains 380 secure calandria tubes in a stable vessel with a $D_2O$ moderator, resulting in a core consisting of approximately 100,000 kg of natural $UO_2$. In each pressure tube, the coolant passes through about 265 $^oC$ and exits at roughly 310 $^oC$; a typical CANDU core is about 4 m high and about 7 m in diameter [9,12,13].

## 1.3 Moderators

A moderator slows down neutrons in the nuclear reactor so that the neutrons can be absorbed by the fuel and create chain nuclear reactions. The materials used for moderation must possess a specific set of properties, including a high neutron scattering cross-section and low neutron absorption cross-section. As a result of collisions between neutrons and nuclei, a moderator should be able to slow down neutrons to an acceptable speed. For this reason, the lighter elements are more efficient moderators [14]. Table 1.1 illustrates the common moderators having a low neutron absorption cross-section but relatively large neutron scattering cross-section.

| Moderator | Neutron scattering cross-section (barns) | Neutron absorption cross-section (barns) |
|---|---|---|
| **Light water ($H_2O$)** | 49 | 0.66 |
| **Heavy water ($D_2O$)** | 10.6 | 0.0013 |
| **Graphite (C)** | 4.7 | 0.0035 |

Table 1.1: Physical constants of common moderators [15]**.**

### *1.3.1 Types of moderators*

There are different types of moderating materials, each with its conditions under which it is most efficiently used. Typically used moderator materials are light water, heavy water, and graphite.

(i) Light water ($H_2O$) — is commonly used in light water reactors. Hydrogen operates well as a neutron moderator due to its mass, almost identical to that of a neutron. One collision will significantly reduce the neutron's speed resulting from the laws of conservation of energy and momentum. Besides, light water is easily accessible and inexpensive. However, the neutrons are relatively more likely to be captured by $^{238}U$ and less likely used to fission $^{235}U$, so light water reactors require enriched uranium to operate.

(ii) Heavy water ($D_2O$) — is commonly used in heavy water reactors (e.g., CANDU). Heavy water has comparable benefits to light water, with the addition of deuterium atoms creating a lower neutron absorption cross-section. The reactors with heavy water moderator can utilize natural uranium.

(iii) Graphite (carbon) — is commonly used in pebble-bed reactors (PBR) and reactor Bolshoy Moshchnosty Kanalny (RBMK) reactors. Like a heavy water reactor, some of these reactors can use natural uranium. However, at high temperatures, graphite can be oxidized, reducing its efficiency as a moderator [16].

## 1.4 Control rods

To control the fission reaction of the nuclear fuel, the control rods in the reactor will adjust the number of slow neutrons and to maintain the fission chain reaction at a safe level. These control rods consist of strong neutron absorbers such as boron (B), hafnium (Hf), or cadmium (Cd). Their insertion controls the reactor in multiple ways during the power operations, and when fully inserted, they could shut down the reactor operation. While some classes of power reactors have channels reserved for the control rods within the designed fuel assemblies, some systems place the control rods between the fuel assemblies [17]. The energy produced from the fission process is generally in the form of the kinetic energy of the fission fragments, which is usually transferred to the coolant in the form of water. The water acts as both a neutron moderator, as it slows down the fission neutrons to the thermal energies, and as heat transfer fluid. The chain reaction is monitored by control rods. In the core, the thermal energy is removed by the water to an exterior thermal-energy

converter. For example, in BWRs, steam is released for use in the turbine. Similarly, in PWRs, a heat exchanger releases steam for the turbine[18].

### 1.5 Nuclear fission

Nuclear fission is the primary process of generating nuclear energy in a nuclear reactor. An unstable nucleus must first interact with a neutron before any nuclear fission takes place. The energy from the fission process makes use of varying binding energies of the nucleus of the atom. A typical distribution of fission product yield is shown in Figure 1.3, where the atomic mass of fission products is plotted against the percentage yield in a fuel composed of 65% Uranium and 35% Plutonium. These products resulting from fission reactions are regulated by statistical probability, but it is difficult to predict the precise way in which a single nucleus will split. Therefore, the law of conservation of energy is required to evaluate the total number of nucleons (protons or neutrons), and energy that is produced [19].

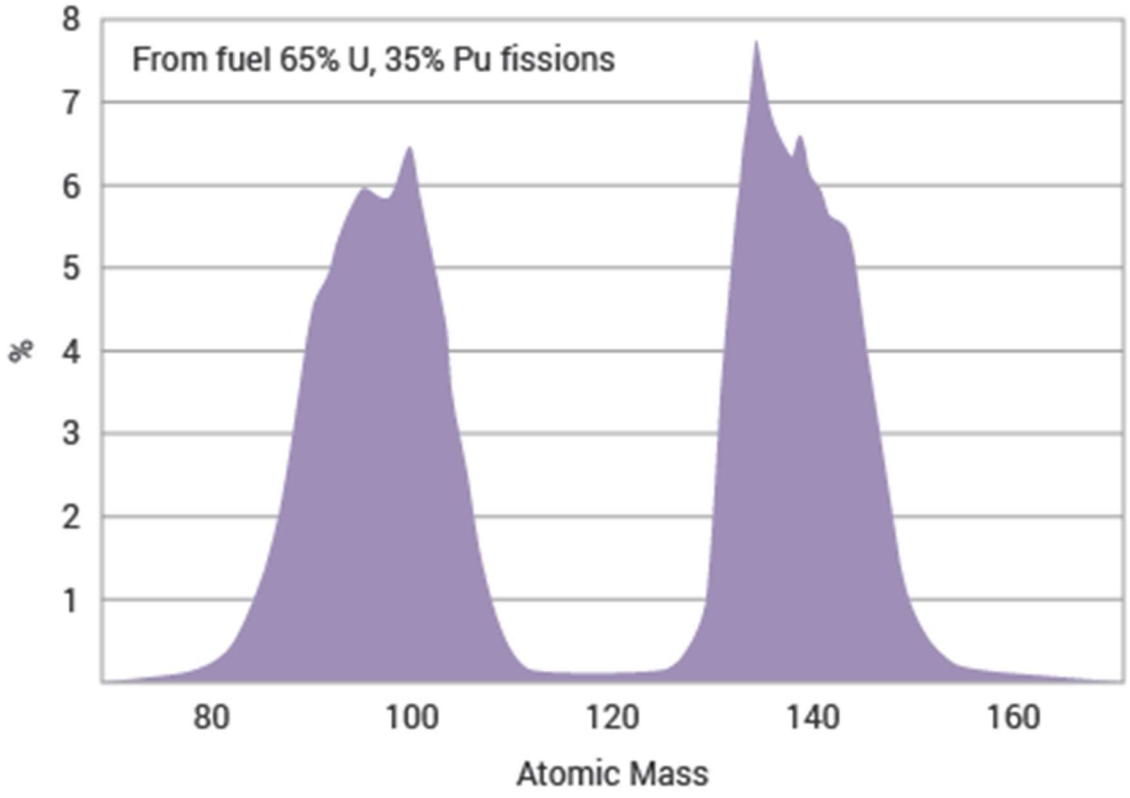


Figure 1.3: Distribution of Fission Products across the periodic table [20].

The typical fission reactions can be illustrated as:

$$n + {}^{235}_{92}U \rightarrow {}^{141}_{56}Ba + {}^{92}_{36}Kr + 3n + energy\ (170\ MeV) \quad (1.1)$$

$$n + {}^{235}_{92}U \rightarrow {}^{140}_{54}Xe + {}^{94}_{38}Sr + 2n + energy\ (200\ MeV) \quad (1.2)$$

Equation (1.1) above illustrates the conservation of nucleons, which is 235 + 1 = 141 +92 + 3, but the energy released is known to be equivalent to the small loss in the atomic mass. However, the fission products of Ba and Kr isotopes will further undergo beta decay and form the more stable isotopes of neodymium (Nd) and yttrium (Y), with the production of several electrons [19]. This beta decay, with some additional gamma rays, makes the fission products highly radioactive.

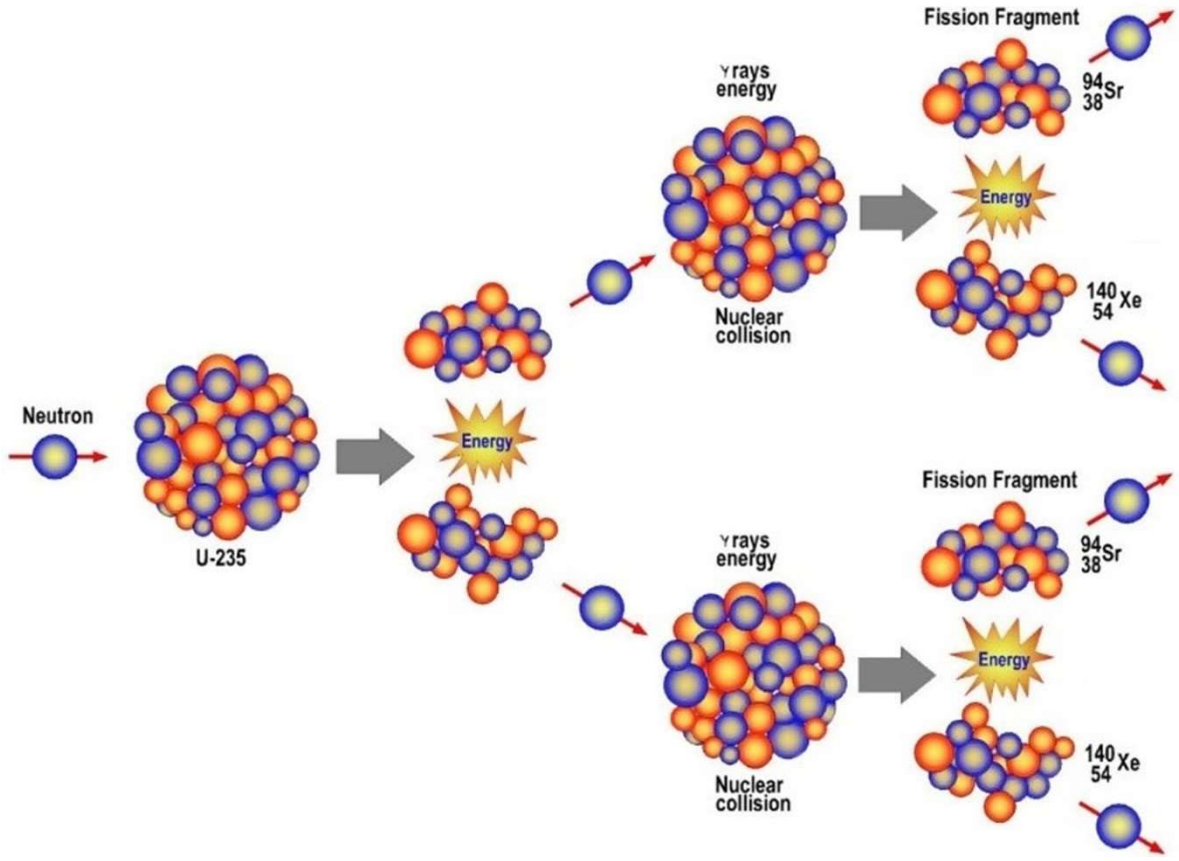


Figure 1.4: Schematic diagram of the fission process involving a Uranium-235 nucleus capturing a neutron to produce three neutrons, Strontium-94 and Xenon-140.

### 1.6 Nuclear fission reaction rate

In nuclear and particle physics, the interactions of neutrons with matter can be either absorption or scattering reactions. Absorption can result in the disappearance of free neutrons, leading to a nuclear fission reaction. Scattering results in the change of neutron energy and the direction of a neutron's motion [10]. Therefore, the probability of occurring of the reactions depends mainly on the neutrons' energy and the characteristics of the nucleus of the atom with which neutron is interacting. We can calculate the rate of reaction of the neutron with the target through the following equation:

$$R = \Phi_0 \, \sigma(nV) \tag{1.3}$$

Where $R$ is the reaction rate, $\Phi_0$ is thermal neutron flux (neutrons/cm$^2$/s), $\sigma$ is thermal neutron cross-section of $^{235}$U (cm$^2$), $n$ is the density (atoms/cm$^3$), and $V$ is the volume (cm$^3$).

For example, a typical CANDU reactor fuel reaction rate can be calculated $N = nV$ (number of target nuclei in a fuel element of volume $V$):

$$N = nV = \rho \, V \times Enrichment \times \frac{N_A}{M} \tag{1.4}$$

Where $\rho$ is the density of material (g/cm$^3$), $V$ is the volume, $M$ is the molar mass of an element (g/mol), $N_A$ is Avogadro's number $6.022 \times 10^{23}$ mol$^{-1}$ [21].

A typical CANDU reactor uses cylindrical-shape $UO_2$ fuel pellets of 12 mm diameter and 20 mm height. We can consider the density of $UO_2$ to be 10.6 g/cm$^3$, with molar mass 270.03 g/mol, and enrichment 0.7 wt%, an average thermal neutron cross-section $\sigma = 585 \times 10^{-24}$ cm$^2$, thermal neutron flux of $\Phi_0 = 10^{14}$ (neutrons/cm$^2$/s).

From equation (1.4):

$$N(U^{235}) = 10.6 \times \pi \times (0.6)^2 \times (2) \times \left(\frac{0.7}{100}\right) \times \frac{6.022 \times 10^{23}}{270.03}$$

$$= 3.74 \times 10^{20} \; (atoms).$$

From equation (1.3):

$$R = 10^{14} \left(\frac{\text{neutrons}}{cm^2 s}\right) \times 585 \times 10^{-24} (cm^2) \times 3.74 \times 10^{20}$$

$$= 2.19 \times 10^{13} \; (fission/s).$$

## 1.7 Nuclear fuel

### *1.7.1 Uranium dioxide ($UO_2$) fuel*

Over the last many years, the energy sector has undergone immense changes. Energy consumption has been increasing dramatically, and as a result, we are experiencing the exhaustion of fossil energy resources and environmental pollution, which threatens us with an increase in greenhouse gases. Many countries recognize the severity of these issues and seek sustainable and competitive energy sources as a possible solution. Nuclear fuel is a well-known candidate as it is a sustainable, energy-dense fuel. Nuclear reactors accounted for ~11% of the electricity generated in Canada [22,23], a number that is increasing each year.

The frequently used nuclear fuel is uranium (U), generally in the oxide form $UO_2$ [11]. Uranium has two isotopes uranium-235 ($^{235}U$) and uranium-238 ($^{238}U$). In nuclear power reactors, $^{235}U$ is required for nuclear fuel to sustain a chain reaction. A typical chain reaction is shown in Figure 1.4. Unfortunately, natural uranium contains only 0.72% of $^{235}U$ and the remaining 99.27% of $^{238}U$. Therefore, the concentration of $^{235}U$ must be enhanced by enrichment [24]. For instance, the generation III boiling water reactors (BWR) and the pressurized water reactors (PWR) need 2.5% and 3.5% of enrichment, respectively; light water ($H_2O$) absorbs neutrons and slows them down. The Canada Deuterium Uranium (CANDU) and Magnox reactors can use natural uranium ($^{238}U$) as fuel without any enrichment due to the use of heavy water ($D_2O$) and graphite as a moderator [9].

However, the $UO_2$ fuel can withstand harsh irradiation environments, it has high melting points, and phase stability; reduces radioactive waste; and has enhanced oxidation resistance compared to metallic, nitrides, silicides, and mixed oxide fuels [25,26]. Nevertheless, the major drawback of the present $UO_2$-zircalloy system is the low thermal conductivity of the $UO_2$ fuels, which further decreases with oxidation, increasing temperatures, and radiation dosages. Therefore, the search for fissile materials with enhanced thermal conductivity is necessary. The concept of adding high thermal conductivity material into a $UO_2$ fuel pellet has been widely studied [25]. An essential parameter in the reactor design and safety of $UO_2$ is the thermal conductivity that governs the transfer of heat produced from the fission to steam and electricity [22]. Accident-tolerant fuels (ATFs) are expected to improve fuel performance during regular operation due to enhanced thermophysical properties [25,27].

### *1.7.2 Accident-tolerant fuels (ATF's)*

Accident-tolerant fuel became a significant focus area after Fukushima, investigating the accident-tolerance properties of fuel materials has become an important issue. Currently, uranium dioxide is the standard fuel use in nuclear reactors, but the fact that the thermal conductivity degrades as temperature increases necessitate the search for fissile materials with enhanced thermophysical properties. Recently, ATF's concepts are promising due to improved thermophysical properties compared to $UO_2$ fuel, with the necessary thermal conductivity [3,28–30]. ATF's can be classified as metallic and composite fuels.

Metallic fuels, namely Uranium Molybdenum (UMo), Uranium Nitride (UN), Uranium Diboride ($UB_2$), and Uranium Silicide (U-Si) and its compounds are considered as nuclear reactor fuels. In metallic fuels, the metal elements are alloyed by various kinds' fabrication like powder metallurgy route, tri-arc melting, and liquid phase sintering, and so on with some different additives. It has been explained that the additive element concentration up to 10 wt. % can exhibit favorable outcomes relating to fissile uranium density, and irradiation performance [31]. The metallic fuels have superior mechanical properties formed by the concentration of metal range [32]. Hence, the advantages of metallic fuels are much higher heat conductivity than oxide fuels, but they cannot be used at high temperatures.

The metallic fuels are usually alloyed with the standard pure uranium, the alloy elements like Al, Zr, Si, Mo, etc., because this kind of metallic fuel has a higher fissile atom density. Furthermore, the suggested elements are also used with plutonium and actinides as a part of the nuclear fuel cycle. These fuels have high thermal conductivity due to their electronic contribution. Metallic fuels seem to be promising, but they have the main limitations related to high-temperature oxidation, low melting point, and fuel swelling, which impact the possible application as accident-tolerant fuel. Upon the critical evaluation of the limitations of the proposed metallic fuels, there is a need for future research to develop composite fuels.

In composite fuels, the excellent thermal properties, good fissile material density, good irradiation performance, and superior mechanical properties are achievable, depending on the concentration of metal added [31,33]. The additive materials, such as Mo, BeO, SiC, and diamond, have been proposed to improve the thermophysical properties of $UO_2$ [34,35]. The fundamental features that make these additives candidate materials are high thermal conductivity, high melting point, high

boiling point, and low thermal neutron absorption cross-section [35]. In metallics, the thermal conductivity increases with increasing temperature, opposite to $UO_2$. Of the mentioned materials, Mo is a primary candidate due to its low thermal neutron absorption cross-section, phase stability, and high melting point [33,36].

The composite fuels can be created in a few ways, by producing a higher heat conducting percolation pathway or a higher thermal conducting secondary particle distributed homogeneously in a matrix material ($UO_2$). However, most thermal energy could be conducted through a percolation pathway because thermal energy must pass through both higher thermal conducting secondary particles and lower thermal conducting $UO_2$ matrix in the composite. In turn, forming a higher heat conducting percolation pathway can lead to more efficiency of conducting heat because less thermal energy is conducted through the lower thermal conducting $UO_2$ matrix. Therefore, composite fuel manufacturing containing such a percolation pathway or a higher thermal conducting secondary particle distributed homogeneously in a matrix material ($UO_2$) is challenging. To obtain the desired properties of the composites, it is also essential to ensure that the pellets have a uniform distribution of materials and high densification. To achieve high density and uniform distribution, the choice of synthesis route is crucial. Previous studies by Finkeldei et al. [26] and Kim et al. [35] attempted to produce $UO_2$-Mo composite fuel through conventional sintering; these studies show that although significant improvements have been made in traditional sintering of $UO_2$-Mo, sintering by the conventional methods is limited and cannot be used to produce the dense high thermal conductivity $UO_2$-Mo pellets.

## 1.8 Objectives of the thesis

The general objective of my research is to investigate the microstructural and thermophysical properties of $UO_2$-Mo composite fuel using experimental procedures. Therefore, the specific objectives are as follows:

Objective 1: To evaluate the microstructural properties such as morphology, grain size, texture, and grain boundary character distribution of the $UO_2$-Mo pellets. Also, to evaluate the Mo particle size experimentally, to tune the microstructural characteristics of $UO_2$-Mo composite fuel.

Objective 2: To optimize the high densification of pure and Mo doped $UO_2$ pellets, and to determine the structural analysis of the $UO_2$-Mo pellets.

Objective 3: To enhance the thermophysical properties of $UO_2$-Mo composite fuel pellets compared with the $UO_2$ pellets. Also, to analyze different processing parameters on the thermophysical properties of composite fuel pellets.

Characterization of the samples was done to obtain phase distribution and morphology using energy dispersive spectroscopy (EDS), and scanning electron microscope (SEM)/ electron backscattered diffraction (EBSD). Structural analysis was obtained using X-ray diffractometry (XRD), and the thermophysical properties were analyzed using the laser flash technique.

# CHAPTER 2
# LITERATURE SURVEY

## 2.1 Degradation of uranium dioxide ($UO_2$) fuel

Uranium dioxide is the standard fuel use in nuclear reactors, but the fact that the thermal conductivity degrades as temperature increases necessitate the search for fissile materials with enhanced thermophysical properties. Recently, accident-tolerant nuclear fuel concepts are promising due to improving thermal properties as compared to $UO_2$. During the reactor operations, the fuel is exposed to high temperatures and water vapor. The potential availability of oxygen and water may also impact the behavior of accident-tolerant fuel. ATF fuel has to withstand also high elevated temperatures during the operation conditions. However, accident-tolerant nuclear fuel is usually alloyed with metallic elements and metals often oxidize at a high rate at high temperatures. According to the following literature review, the $UO_2$ with the addition of Mo showed less oxidation than other accident-tolerant nuclear fuels. Therefore, the literature survey will discuss accident-tolerant fuels with high oxidation resistance at high temperatures.

### *2.1.1 Degradation of $UO_2$ fuel in the air*

The oxidation of uranium dioxide ($UO_2$) exposed to air during normal or high-temperature operating conditions, has been widely investigated for 40 years [37]. Oxidation is relevant in various stages, including dry storage, utilization of disposing of nuclear fuel, storage of $UO_2$ powder, and fuel-recycling processes [38,39]. The oxidation of $UO_2$ fuel is a two-step reaction:

$$UO_2 \rightarrow U_3O_7/U_40_9 \rightarrow U_3O_8. \quad (2.1)$$

The $UO_2$ starting material adopts a crystal structure like calcium fluoride ($CaF_2$). The oxidation of the intermediate products, tetragonal oxide ($U_3O_7$), or triuranium octoxide ($U_3O_8$), are by-products of this structure because the interstitial oxygen atoms occupy vacant cubic sites in the fluorite-type lattice [40,41]. The formation of $U_3O_7$ and $U_4O_9$ from $UO_2$ results in a slight volume reduction, as $U_3O_8$ has a distinctly different crystal structure and density that is 23% less than that of $UO_2$, which results in a 36% net volume increase [37]. Thus, the formation of $U_3O_8$ can result in the sheath's splitting, which would also complicate subsequent handling and the disposal of nuclear fuel [42,43].

### *2.1.2 Degradation of $UO_2$ fuel in steam*

The oxidation state of nuclear fuel depends on the fission products' release from the defective rods. When the coolant enters via the defect site from the fuel-to-clad gap oxidation will occur [44]. After initial oxidation of the fuel sheath, a significant amount of hydrogen is produced, fuel oxidation occurs, and hyperstoichiometric urania ($UO_{2+x}$) is formed [45]. Higher oxidation state oxides are built with different structures and lattice constants, and as the concentration of oxygen in the interstitials increases, and the concentration of oxygen vacancy decreases [46]. This can lead to a rise in the level of uranium vacancies to maintain local electrical neutrality. An increase in the oxygen/uranium (O/U) ratio leads to increased uranium vacancies and greater diffusion of fission products. Fuel oxidation can significantly enhance fission-product transport by diffusion, as described by Szpunar *et al.* [46]. It was also observed experimentally [45,47] that fuel oxidation significantly increases fission products' volatility. Furthermore, the higher number of defects in hyperstoichiometric uranium dioxide drastically decreases the phonon contribution to the thermal conductivity, as identified experimentally by Amaya *et al.* [27,48]. This fuel thermal conductivity reduction can cause a significant temperature increase in operating fuel elements. Therefore, it is crucial to monitor the fuel oxidation state when identifying accident scenarios accurately.

## 2.2 Degradation of accident-tolerant fuels (ATF's)

Current metallic composite fuel concepts are promising due to their improved thermomechanical properties in comparison to $UO_2$. During nuclear plant operations, the fuel is exposed to high temperatures and water vapor. This oxygen and water may also impact the behavior of the fuel. Therefore, it is essential to understand the oxidation kinetics of metallic composite fuels in high-temperature environments and the impact that this has on the real-time application of the accident-tolerant fuels. Fuels with lower oxidation resistance at high temperatures are inappropriate for use in the reactors and are inadequate to be used as the accident-tolerant fuels to prevent accidents.

### *2.2.1 Degradation of UN-$UO_2$ accident-tolerant composite fuel*

UN-$UO_2$ composite pellets were subjected to hydrothermal oxidation in a water-filled static autoclave at temperatures from 250 to 350 ºC and pressure of 16.5 MPa [49]. The post-autoclave X-ray diffraction (XRD) peaks of uranium nitride (UN)- 5 wt% $UO_2$ and UN-10 wt% $UO_2$ pellets exhibited the patterns that correspond to α-$U_2N_3$; some primary peaks overlapped due to the presence of these two phases. The XRD patterns illustrated a reduction in the full width and half maximum (FWHM) of the first two peaks of $UO_2$ at (29.0 and 33.6 2θ values). At temperatures of 275 and 300 ºC, the patterns of 5 and 10 wt% specimens suggest that the $UO_2$ crystallites increased in size during the hydrothermal oxidation process. The resultant peak broadened due to an oxynitride layer from dissolved oxygen or nitrogen into the $UO_2$ and $UN_2$ lattices [49,50]. There exists also, microstructural studies using a scanning electron microscope (SEM) in backscattered electron (BSE) mode, revealing that the oxidation process firstly attacks the grain boundaries and spallation beginning at the corners of the pellet [49]. Further, attacks increase with increases in autoclave temperature. The surfaces of UN- 5 wt% $UO_2$ and UN-10 wt% $UO_2$ composites corroded at 250 ºC, where dark and light phases are noted, as shown in Figure 2.1.

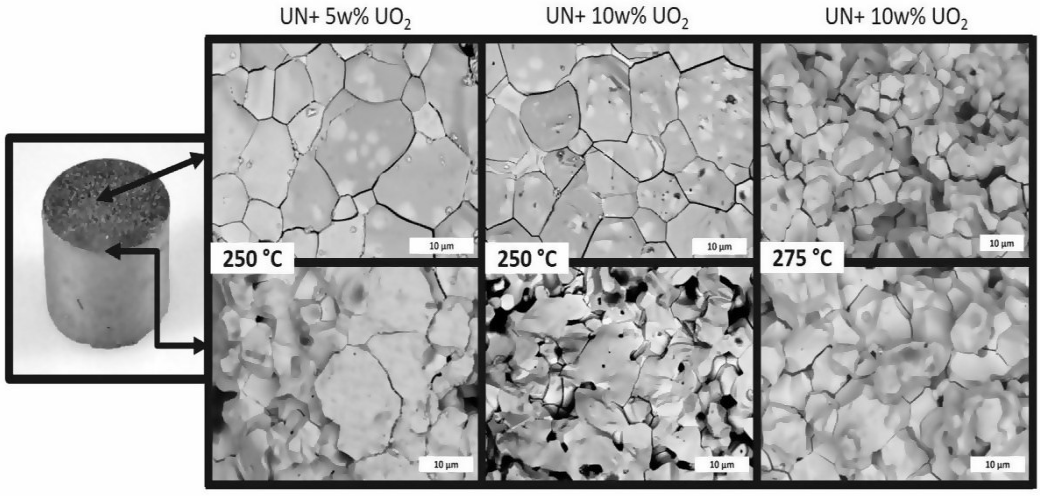


Figure 2.1: SEM micrographs of UN-5 wt% $UO_2$ and UN-10 wt% $UO_2$ composites pellets corroded at 250 ºC and UN-10 wt% $UO_2$ composites pellets corroded at 275 ºC. The top images represent the middle region of the pellets, which exhibit less corrosion; the bottom images are taken from the outer edge of the pellets and are heavily corroded. The edge and grain boundaries are attacked [49].

The dark phase was observed as an oxide with energy dispersive spectroscopy (EDS) analysis shown in Figure 2.2. These combined micrographs with EDS analysis show that the oxide nucleates on grains and propagates through the grains' surface. The increase in autoclave temperature at 275–350 °C shows that the grains exhibited clear separation at the grain boundaries. The individual grain sludge from 275–300 °C show less granular deterioration than pellets at 325–350 °C, which show a more substantial attack. However, Rao *et al.* [51] and Sunder *et al.* [52] claimed that the UN converts quickly to $UO_2$ as the final phase upon exposure to water, or $U_3O_8$ in pure UN specimens, which had no starting $UO_2$ phase.

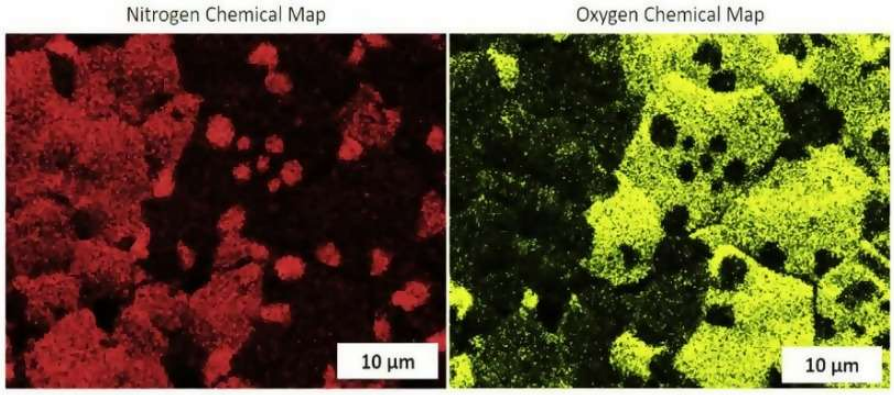


Figure 2.2: EDS analysis of an UN-5 wt% $UO_2$ composite pellet surface corroded at 250 °C showing distinct nitrogen and oxygen-rich regions [49].

### *2.2.2 Degradation of UN-$U_3Si_2$ accident-tolerant composite fuel*

In a study by Johnson *et al.* [53], the authors explored the oxidation behavior of various accident-tolerant fuels candidates such as UN, $U_3Si_2$, $U_3Si_5$, and UN-$U_3Si_2$ (10%) composites under different conditions, which were then evaluated and compared with the standard $UO_2$ as a reference point. These oxidation reactions occur in any high-temperature, high-oxygen environment, and all of the fuels, as mentioned earlier, can oxidize. Generally, in light water reactors (LWR), oxidation will be driven by interactions between fuel and water. In this case, the equations projected for the oxidation of the fuels can be given as follows:

$$3UO_2 + 2H_2O \rightarrow U_3O_8 + 2H_2 \quad (2.2)$$

$$3UN + 8H_2O \rightarrow U_3O_8 + 3NH_3 + 3.5H_2 \quad (2.3)$$

$$U_3Si_2 + 12H_2O \rightarrow U_3O_8 + 2SiO + 12H_2 \quad (2.4)$$

$$U_3Si_5 + 18H_2O \rightarrow U_3O_8 + 5SiO + 18H_2 \quad (2.5)$$

In each case, a reduction in density is exhibited between the initial phase and $U_3O_8$ (final product for each reaction). The reduction of these outcomes is from converting the initially solid material into finer particulates and the formation of hydrogen gas. The authors explored the thermo-gravimetric analysis (TGA) in high temperatures in the air environment compared to steam environments. In air environments, the oxidation occurs solely through reaction with dioxygen ($O_2$) gas, while the product of oxidation remains $U_3O_8$. The existing studies focus on relating the differences in reaction rate for the various fuel candidates compared to $UO_2$, as shown in Figure 2.3.

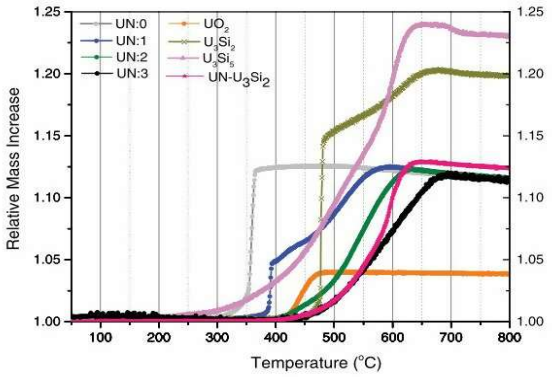


Figure 2.3: TGA analysis of the oxidation reactions of $UO_2$, UN, $U_3Si_2$, $U_3Si_5$, and UN-$U_3Si_2$ composite fuels [53].

In the case of standard $UO_2$, the onset oxidation reaction occurred at 405 ºC, while the maximum rate of 10% per minute was noted at 440 ºC. The formation of $UO_2$ to $U_3O_8$ was studied by McEachern *et al.* [37]. This reaction typically causes a 3.95% mass gain and causes the creation of a fine powder residue. In comparison, for the UN, the onset of the oxidation reaction occurred at 320 ºC, and the maximum rate was noted at 360 ºC. The oxidation itself is very rapid and reached a peak consumption rate of nearly 50% per minute. A final mass gain of 11.4% was noted, suggesting the production of $U_3O_8$. This assumption was confirmed by the EDS of the final results, which showed 15.1% ± 0.2 oxygen [54]. In the case of $U_3Si_2$ and $U_3Si_5$, the oxidation reaction was also rapid, and the gained mass was 20% and 24%, respectively, consistent with the oxidation reactions proposed in Equations 2.4 and 2.5, suggesting the production of $U_3O_8$ and SiO [55]. The UN-$U_3Si_2$ (10%) composite showed a similar trend like the UN's oxidation reaction with a slight mass gain in the composite. This seems to suggest a more complex behavior of oxidation between the UN and $U_3Si_2$. These results indicate that the oxidation of highly porous UN and $U_3Si_5$ is noticeably less than of the other composites.

### *2.2.3 Degradation of U-10 wt% Mo accident-tolerant fuel*

Kang *et al.* [56] explored the oxidation behavior of U-10 wt% molybdenum (Mo) fuel in the air at ~200–500 ºC. It was noted through XRD studies that U-10 wt% Mo was transformed entirely to $U_3O_8$ at temperatures above 400 ºC. The addition of 10 wt% Mo lowers the oxidation rate of uranium at 200–500 ºC. A previous study by Antill *et al.* [57] also noted that the addition of Mo, copper (Cu), and niobium (Nb) in uranium reduced the oxidation in air and carbon dioxide at 500 ºC. A silicon alloy was reported to have higher oxidation in carbon dioxide at the most elevated temperatures. There exist, however, commonly-known stable uranium oxides such as $UO_2$, $U_3O_8$, $UO_3$, $U_4O_9$, and metastable uranium oxides of $U_2O_5$ and $U_3O_7$. After 40 hours of air oxidation, the U-10 wt% Mo has formed $UO_2$ and $U_3O_7$ at 200 ºC, while $U_3O_8$ was observed at a temperature of 300 ºC. After the creation of $U_3O_8$, there is no other oxide phase but $UO_2$ and $U_3O_7$ above 400 ºC. Figure 2.4. (a) shows mass gain per unit area during the process of air oxidation over time. Figure 2.4. (b) represents the weight gain per unit time against the temperature. A U-Mo alloy, uranium, and $U_3S_i$ are shown in the plot. When comparing the uranium and $U_3S_i$ fuels, the U-10 wt% Mo fuel has lower oxidation in air.

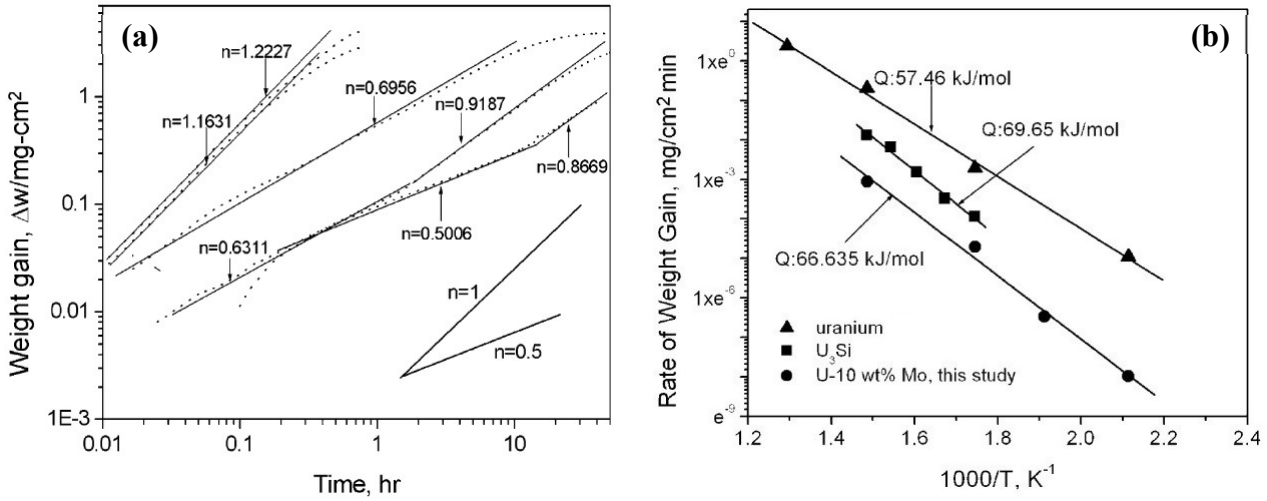


Figure 2.4: (a) The weight gain per unit area versus time at ~200–500 ºC, (b) Rate of weight gain versus 1000/T [56].

### *2.2.4 Degradation of Mo-cermet fuel containing $PuO_{2-x}$.*

The oxidation of a prototypic Mo-cermet fuel having $PuO_{2-x}$ was experimentally studied by Miwa *et al.* [58]. In this study, Mo-cermet fuel holding 50 vol% $PuO_{2-x}$ with 2% of $UO_2$ was fabricated via a conventional powder metallurgical route. Analysis of the fabricated pellets through XRD showed the two phases of $PuO_{2-x}$ and Mo with a fluorite type body-centered cubic (BCC) crystal structure. The cross-sectional optical microscope image of these phases is shown in Figure 2.5. (a), The grey represents the oxide phase, the white represents the metal phase, and the black shows the pores in the pellet with an average diameter of approximately 5 µm. Similarly, a TGA analysis was performed using 100 mg pieces of the specimens to determine the O/Pu ratio of $PuO_{2-x}$ in the Mo-cermet pellets at pre-determined temperatures, precisely ~1200 ºC as shown in Figure 2.5. (b). It was noted that the Mo-cermet's weight gain started at 1200 ºC; the oxygen potential ($\Delta\bar{G}_{O_2}$) of $Mo/MoO_2$ was also recorded at 1200 ºC. Because of the oxidation potential effects the thermochemical behaviors of the oxide nuclear fuel system, it is essential to determine the composition, temperature, and oxygen-to-metal ratio (O/Pu) ratio (2.00-$x$). The oxygen potential is illustrated by the following relationship:

$$\Delta\bar{G}_{O_2} = RT\ In\ PO_2 \tag{2.6}$$

Where $\Delta\bar{G}_{O_2}$ is the oxygen potential, $R$ is the gas constant, $T$ is the temperature (ºC), and $PO_2$ is equilibrium oxygen partial pressure.

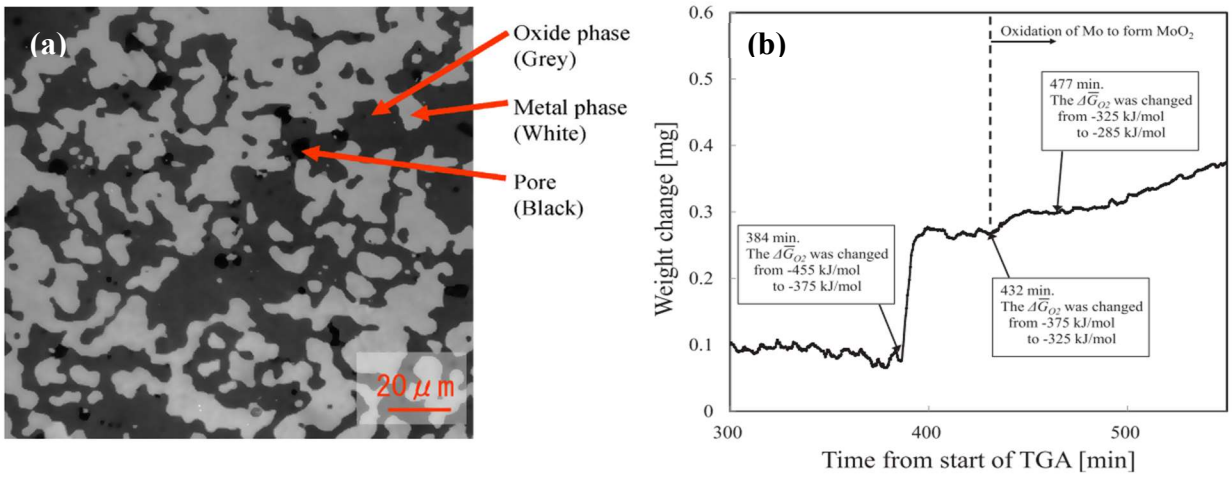


Figure 2.5: (a) Optical image of the cross-sectional prototypic Mo-cermet fuel pellet. (b) TGA analysis of the Mo-cermet fuel specimen during oxidation at 1200 ºC. The oxygen potential of $Mo/MoO_2$ observed at 1200 ºC is about -328 kJ/mol [58].

### *2.2.5 Degradation of Ce doped $UO_2$ accident-tolerant fuel*

Ha *et al.* [59] studied the oxidation of cerium (Ce) doped $UO_2$ through TGA analysis. The oxidation reaction through the dominant pathway occurred in two steps:

$$U_{1-y}Ce_yO_{2-\delta} \rightarrow (U_{1-y}Ce_y^{4+})_4O_9 \rightarrow (U_{1-y}Ce_y^{4+})_3O_8 \quad (2.6)$$

Given the increase in Ce content (0.136 to 0.332), an alternate pathway is proposed as:

$$(U_{1-y}Ce_y^{4+})_4O_9 \rightarrow (U_{1-y}Ce_y^{3+})_4O_9 \quad (2.7)$$

The increase in Ce content stabilizes the cubic $(U_{1-y}Ce_y)_4O_9$ phase excludes the creation of a metastable tetragonal $(U_{1-y}Ce_y)_3O_7$ phase, and prevents the creation of $(U_{1-y}Ce_y)_3O_8$ proportional to the Ce content. The $UO_2$ oxidizes changing a face-centered cubic (FCC) structure to orthorhombic $U_3O_8$. This results in the disruption of fuel elements owing to the volumetric expansion related to the structural change [60]. In the evaluation of Ce on the oxidation of $UO_2$, weight changes were measured in terms of temperature under constant airflow. The differences in the Ce content was calculated from the weight changes, as shown in Figure 2.6 (a). The oxidation reaction heats noted by differential scanning calorimetry (DSC) are shown in Figure 2.6 (b). It was observed that the oxidation of $UO_2$ is carried through in two steps, such as $UO_2$ to $U_4O_9$ and $U_4O_9$ to $U_3O_8$ [61–63]. These results show the two transitions for Ce contents from 0.025 to 0.092, as shown in Figure 2.6. The reaction curves in Figure 2.6 (b) shift to elevated temperature as the Ce content is increased, which shows the retardation of the oxidation reaction upon the addition of Ce ions.

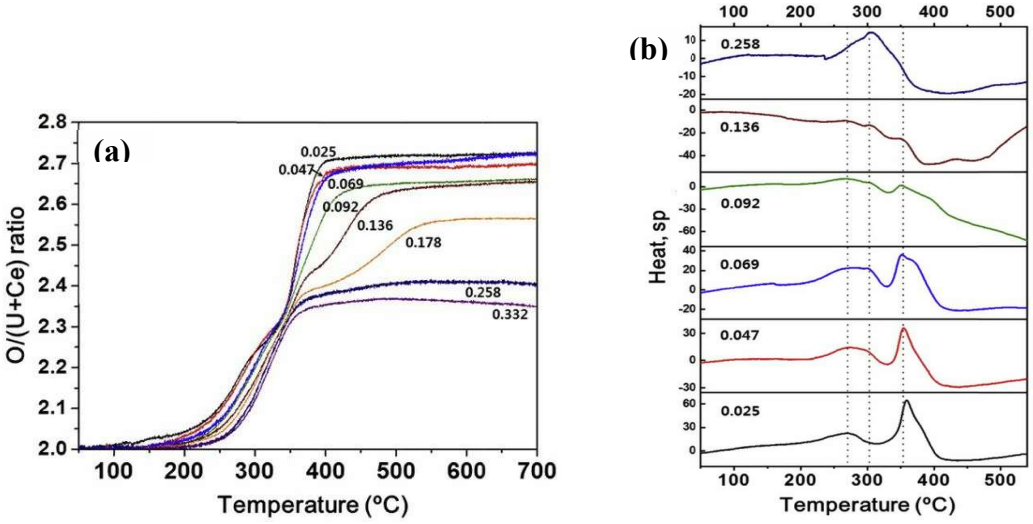


Figure 2.6: TGA (a) and DSC (b) analysis during air oxidation as a function of Ce content from (0.025 to 0.332) [59].

### *2.2.6 Degradation of Mo doped $UO_2$ accident-tolerant fuel*

The oxidation behavior of Mo in spent $UO_2$ fuel was explored by Keong *et al.* [64]. In this study, on the addition of Mo in the $UO_2$ matrix, the Mo content (atom %) was about 1%, 2%, 4%, 8%, and 15%, respectively. The XRD peaks revealed the oxidation of Mo doped $UO_2$ at 300 °C, 450 °C, and 600 °C, as shown in Figure 2.7. Previous studies showed that the U-O system could display oxide phases such as stable cubic $UO_2$, $U_4O_9$, (metastable tetragonal $U_3O_7$), and the (orthorhombic $U_3O_8$) [64,65]. In the $UO_2$-Mo matrix, the $UO_2$ was oxidized and formed $U_3O_7$ and $U_3O_8$, as shown in Figure 2.7. (a, b). At 450 °C, the $U_3O_8$ phase was observed as the primary phase with a minimal amount of $U_3O_7$ phase with high Mo content of [15 at.%]. The $U_3O_8$ intensity was decreased when the Mo content increased, resulting in the inhibition of oxidation of Mo. The monoclinic $UO_2MoO_4$ phase was observed for specimens with high Mo content of [15 at.%] at 600 °C, as shown in Figure 2.7. (c).

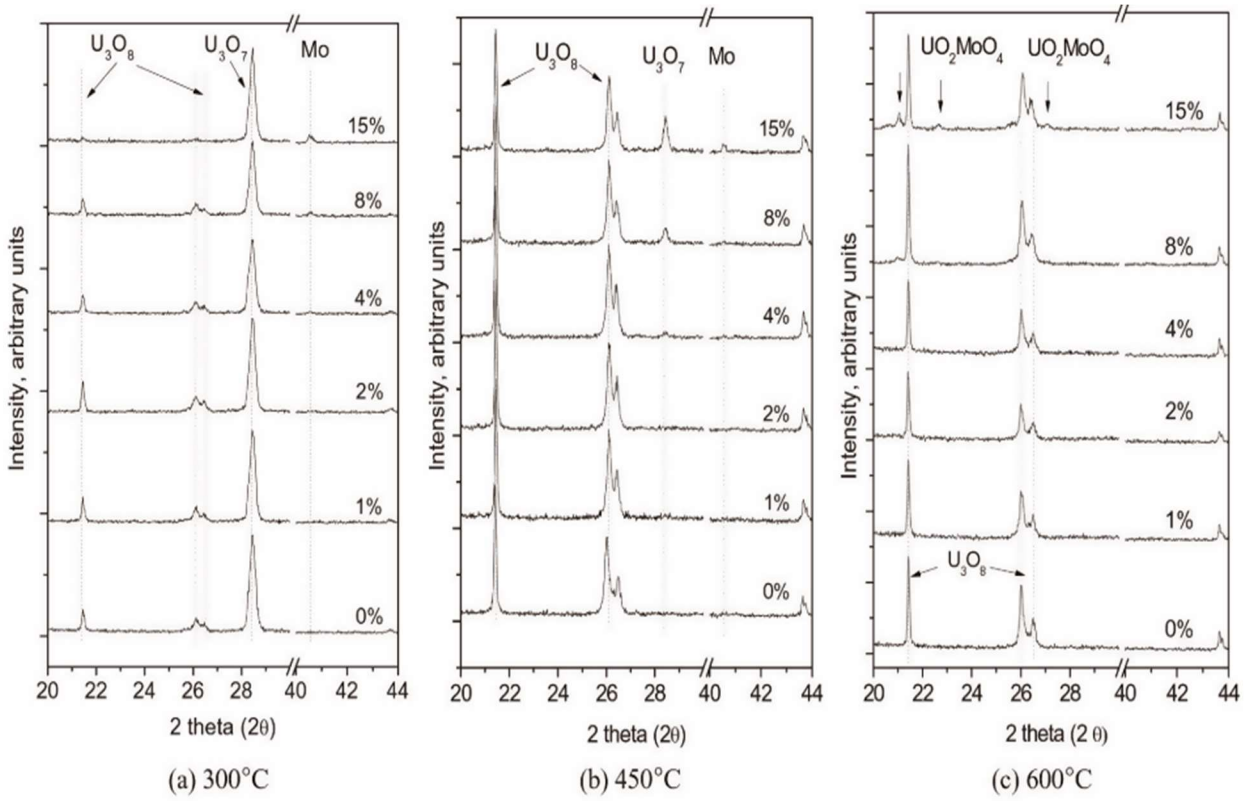


Figure 2.7: XRD patterns of Mo doped $UO_2$ after air oxidation at (a) 300 °C, (b) 450 °C, and (c) 600 °C for 10 minutes [64].

In the oxidation kinetic curves, the weight gain of Mo doped $UO_2$ was observed by TGA. It was noted that the maximum measured weight gains at 600 °C were 3.8%, 3.9%, 4.4%, 4.7%, 5.5%, and 6.6% for the specimens with Mo content 0%, 1%, 2%, 4% 8%, and 15% respectively, as shown in Figure 2.8. There are two different cases studied by considering a metallic precipitate of Mo in a $UO_2$ matrix and $(U_xMo_y)O_2$ mixed oxide as a solid solution (x+y=1) or the oxide precipitate as an initial phase. The oxidation reaction of Mo-precipitated uranium oxide can be illustrated as follows:

$$3\,UO_2 + \tfrac{1}{2}\,O_2 \;\rightarrow\; U_3O_7 + \tfrac{1}{2}\,O_2 \;\rightarrow\; U_3O_8 \tag{2.8}$$

$$U_3O_8 + 3Mo + 5O_2 \;\rightarrow\; UO_2MoO_4 \tag{2.9}$$

The two-step oxidation reaction process of $UO_2$ oxidized to form $U_3O_8$ is shown in Equation 2.8. Additional oxidation was observed with Mo to produce $UO_2MoO_4$, as shown in Equation 2.9. In the initial stage, the Mo oxidation was not observed in the $UO_2$ matrix. Mo inhibits the oxidation reaction from $UO_2$ to $U_3O_8$ due to the protecting effect of the $Mo/MoO_2$ couple. It was observed that after $UO_2$ oxidation, it produces $U_3O_8$. When $U_3O_8$ reacts with Mo, it will then oxidize to $UO_2MoO_4$. These studies are also in good agreement with the oxidation reactions suggested by Imoto *et al.* [66].

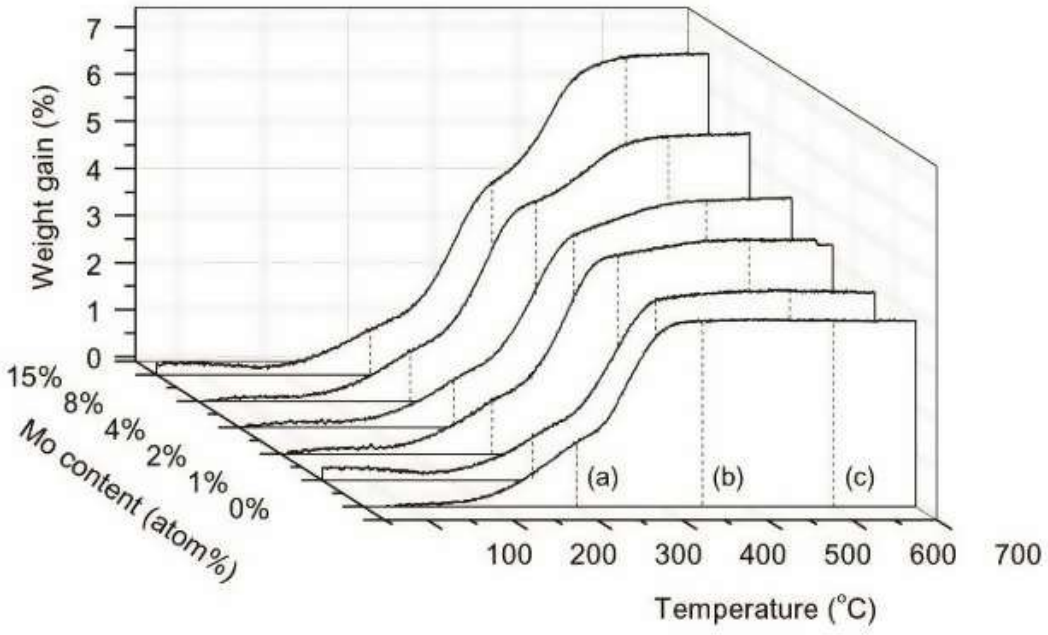


Figure 2.8: TGA analysis of the oxidation reaction of Mo doped $UO_2$ spent fuel [64].

However, during normal operations, the fuel is exposed to high temperature and water vapor. The potential availability of oxygen and water may also impact the behavior of the fuel. It was evident from the literature that, apart from Mo-doped $UO_2$ spent fuel, remaining fuels such as UN, UN-$UO_2$, UN-$U_3Si_2$, U-Si compounds, and U-Mo oxidizes in air. TGA analysis shows significant weight gain at elevated temperatures, whereas the XRD patterns illustrate the formation of an oxide phase. All of these fuels have an oxide $U_3O_8$ at the initial stage of oxidation, and the added metal was oxidized at high temperatures. For example, the oxidation of Mo in $UO_2$ was observed at 600 $^oC$ and was represented by $UO_2MoO_4$, as shown in Figure 2.7. However, the addition of Mo, Nb, and Cu reduced the oxidation attack in uranium. In conclusion, it has been experimentally demonstrated that the addition of metal to nuclear fuels improved thermophysical and mechanical properties. However, metals oxidize and have substantial mass gains at high temperatures. When considering fuels with metallic elements, Mo did not oxidize at normal reactor operating temperatures, and weak oxidation was observed at high temperatures. Thus, Mo can be a potential additive material in nuclear fuels and can be considered to use accident-tolerant fuels.

# CHAPTER 3
# MATERIALS AND METHODOLOGY

## 3.0 Overview

In this chapter, the materials selected, and the experimental techniques used are described. The experimental procedures for characterizing the microstructural and thermophysical properties of nuclear fuels are analyzed, and the added elements are discussed. The fabrication of $UO_2$ and $UO_2$-Mo composite samples using the spark plasma sintering technique is analyzed.

## 3.1 Materials

The materials used in this project were:

The commercial uranium dioxide ($UO_2$) powder provided by Cameco (Saskatoon, Canada).

Alfa Aesar provided the molybdenum (Mo) particle size of 150 μm with a purity of 99.9% (CAS: 7439-98-7).

Sigma-Aldrich supplied the Mo particle size of 100 nm with a purity of 99.8%.

Alfa Aesar provided the Mo particle size of 60–80 nm with a purity of 99% (CAS: 7439-98-7).

US Research Nanomaterials Inc supplied the Mo particle size of 35–45 nm with a purity of 99.9% (CAS: 7439-98-7).

## 3.2 Methodology

The fabrication and various characterization techniques used in this research work are described below.

### *3.2.1 Powder blending*

The planetary ball mill used to blend the powders of $UO_2$ and Mo for making the composite pellets (shown in Figure. 3.1) was manufactured by Torrey Hills Technologies, LLC U.S.A. These powders were milled in container cups of stainless steel (285 ml capacity) with a ball to powder ratio of 8:1 for 2 hours with a milling speed maintained at 200 revolutions per minute (RPM). Isopropanol was used as the process control agent, and the six wt% solution was inserted with $UO_2$-Mo powder before milling.

Figure 3.1: Planetary ball mill (Torrey Hills-ND2L) at the material science laboratory, University of Saskatchewan.

### *3.2.2 Fabrication by spark plasma sintering*

Spark plasma sintering (SPS) uses a combination of pressure, temperature, and electric current to sinter composite powder compacts. In SPS, the graphite die-punch is loaded with the composite powder to be fabricated and positioned between hydraulic rams. Pulsed direct current (DC) is then passed through the die-punch system, while the uniaxial pressure is simultaneously applied. A schematic of the SPS mechanism is shown in Figure 3.3. Generally, the applied field is low (~volts), and the allowed electric current flow through the die is high (~thousands of amps), which heats the die and powder and, combined with the instantaneous pressure, join the composite powder particles together [67–69]. In this project, the samples were fabricated using the Thermal Technology LLC 10-3 system located at the Kelowna campus, University of British Columbia (shown in Figure 3.2).

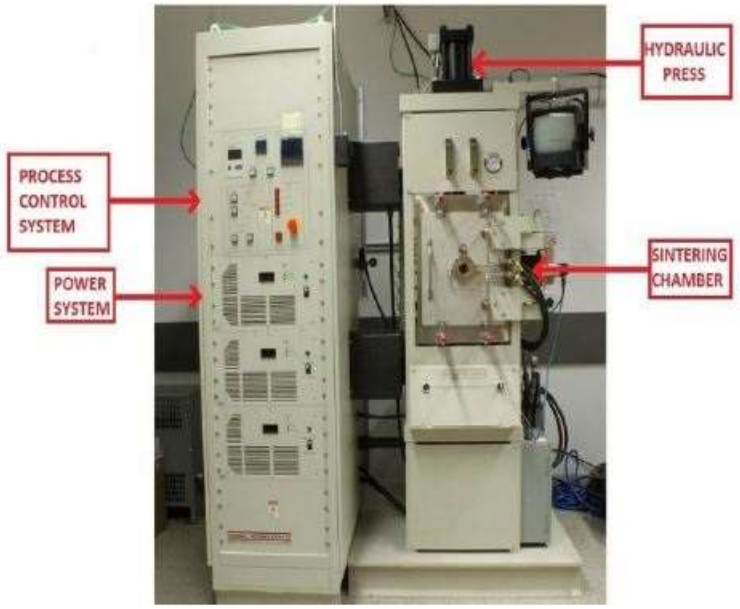


Figure 3.2: SPS equipment- Thermal Technology LLC 10-3 system at the Kelowna campus, University of British Columbia.

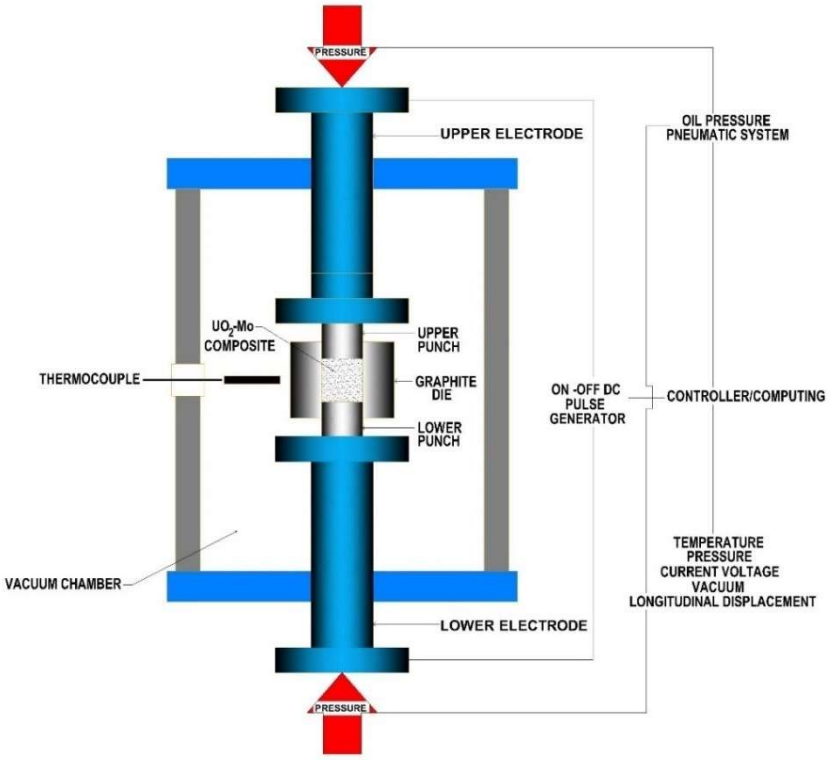


Figure 3.3: Schematic diagram of the SPS sintering technique.

Compared to traditional sintering, SPS is the preferred method for the manufacturing of composite fuels [25,68,70,71]. It has been concluded that composite materials processed under SPS have achieved high densification using lower sintering temperatures, as well as improved mechanical properties over shorter holding times (minutes) [25,68,70,71]. There are many reasons for the higher densification rate achieved using SPS [72]. Overall, the following mechanisms are the most frequently discussed:

(i) Spark—According to the spark theory, there is a spark generated between the powder particles during SPS processes. The region where this spark strikes the powder particles is exposed to spark impact pressure, which also heats the composite powder particle surface and enables bonding between powder particles [68,73,74].

(ii) Plasma—Researchers believe that because of the electric potential during the SPS fabrication, the sintering atmosphere procedures plasma. This plasma cleans the powder particle's surface and helps in the fabrication process [72].

(iii) Joule heating—This theory explains that the powder particles are heated due to Joule heating. Subsequently, the surface resistance of powder particles is higher than the powder bulk resistance; the interface between the powder particles is exposed to very high temperatures. However, this theory is limited to illustrating the efficiency of SPS for non-conductive materials. Joule heating theory claims that powder surfaces encounter temperatures as high as the melting point of the starting material's [75].

(iv) Electric field enhanced diffusion—In general, fundamental diffusion theories illustrate that the distribution of metal particles is improved by the presence of an electric field [76]. Hence, the electric field present in SPS is believed to contribute to higher powder densification [68,74,77].

The SPS process is beneficial when fabricating a wide array of materials, including ceramics, composites, metals, and polymers [25,78–80].

## 3.3 Materials characterization techniques

### *3.3.1 X-ray diffraction*

X-ray diffraction (XRD) is one of the powerful non-destructive methods used to characterization the crystalline material. In this project, XRD was used to identify the phase composition of nuclear fuel materials. The XRD is based on the interfaces of the X-ray and the sample. The X-rays are produced by the cathode X-ray tube. The collimated rays are then focused on the material. Hence the wavelength ($\lambda$) of X-rays is of the same order of magnitude as the lattice spacing ($d$) in the specimen; the X-rays are diffracted in the material by following the Braggs law, equation (3.1). The diffraction angles of $2\theta_B$ are recorded and used to determine the structure of the material.

$$n\lambda = 2d\ sin\theta_B \tag{3.1}$$

The XRD patterns of the powder and sintered samples are characterizations using a BRUKER D8 Discover with chromium $K_\alpha$ radiation of $\lambda$ =2.291 Å. The 2θ angle scanned from 20$^o$ to 110$^o$. Figure 3.4 represents the XRD equipment used in this research, having a Bragg Brentano geometry; adopted the following conditions: voltage 40 kV, 40 mA, step mode, and the sample oscillation XY plane with an amplitude of 2mm. The Xpert High Score Plus software is used to fit the peak profile for phase identification of the specimens.

Figure 3.4: The Bruker D8 Discovery XRD equipment at the material science laboratory, University of Saskatchewan.

### *3.3.2 Scanning electron microscopy/electron backscattered diffraction*

The powder and pellet samples' microstructural characterization was carried out using a versatile Field Emission Scanning Electron Microscope (SEM) Hitachi Su 6600. The Hitachi Su 6600 model shown in Figure 3.5, is also equipped with an Oxford Instruments NordlysNano Electron Backscatter Diffraction (EBSD) detector and Energy Dispersive Spectrometry (EDS) detector that acquires diffraction patterns using AZTEC 2.0 data acquisition software in the form of backscattered electrons recorded by the phosphor screen detector. The EBSD was used to analyze the grain structure, grain boundary misorientation, coincidence site lattice-type boundaries, and texture of the specimens. The SEM and EBSD scans were measured with an acceleration voltage of 20 kV and a working distance of 9-10 mm. The post-processing of the obtained scans is completed using Channel 5 software by Oxford Instruments.

Figure 3.5: Hitachi Field Emission (SU 6600) SEM equipped with an Oxford Instruments NordlysNano EBSD and EDS at the material science laboratory, University of Saskatchewan.

### *3.3.3 Density measurement*

The Archimedes principle is used to measure the pellet densities. TORBAL (AGCN200) density measurement equipment with a resolution of 0.0001g for accuracy in determining each pellet's density by immersing the pellets into the distilled water. The three readings were recorded for each specimen, and the average data with the error bar was reported. The density was calculated by the Archimedes principle [81] since the unknown densities can be computed by measuring the mass in air and weight in water using the following equation (3.2):

$$Relative\ density\ (RD) = \frac{W_{air}}{W_{air} - W_{H_2O}} \qquad (3.2)$$

Where $W_{air}$ is the pellet's weight in air and $W_{H_2O}$ represents the weight of the pellet in water measured in the same units.


Figure 3.6: Mass balance from the TORBAL (AGCN200) apparatus at the material science laboratory, University of Saskatchewan.

### *3.3.4 Thermal conductivity analysis by laser flash technique*

The laser flash analysis is used to measure the thermal diffusivity ($\alpha$), specific heat capacity ($C_p$), and thermal conductivity (λ) of the sintered pellets. In this technique, a high-power laser pulse (450 μs pulse width) from a solid-state Nd: glass laser pulse is used to illuminate the pellet's front face. Simultaneously, the resulting temperature rise is observed on the rear face with liquid nitrogen cooled InSb infrared detector. The specimen is coated with the graphite spray for good absorption and emissivity of the laser pulse. The measurements were performed in the argon atmosphere, starting from room temperature to 900 ºC. By measuring the time taken for the temperature rise in the rear face, the laser flash technique records the thermal diffusivity (α) of the samples using the Parkers relations [82] given as shown in equation (3.2):

$$\alpha = 0.1388 \times \frac{L^2}{t_{\frac{1}{2}}} \tag{3.2}$$

Where $L$ is the thickness of the sintered sample, and $t_{1/2}$ is half of the maximum time for the signal to catch the detector. Since the measured $\alpha$, the thermal conductivity as a function of temperature $\alpha(T)$ measured using the relation (3.3):

$$\alpha(T) = \frac{\lambda(T)}{\rho(T) \times C_p\,(T)} \tag{3.3}$$

Where $\rho(T)$ is the density, and $Cp\ (T)$ is the heat capacity at constant pressure as a function of temperature. The apparatus used to measure the thermal diffusivity ($\alpha$), and thermal conductivity (λ) was TA instruments (DLF-1/EM-1300), shown in Figure 3.7.

Figure 3.7: Laser flash equipment (DLF-1/EM-1300) from TA Instruments at the material science laboratory, University of Saskatchewan.

The pellets used in this analysis were disc-shaped and diameter about 12 mm to 12.7 mm in diameter and the thickness in the range of 2 mm to 3 mm. The specimen thickness was determined by averaging six values measured using a calibrated micrometer. The standard deviation of the average thickness was less than 0.02 mm. The density and thickness of the sintered pellets were measured and remain constant during the whole procedure.

# CHAPTER 4

# FABRICATION AND MICROSTRUCTURAL ANALYSIS OF $UO_2$ AND $UO_2$-Mo COMPOSITES

## 4.1 Brief introduction

### *4.1.1 Fabrication mechanisms*

Fabrication mechanisms of polycrystalline materials facilitate the transport of matter along specific paths such as lattice, grain boundary, and surface. There are six types of mechanisms of matter transport during the fabrication of polycrystalline materials such as I. Surface diffusion, II. Lattice diffusion (from the surface), III. Vapor transport, IV. Grain boundary diffusion, V. Lattice diffusion (from grain boundary), and VI. Plastic flow, as demonstrated in Figure 4.1. All these mechanisms correspond to bonding and neck growth among the particles. They can also be commonly categorized as densifying and nonidentifying mechanisms [83,84].

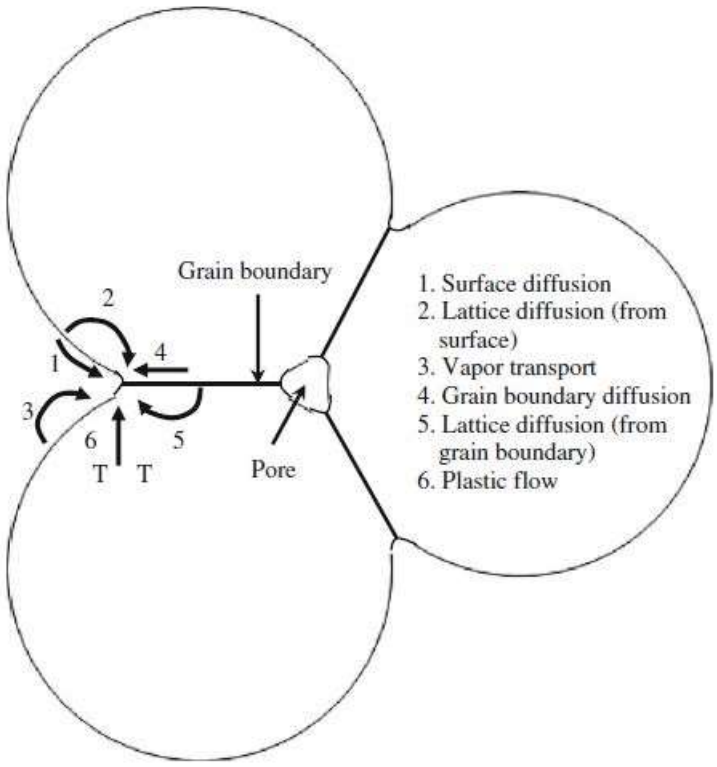


Figure 4.1: Schematic representation of sintering mechanisms in polycrystalline materials [84,85].

(i) Non-densifying mechanisms include surface diffusion (diffusion of atoms along the surface of the particle), lattice diffusion from the surface (atoms from surface diffuse to lattice), and vapor transport (the evaporation of fragments that condense on a distinct surface). Therefore, these (mechanisms 1, 2, and 3) result in neck coarsening without densification.

(ii) Densifying mechanisms include grain boundary diffusion, in which (atoms diffuse along through grain boundaries), lattice diffusion from grain boundary (atom from grain boundary spreads through lattices), and plastic flow (dislocation triggers the flow of matter). These mechanisms (4, 5, and 6), can lead to neck growth, densification, and plastic flow through dislocation motion [83].

### *4.1.2 Fabrication of $UO_2$ and $UO_2$-Mo composites by SPS*

The $UO_2$-Mo powder was sintered in an argon atmosphere using LLC 10-3 spark plasma sintering (SPS) equipment manufactured by the Thermal Technologies system at the University of British Columbia (Kelowna, BC) Canada. The powder was incorporated into the graphite die with an internal diameter of 12 mm to 12.7 mm. A thin graphite foil (0.125 mm) was used at tooling powder interfaces to prevent friction and reaction between $UO_2$-Mo and tooling. The die was spread inside an analytical balance before filling up the powder. Once the powder-filled up, the punch incorporated into the graphite die. A grafoil disk was placed between the powder and the punch of the system. The die was then placed in the SPS chamber with a carbon sleeve. The carbon sleeve is utilized to decrease radiation heat loss at high temperatures.

Once the entire die assembly was inside the chamber, then the Argon and sintering procedure was started. An optical pyrometer monitored the temperature during the experiment. The temperature, chamber pressure, voltage, and current were observed as a function of time. The temperature of the $UO_2$ pellets was in the range of 1000 ºC to 1300 ºC. Whereas $UO_2$- Mo-10 vol% composite fuel pellets were prepared at a temperature range from 1300 ºC to 1800 ºC at heating and cooling rate of 50 ºC/min, 75 ºC/min, 100 ºC/min, and 125 ºC/min. The sintering pressure was in a range of 60 MPa and a continuous holding time of 0.5 min. After the sintering process, the pellets grounded using 500-grid sandpaper to remove the graphite foil for further characterization.

### *4.1.3 Microstructural features*

The microstructural analysis of $UO_2$-10vol% Mo powder and pellets was carried out to study the impact of Mo particle size on the development of homogeneous pellets and the evaluation of the porosity. The porous samples are expected to have lower thermal conductivity than high-dense pellets, and therefore, high-density composite fuel pellets are desirable in the fabrication of enhanced thermal conductivity fuel pellets. Yeo *et al.* [25] achieved the higher thermal conductivity of the composite pellets containing small SiC particles than the large-diameter SiC particles in the $UO_2$ matrix. In contrast, microstructural defects such as micro-cracks in nuclear fuel could be a significant problem in releasing fission gasses during the nuclear reactor operation. The 15% production of inert gases such as Helium ($_2$He), Krypton ($_{36}$Kr), and Xenon ($_{54}$Xe) are the constituents of the Uranium fission process [86]. These gas atoms form bubbles in the nuclear fuel and release from the fuel when they reach any open porosity connected to the free volume.

The micro-cracks create open porosities, and a large amount of fission gas can be release through micro-cracks. Once the gas release to free space in the fuel pin, the pressure inside the fuel pin increases to a higher degree and this can contribute to cladding rupture and reduce the safety margin. However, the micro-cracking and interfacial debonding exist in many sintered composites and are a consequence of different coefficients of thermal expansion (CTE) of the matrix and the particles [87–91]. Lu *et al.* [89] observed the thermal cracking in several intermetallic composites and noted that an optimum particle size exists at which the micro-cracking is suppressed. The larger particle size induces higher compressive stress due to the lower surface-area-to-volume ratio [87]. Moreover, researchers such as Todd *et al.* [87] and Watts *et al.* [92] investigated how micro-cracks reduced the strength, modulus, and hardness of the composites. Subsequently, these thermal cracks and the interfacial debonding in composite fuel pellets create abstracts in the pathway for heat conduction. The extensive cracking and poor interfacial contact could lead to lower thermal conductivity.

## 4.2 Methodology

### *4.2.1 Starting powder*

The powders of $UO_2$ and Mo were milled in a high energy planetary ball mill (Torrey Hills-ND2L) containing stainless steel (285 ml capacity) cups with a ball to powder ratio of 8:1 for 2 hours, and the milling speed was maintained at 200 revolutions per minute (RPM). Isopropanol was used as the process control agent (PCA), and the six wt% of it has assorted with $UO_2$-Mo powder before milling. These powders were then characterized by the x-ray diffraction (XRD), and energy dispersive spectroscopy (EDS) and revealed a secondary phase in the matrix material ($UO_2$). The SEM micrograph of the $UO_2$-Mo powder provided in Figure 4.2 indicates that the Mo particle has a spherical shaped morphology, and the size has ranged between 5µm to 150µm, respectively. The grain size, texture, and grain boundary characters were analyzed using Hitachi SU6600 high-resolution electron backscatter diffraction (EBSD). The pellets were polished to mirror finish by grinding them with silicon carbide papers starting with 46 µm and gradually going down to 5 µm. After cleansing with the SiC papers, the pellets were polished using 3 µm MD mol cloth with 3 µm MD Mol suspension and also using 1 µm MD Nap cloth with 1 µm MD Nap suspension. The microstructural studies on the cleaned samples were carried out using a scanning electron microscope (SEM) and electron backscatter diffraction (EBSD).

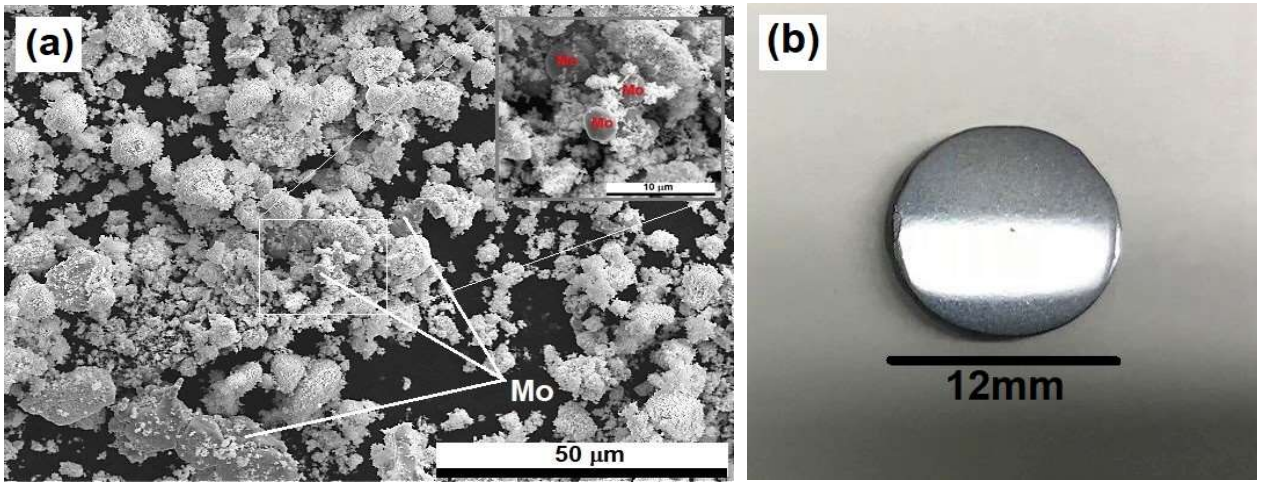


Figure 4.2: (a) SEM micrograph of the $UO_2$-Mo powder, (b) SPS sintered $UO_2$-Mo (98%) pellet of diameter 12 mm × 3 mm thickness. Sintering was done at 1800 $^oC$ 60 MPa pressure and 0.5 min.

## 4.3 Results and discussion

### *4.3.1 Elemental distribution of $UO_2$-Mo composite by EDS*

The homogeneous distribution of Mo particles in the $UO_2$ matrix is observed using energy dispersive spectroscopy (EDS) shown in Figure 4.3. To understand the influence of Mo particle size and distribution of the second phase particles in the $UO_2$-10vol% Mo composite, evaluated the composite with constant milling conditions and volume percentage. The 10vol% of different Mo (micro and nanoparticles) of 150 μm, 100 nm, 60-80 nm, 35-45 nm was incorporated in the $UO_2$ using planetary ball milling. The effect of the ball-to-powder ratio (BPR) and the milling time was optimized. After milling at different BPR and various time intervals, it was noted that BPR 8:1 (eight times balls and the one-time powder mass) for 2hrs shown a good distribution without any contamination. And the milling speed was maintained at 200 revolutions per minute (RPM).

The pictures of composites obtained with different diameters of Mo particles are shown in Figure 4.3 (a-d). The uniformity of Mo distribution in $UO_2$ was observed for particles of different size 35-45 nm, 60-80 nm, 100 nm, as shown in Figure 4.3 (a, b, c), respectively. The more homogeneous distribution of small Mo particles was related to lower compressive stress due to the higher surface-area-to-volume ratio of the smaller particles. The homogeneous distribution of Mo particles influences morphology, by minimizing the porosity and reduces the visible micro-cracks in the sintered pellets as shown in Figure 4.4. Therefore, microstructural defects such as micro-cracks in fuel can be a significant problem in releasing fission gasses during the nuclear reactor operation. Micro-cracks create open porosities, and a large amount of fission gas can be release through micro-cracks. Also, non-homogeneous large size Mo particles support the hypothesis that micro-cracking and interfacial debonding is responsible for the reduction in thermal conductivity of $UO_2$-Mo composite. In Figure 4.5, the 150 μm Mo particle composite has the most severe micro-cracks, and the large interfacial debonding can result in reduced thermal conductivity.

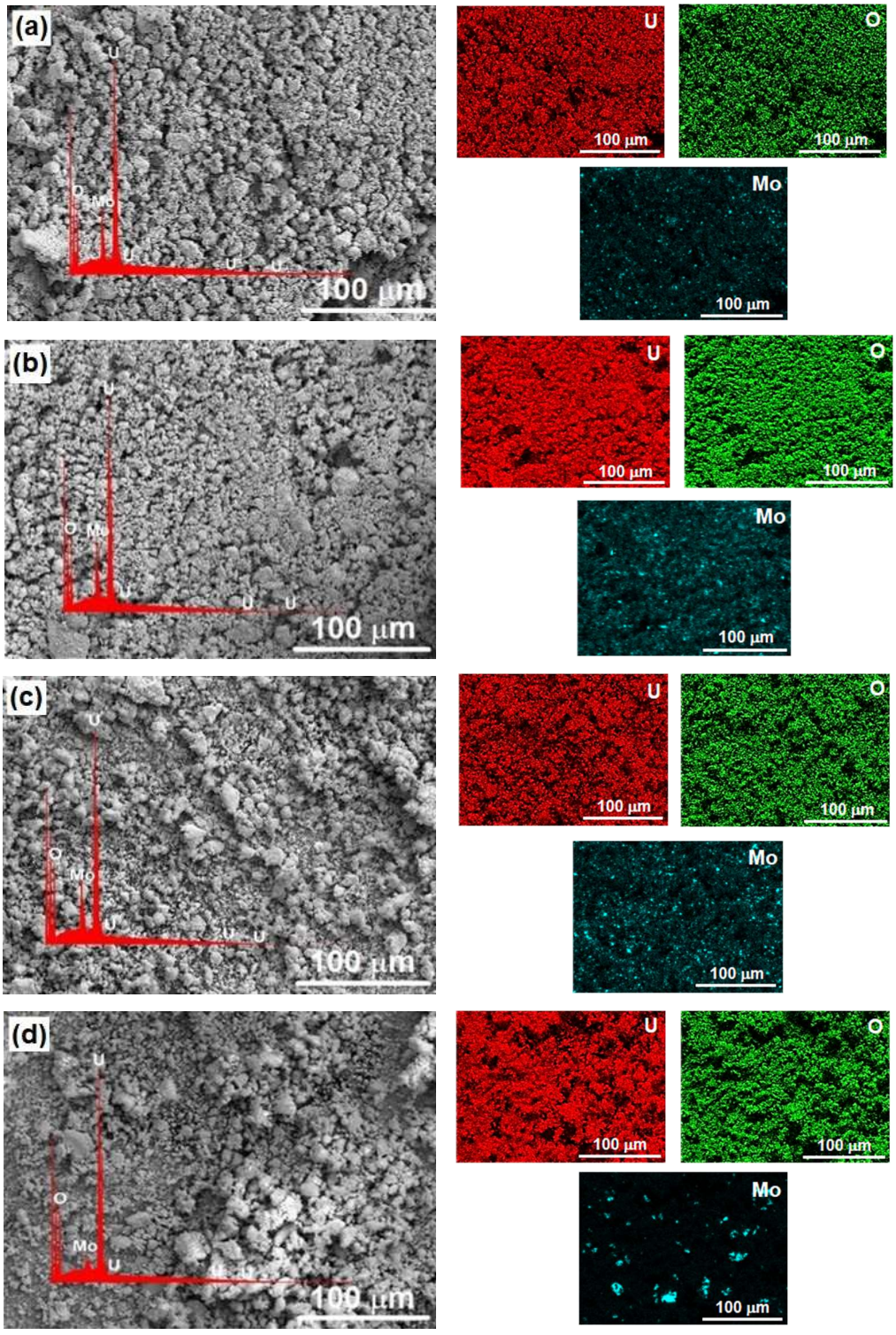


Figure 4.3: Elemental distribution of $UO_2$-Mo composite. EDS spectrum and elemental mapping of $UO_2$-10vol% Mo composite with various diameters of Mo particle. (a) 35-45 nm. (b) 60-80 nm. (c) 100 nm. (d) 150 µm. Note the homogeneous distribution of Mo in the $UO_2$ matrix identified in small size Mo particles in a, b, c.

### *4.3.2 Size effect of Mo particles on $UO_2$-Mo composite by SEM*

The SEM was used to analyze the micro-morphologies of the $UO_2$-10vol% Mo composite sintered pellets containing the different sizes of Mo particles, namely 35-45 nm, 60-80 nm, 100 nm, and 150 µm. All the other conditions were kept constant during the sintering process. Figure 4.4 shows the microstructures of these composites, where the Mo particles appear black, and the brighter area indicates the $UO_2$ matrix. The Mo particles seemed to be homogeneously distributed in the composites as shown in Figure 4.4 (a-c). However, as shown in Figure 4.4 (d), the composite containing 150 µm Mo particles, have distinct radial micro-cracks observed at the interface between a Mo particle and $UO_2$ matrix.

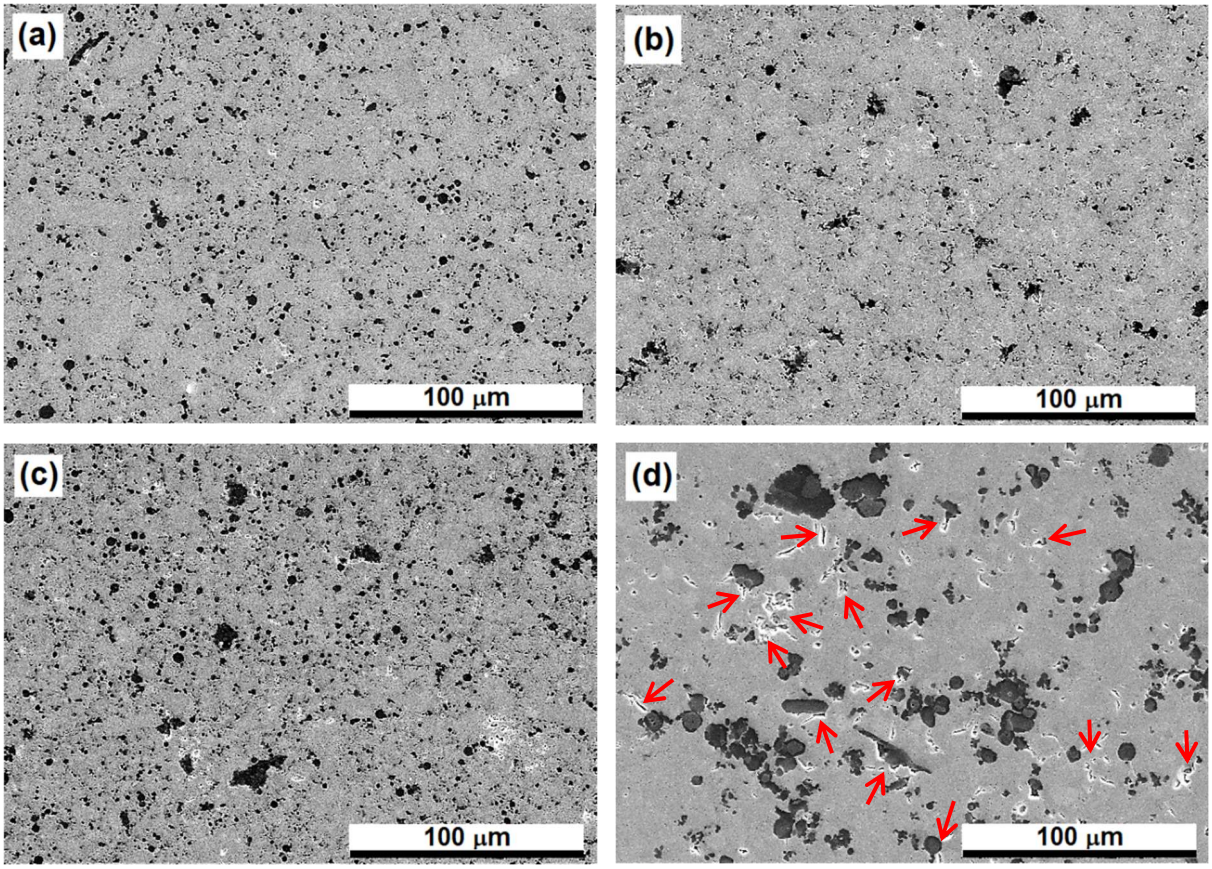


Figure 4.4: Microstructure of $UO_2$-10vol% Mo composite pellets containing various diameter of Mo particle. (a) 35-45 nm. (b) 60-80 nm. (c) 100 nm. (d) 150 µm. Note micro-cracks are originating from large size Mo particles in d.

The interfaces between the $UO_2$ matrix and Mo particles in $UO_2$-10vol% Mo composite pellets with different sized Mo are shown in Figure 4.5. The micro-cracks originating from the large-size Mo particles are presented in Figure 4.5 (d), indicating that micro-cracking is less severe in composite with Mo particles of size 35-45 nm, 60-80 nm, and 100 nm compared to the composite containing 150 µm size Mo particles. There were no visible cracks in the microstructure in the composite pellets containing smaller size Mo particles. It is also understood that with increasing particle size, there is a more significant separation between the Mo particle and the $UO_2$ matrix. Figure 4.5 (d) shows the interfacial debonding between $UO_2$ and Mo particles. These results support the hypothesis that micro-cracking and interfacial debonding is responsible for the reduction in thermal conductivity of $UO_2$-Mo composite containing large size Mo particles. The 150 µm Mo particle composite has the most severe micro-cracks, and the large interfacial debonding can result in reduced thermal conductivity.

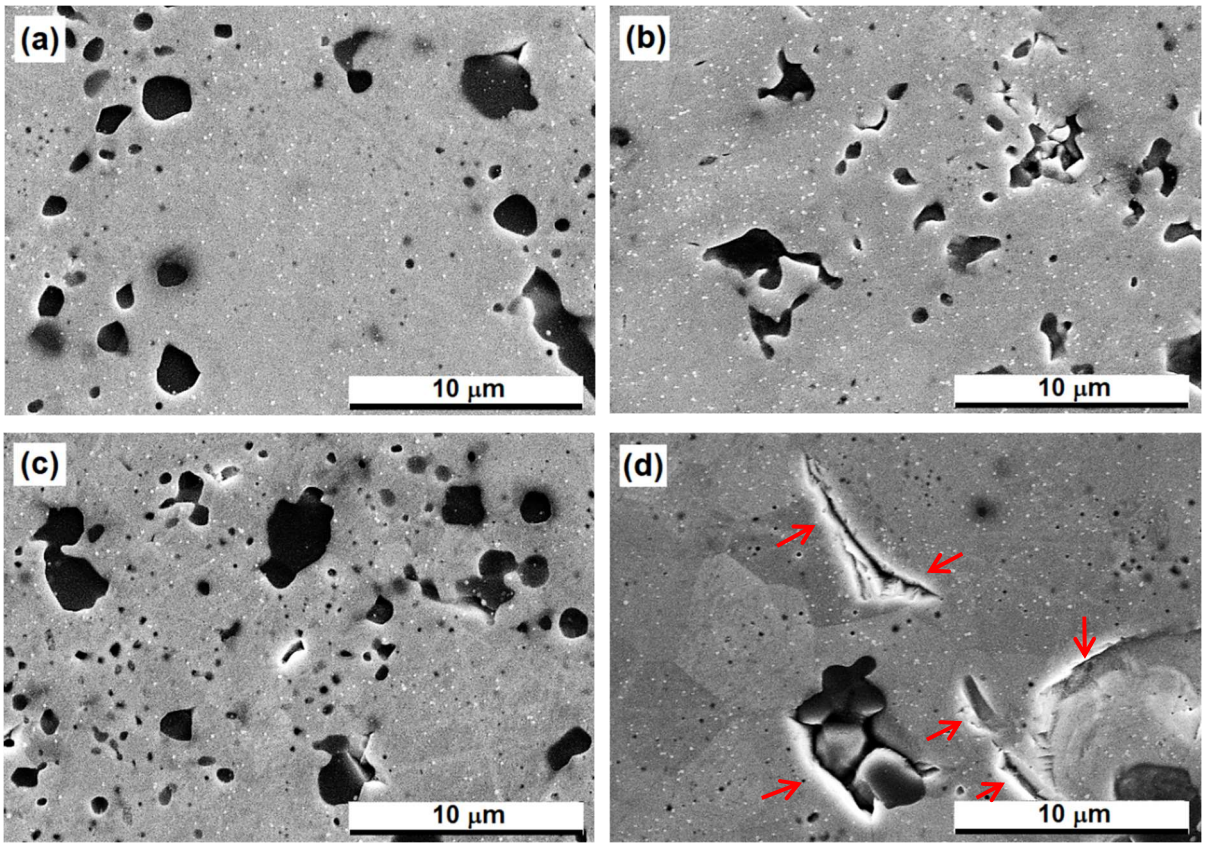


Figure 4.5: Mo particles in $UO_2$-10vol% Mo composite pellets with various mean diameters. (a) 35-45 nm. (b) 60-80 nm. (c) 100 nm. (d) 150 µm. Arrows identify the micro-cracks in the matrix and between Mo particles.

### *4.3.3 Grain size, texture, and grain boundary characters from EBSD*

#### *4.3.3.1 Grain size*

An EBSD analysis represents the grain boundary characteristic features of $UO_2$-Mo composite pellets compared to those of $UO_2$ pellets. Previous studies on $UO_2$ have shown that the fuel pellet's grain size plays an essential role in the fission gas release and swelling [25,93]. The grain size also influences the creep; for instance, when the stress is lower than the threshold stress, the creep rate is inversely proportional to the square of grain size [94]. Since grain size plays a significant role in the fuel's performance, it is essential to have control over the grain size of the composite fuel pellets. The analysis of an EBSD allows the creation of orientation maps that visually and quantitatively represents the grain size of the sintered pellets. Orientation maps also illustrate the microstructural differences in a sintered structure like the porosity and the preferred orientation of the grains.

The mechanism of grain growth was mainly affected by the sintering temperature. Figure 4.6 (a) represents the SPS $UO_2$ pellet at 1300 ºC sintering temperature having an approximate grain size of 5.5 µm. Whereas, Figure 4.6 (b, c, d) shows the orientation maps for the SPS $UO_2$-Mo composite as a function of sintering temperature from 1300, 1500, and 1800 °C with an average grain size of 0.9 µm, 2.4 µm, and 5.6 µm processed with an applied constant pressure of 60 MPa, constant heating and cooling rate 100 ºC/min and a constant hold time of 0.5 min. It seems that $UO_2$ without any additives has the largest grain size. The grain size was reduced after molybdenum's addition because the insoluble second-phase particles were dispersed randomly in the polycrystalline solid. Therefore, the grain boundary movement during sintering was pinned by the particles, and as a result, the grain size in the matrix decreased. The $UO_2$-Mo pellets have 84% smaller grains than that of the $UO_2$ pellets as shown in Figure 4.6 (b).

Consequently, a comparable grain size of $UO_2$ and $UO_2$-Mo was observed at 1300 and 1800 ºC sintering temperature. This outcome is because the addition of Mo decreases the grain size of $UO_2$ pellets. Therefore, the higher the amount volume of secondary phase particles the more important the pinning effect, which leads to the smaller grain size. However, the sintering temperature can be increased in the $UO_2$-Mo composite pellets to obtain the grain size comparable with that in the $UO_2$ pellets.

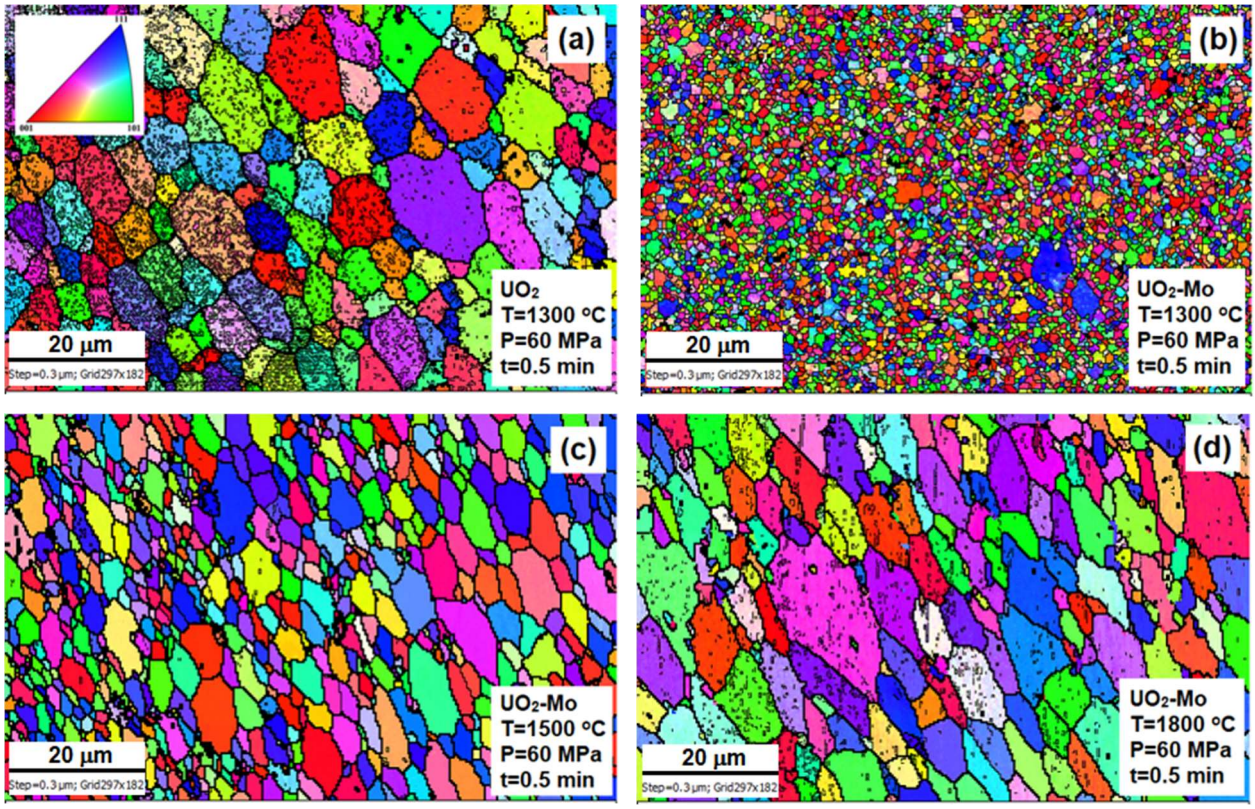


Figure 4.6: (a) EBSD maps of $UO_2$ at 1300 ºC sintering temperature with an average grain size of (5.5 µm), (b) $UO_2$-Mo at 1300 ºC sintering temperature with an average grain size of (0.9 µm), (c) $UO_2$-Mo at 1500 ºC sintering temperature with an average grain size of size (2.4 µm) (d) $UO_2$-Mo at 1800 ºC sintering temperature with an average grain size of (5.6 µm).

### *4.3.3.2 Texture (Inverse pole figures)*

On the micro-texture of the specimens, Figure 4.7 presents the comparison of the inverse pole figure (IPF) triangle of three $UO_2$-Mo samples sintered at 1300 ºC, 1500 ºC, and 1800 ºC. In IPF, the distinct colors represent each grain's crystallographic orientation in such a way that the normal vector of the grain is parallel to the normal direction (ND) of the specimen. For example, the blue color grains correspond to <111>//ND, the green color grains correspond to <011>//ND, and the red color grains have <001>//ND orientation. The results demonstrate that the grain growth activated in SPS occurred with preferential crystallographic orientation, i.e., in $UO_2$-Mo composite with and without grain growth, a preferred orientation is observed. The critical feature to be noted, as the SPS method, creates a steady current flow since the top and bottom of the sample could lead to abnormally oriented grain growth.

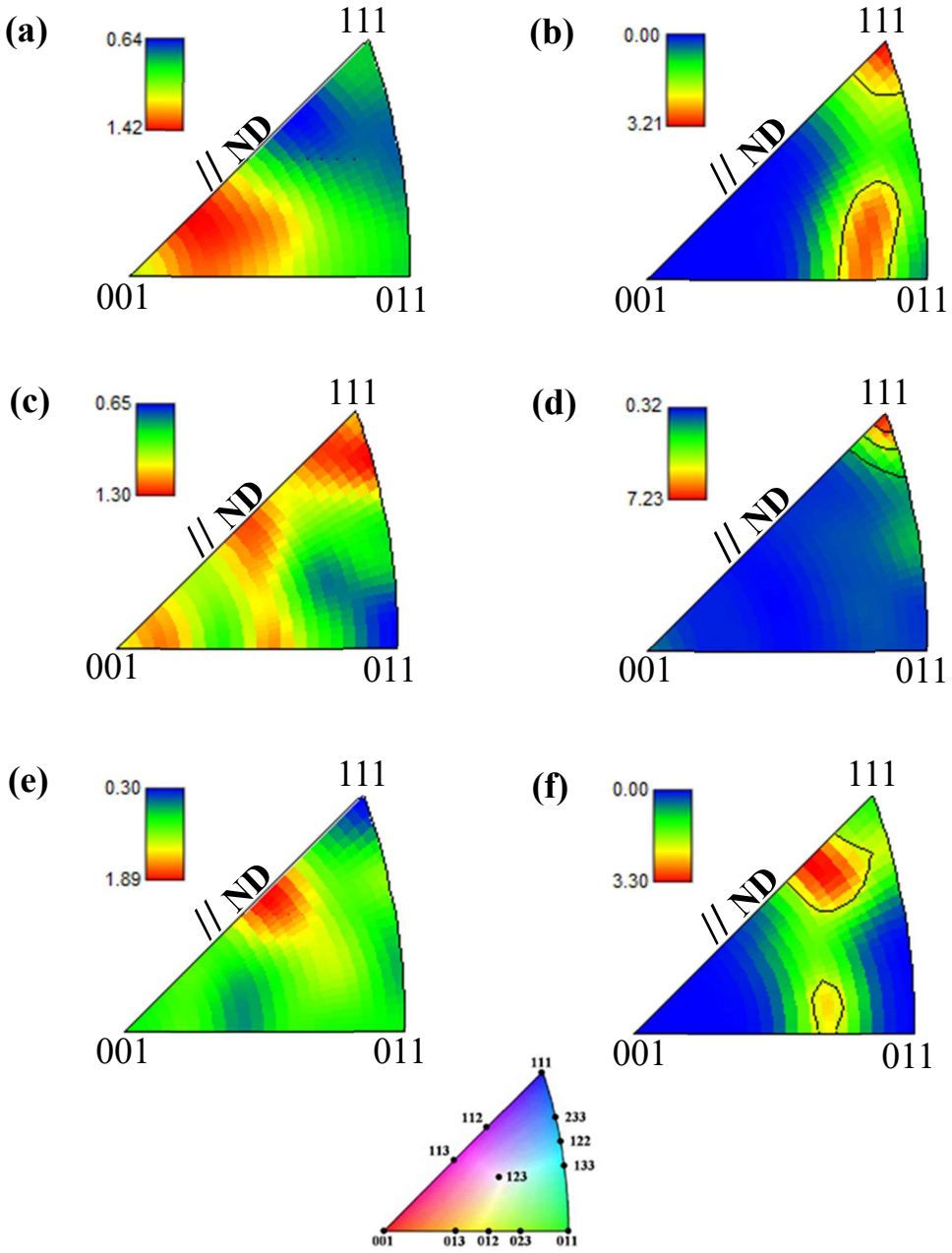


Figure 4.7: Inverse pole figure of $UO_2$-Mo composite pellets with various sintering temperatures. (a,b) 1300 ºC. (c-d) 1500 ºC. (e,f) 1800 ºC. Similarly, (a,c,e) shows the $UO_2$ phase, and (b,d,f) shows the Mo phase in the composite. Constantly applied pressure 60 MPa and a constant sintering time of 0.5 min.

The texture of $UO_2$ is rather weak oriented near <001>//ND at sintering temperature 1300 ºC and moving to <111>//ND during the sintering process at 1500 ºC. Similarly, at 1800 ºC, the crystallographic orientation of the grains deviates from <111>//ND towards <112>//ND. This behavior could be attributed to the increased sintering temperature shown in Figure 4.7 (a, c, e). The texture of Mo is stronger and is oriented near <111>//ND with a significant spread near <011>//ND during the sintering process at 1300 ºC shown in Figure 4.7 (b). At 1500 ºC there is a strong <111>//ND texture and according to the previous studies (111) texture played a significant role in enhancing the interfacial exchange energy [95] and the oxidation resistance of grains found to increase in the order of (001) < (011) < (111) [94]. Since different textures were observed, this demonstrates that the SPS sintering is a powerful tool for producing $UO_2$-Mo composite pellets with a wide array of microstructural features.

#### *4.3.3.3 Grain boundary character distribution (GBCD)*

The grain boundaries' misorientation angle analyzed for the $UO_2$-Mo samples sintered at 1300 ºC, 1500 ºC, and 1800 ºC is shown in Figure 4.8. The misorientation angles are represented as a function of sintering temperature by having a constant pressure of 60 MPa and a constant sintering time of 0.5 min. Nerikar et *al.* [96] studied the structural properties of numerous symmetrical tilt boundaries with misorientation angles ranging from 12.7º to 61.9º. They noted that the lower misorientation angles consist of edge dislocations. Whereas, for higher misorientation angles, Schottky defects (point defects in a crystal lattice) were dominant in the grain boundary structure [96].

However, for the high angle misorientation greater than 15º during the deformation; the density of dislocation will increase and the spacing between neighboring dislocations decreases; ultimately, the dislocation's cores will start to overlap and the ordered nature of the boundary will break down. Our experiments revealed that there are very few relative frequencies of high-angle boundaries in the specimens sintered at 1300 ºC, 1500 ºC, and 1800 ºC temperatures, as shown in Figure 4.8. This result reveals that SPS is, so far, the very flexible method for manufacturing the $UO_2$-Mo composite, which can produce high density of the composite.

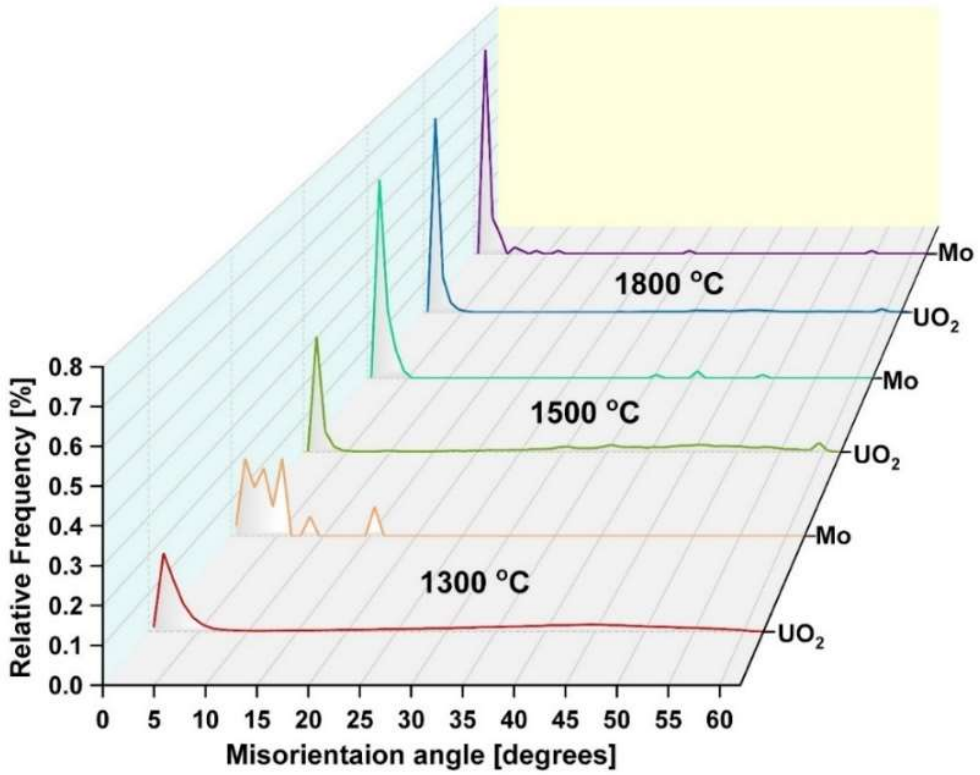


Figure 4.8: Grain boundary character distribution (GBCD) of the $UO_2$-Mo pellets sintered at 1300 $^oC$, 1500 $^oC$, and 1800 $^oC$ sintering temperature at a consistently applied pressure 60 MPa and a constant sintering time of 0.5 min.

#### *4.3.3.4 Coincidence site lattice (CSL) type boundary*

The presence of special/coincidence-site lattice (CSL) boundaries of $UO_2$ and $UO_2$-Mo pellet sintered at 1300 $^oC$ and 1800 $^oC$ sintering temperature with similar grain size is shown in Figure 4.9 (a, b) and the CSL boundaries versus frequency of the $UO_2$ and $UO_2$-Mo composite as shown in Figure 4.9 (c). Based on the misorientation angle of the adjoining grains, the grain boundaries are considered as low-angle grain boundaries (LAGBs), high-angle (random) grain boundaries (HAGBs), and special/coincident-site lattice (CSL) GBs [97,98]. The different CSLs can be classified by Σ value, which represents the inverse of common lattice points in the boundaries that are formed between the two adjoining grains. Previous investigations have shown that low Σ CSL GBs, e.g., Σ3, exhibited higher resistance to numerous types of intergranular degradation than HAGBs [99].

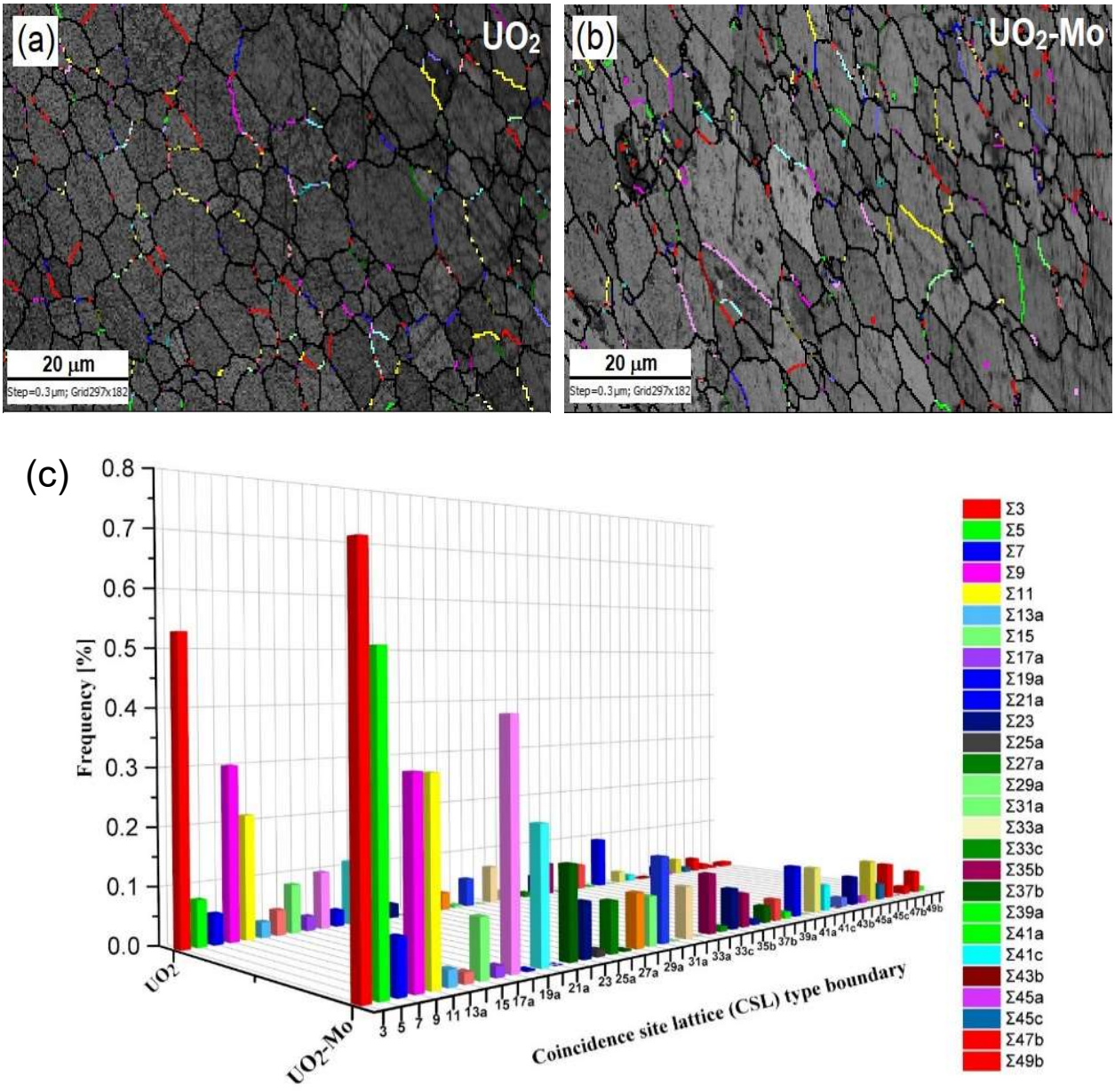


Figure 4.9: EBSD map (a, b) band contrast with coincidence site lattice (CSL) boundaries. (c) CSL boundaries versus frequency of the $UO_2$ and $UO_2$-Mo at similar grain sizes.

However, the high concentration of CSL GBs enhances the properties of the materials. In several aspects, such as lower rates of grain boundary sliding during creep [100,101]. Resistance to solute segregation, precipitation, and intergranular embrittlement [102]. Resistance to high-temperature fracture [103], weldability [104], resistance to intergranular corrosion [105], resistance to corrosion and stress corrosion [102,106,107], and resistance to radiation damage [101,108]. The low Σ boundaries of Σ3, Σ5, and Σ9 GBs shown in red, green, and pink colors. This result indicates that the $UO_2$-Mo composite pellet can produce the significant frequency of the special/coincident-site lattice (CSL) GBs compared to the $UO_2$ pellet.

### 4.4 Summary

$UO_2$-Mo 10vol% composites were fabricated using the SPS technique without any sintering aid such as magnesium oxide (MgO) and Dinitrogen pentoxide ($N_2O_5$). A systematic analysis of the influence of sintering parameters microstructure, grain size, texture, grain boundary features of the $UO_2$-Mo pellets has been presented. It was noted that by varying the Mo particle size, it is possible to tune the microstructural characteristics of $UO_2$-Mo composite fuel. EBSD studies demonstrated that higher sintering temperatures result in larger grain size. By optimizing the sintering parameters, the grain size and texture of the sintered pellets can be controlled. The orientation maps demonstrated that <111> texturing was observed in the pellets sintered at 1500 $^oC$. Our combined experimental investigations suggest that $UO_2$-Mo composite pellets exhibited favorable microstructural features compared to the $UO_2$ pellet.

# CHAPTER 5

# DENSIFICATION AND STRUCTURAL ANALYSIS OF $UO_2$ AND $UO_2$-Mo COMPOSITES

## 5.1 Brief introduction

The X-ray diffraction (XRD) analysis of the uranium dioxide ($UO_2$)-10 vol% Molybdenum (Mo) powder composites and sintered pellets was presented. Demonstrating that there is no formation of any intermetallic products between the two phases during the SPS sintering at temperatures from 1300 $^oC$ to 1800 $^oC$. Both Mo micro and nanoparticles were utilized. An evaluation of the influence of processing conditions on the densification of the $UO_2$-Mo is presented. The results reveal that without any sintering aid, pellets with a density of ~97% theoretical density (TD) can be obtained at a low sintering temperature of 1300 $^oC$, and applied pressure 60 MPa, heating and cooling rate 125 $^oC$/min, and a holding time of 0.5 min. The density of the pellet plays a vital role in the performance of nuclear fuel. The nuclear fuel with the desired density is expected to accommodate fission gas release and avoid possible in-reactor shrinkage [109]. In this analysis, the effect of processing conditions such as sintering temperature, holding time, and heating and cooling time on the density of pellets was presented. The relative density of $UO_2$ and $UO_2$-10 vol% Mo pellets as a function of sintering temperature was measured. The pellet's density increased from 94 - 99 %TD with the change of sintering temperature ranging from 1300–1800 $^oC$. The results revealed that the choice of sintering temperature had a significant influence on the $UO_2$-Mo composite pellet's final density.

## 5.2 Methodology

The sintered specimens were polished to eliminate the residual graphite foil for further experimental procedures such as X-ray Diffraction (XRD). The Archimedes' principle (Torbal density measurement kit) is used to determine each pellet's density. The three readings were recorded for each pellet, and an average with the error bar was plotted. The density measurement was calculated by the Archimedes principle [81]since the unknown densities can be calculated by measuring the mass in air and weight in water, as shown in the equation (3.2).

## 5.3 Results and discussion

### *5.3.1 Structural characterization using X-ray diffraction (XRD)*

Figure 5.1 compares the XRD patterns of the planetary ball milled $UO_2$-10vol% Mo powder, and the SPS sintered pellets of $UO_2$-10vol% Mo sintered at 1300 ºC to 1800 ºC. The XRD peaks of the powder and sintered pellets presented here were indexed based on the crystallographic data from the joint committee on powder diffraction standards (JCPDS) database [110]. The XRD analysis of the $UO_2$-Mo composites carried out using the Cr $K_\alpha$ radiation (lambda=2.291) with a Bragg Brentano geometry; we adopted the following conditions: voltage 40 kV, 40 mA, angle (2θ) ranging from 20 to 110º, mode step, sample oscillation XY plane with an amplitude of 2mm. The XRD results illustrate that the peaks at 42º, 49º, 73º, 88º, and 94º respectively correspond to the crystallographic planes of (111), (200), (220), (311), and (222) of the $UO_2$. The peak at 62º represents the (110) plane of Mo. In the $UO_2$-Mo composite pellets, detected the (110) peak shifted towards the right due to the high sintering temperature, which corresponds to a change of the crystallinity of the material. The resultant peak shifts are in good agreement with the sintered diffraction patterns by Pikalova *et al.* [111] and Ahmad *et al.* [112]. The XRD result in Figure 5.1 of the $UO_2$-10vol% Mo composites, indicates that there is no formation of any by-products or intermetallics during the whole process.

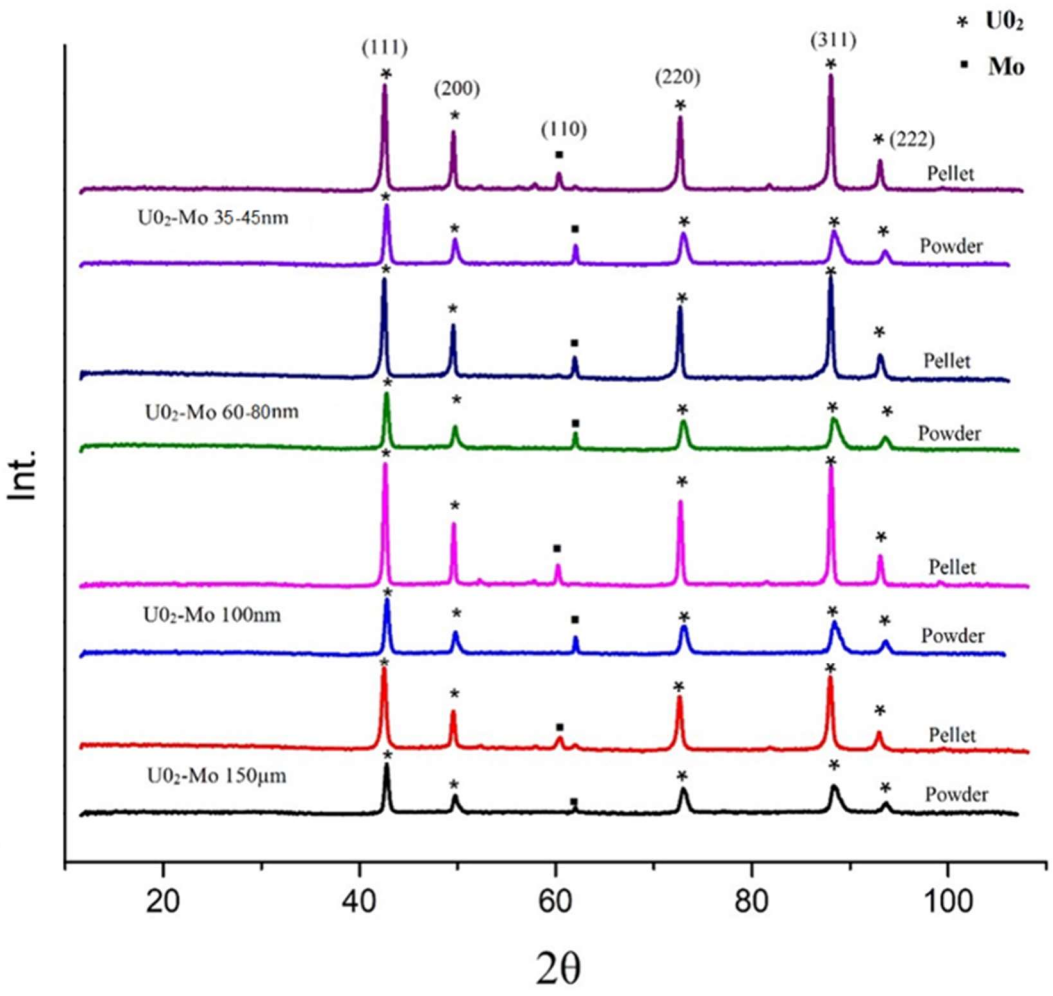


Figure 5.1: X-ray diffraction (XRD) patterns of the powder and sintered $UO_2$-10vol% Mo composite pellets containing various diameters of Mo particle such as 35-45 nm, 60-80 nm, 100 nm, and 150 μm.

### *5.3.2 Density of the fabricated composites*

The density of nuclear pellets plays a significant role in the performance of nuclear fuel. The desired density of the nuclear fuel pellet not only accommodates the fission gas release but also should not cause any in reactor shrinkage of fuel that can occur with low-density fuel [109]. Therefore, having control over the density of the fuel pellet is very important. Thus, various sintering processing conditions on the density of the fuel pellets were analyzed by the Archimedes immersion method.

Table 5.1 shows the complete results of the density measurement of the sintered $UO_2$ and $UO_2$-10vol% Mo composite pellets containing various diameters of Mo particle such as 35-45 nm, 60-80 nm, 100 nm, and 150 μm. In this evaluation, the effect of processing conditions such as sintering temperature, heating, and cooling rate on the pellet densification was evaluated. Figure 5.2 (a) shows the relative density of $UO_2$-10 vol% Mo pellets as a function of sintering temperature. The peak of sintering temperature was varied between 1300 end 1800 ºC keeping all the other sintering conditions constant. The densification of sintered pellets was improved with the increase in the sintering temperature. The results reveal that the choice of sintering temperature had a significant effect on the final density of the pellet. Therefore, rising the sintering temperature from 1300 to 1500 ºC resulted in average density rising from 94% TD to 98% TD. Increasing the sintering temperature further to 1800 ºC resulted in an average density ~98% TD did not cause any considerable difference in the densification, indicating that the maximum compaction of $UO_2$-Mo occurs at a temperature of 1500 ºC.

Therefore, the results revealed that the pellet of the desired density of ~97 %TD could be obtained at a low sintering temperature of 1300 ºC. With other processing parameters like a constant applied pressure 60 MPa, constant heating and cooling rate 125 ºC/min, and in a short time of 0.5 minutes. Under these conditions, a composite with sufficient porosity to accommodate the light-water reactor (LWR) burnup can be obtained. However, under higher testing temperatures the compaction of the pellets ~98% TD the complete closure of the porosity of $UO_2$-Mo pellets was observed. The results obtained from 1500 ºC to 1800 ºC sintering temperature with 100 ºC/min the heating and cooling rates at an applied continuous pressure 60 MPa and a constant holding time of 0.5 minutes are shown in Figure 5.2. Finally, the effect of heating and cooling rate ºC/min on the density of the sintered pellet was analyzed by changing the heating and cooling rate ºC/min between 50 ºC/min 75 ºC/min, 100 ºC/min keeping the sintering pressure at 60 MPa and holing time for 0.5 min. However, at 1800 ºC, further increasing of the heating and cooling rate of 125 ºC/min did not significantly change the density of the samples. Which is in good agreement with the composite of $UN/U_3Si_2$ analyzed by White *et al*. [113]. This demonstrates that a heating and cooling rate of 100 ºC/min is sufficient to get a pellet of $UO_2$-Mo with the desired density. Consequently, the density measurement clearly shows that using SPS we can lower the sintering temperature and the sintering time to 1300 ºC and 0.5 min.

| $UO_2$ and $UO_2$-Mo Composite pellets | Sintering Temperature (°C) | Holding time (min) | Heating rate (°C/min) | Density (%TD) |
|---|---|---|---|---|
| $UO_2$ | 1300 | 0.5 | 50 | 98 |
| $UO_2$ | 1300 | 0.5 | 75 | 99 |
| $UO_2$ | 1300 | 0.5 | 100 | 98 |
| $UO_2$ | 1000 | 5 | 100 | 94 |
| $UO_2$-Mo (150 μm) | 1800 | 0.5 | 50 | 96 |
| $UO_2$-Mo (150 μm) | 1800 | 0.5 | 75 | 97 |
| $UO_2$-Mo (150 μm) | 1800 | 0.5 | 100 | 98 |
| $UO_2$-Mo (150 μm) | 1300 | 0.5 | 125 | 97 |
| $UO_2$-Mo (150 μm) unmilled | 1500 | 0.5 | 50 | 95 |
| $UO_2$-Mo (150 μm) unmilled | 1500 | 0.5 | 75 | 96 |
| $UO_2$-Mo (150 μm) unmilled | 1500 | 0.5 | 100 | 95 |
| $UO_2$-Mo (150 μm) unmilled | 1300 | 5 | 100 | 95 |
| $UO_2$-Mo (100 nm) | 1800 | 0.5 | 50 | 94 |
| $UO_2$-Mo (100 nm) | 1800 | 0.5 | 75 | 89 |
| $UO_2$-Mo (100 nm) | 1800 | 0.5 | 100 | 93 |
| $UO_2$-Mo (100 nm) | 1500 | 5 | 100 | 98 |
| $UO_2$-Mo (60-80 nm) | 1500 | 0.5 | 50 | 96 |
| $UO_2$-Mo (60-80 nm) | 1500 | 0.5 | 75 | 95 |
| $UO_2$-Mo (60-80 nm) | 1500 | 0.5 | 100 | 94 |
| $UO_2$-Mo (60-80 nm) | 1300 | 0.5 | 100 | 96 |
| $UO_2$-Mo (35-45 nm) | 1500 | 0.5 | 50 | 94 |
| $UO_2$-Mo (35-45 nm) | 1500 | 0.5 | 75 | 96 |
| $UO_2$-Mo (35-45 nm) | 1500 | 0.5 | 100 | 98 |
| $UO_2$-Mo (35-45 nm) | 1800 | 0.5 | 100 | 98 |
| $UO_2$-Mo (35-45 nm) | 1300 | 5 | 100 | 96 |

Table 5.1: Density measurement of $UO_2$ and $UO_2$-Mo composite pellets.

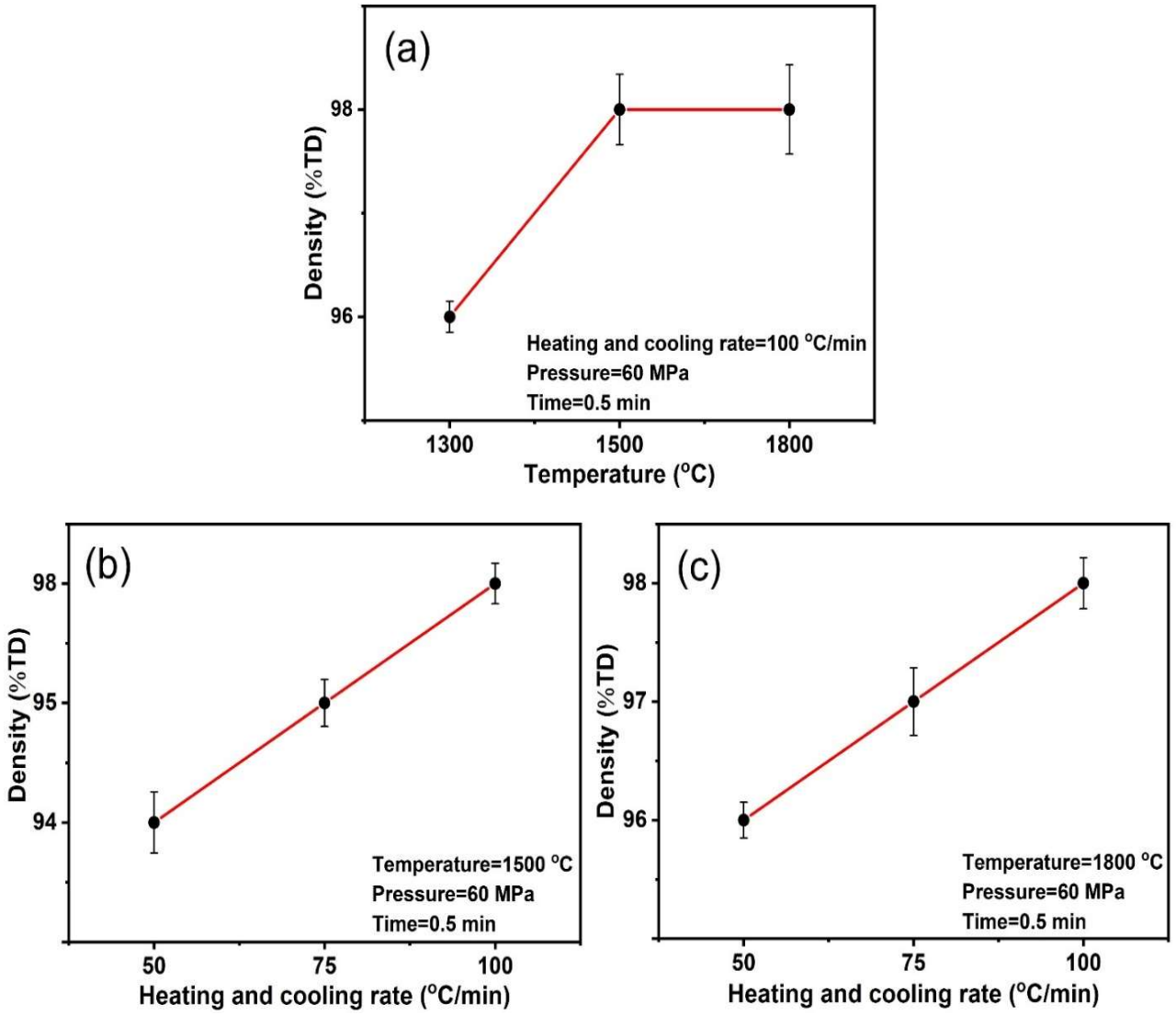


Figure 5.2: The influence of (a) sintering temperature (b) heating and cooling rate °C/min on the densification of the sintered pellets at an applied pressure 60 MPa and constant sintering time 0.5 minutes.

## 5.4 Summary

The densification process is an important stage in the composite fuel manufacturing cycle, however, it is difficult to obtain the dense fuel pellets using traditional sintering techniques. The conventional sintering of nuclear fuels required a maximum sintering temperature higher than 2000 $^{o}$C, and longer holding time, and needs the help of various sintering aid. Therefore, the $UO_2$-Mo composites produced by SPS revealed high-density pellets at a low sintering temperature in a short time without intermetallic products. The $UO_2$-Mo pellet with the desired density of ~97 %TD can be achieved at a temperature as low as 1300 $^{o}$C. An investigation of the influence of processing conditions on the $UO_2$ and $UO_2$-Mo composite pellets' density was explored. The range of sintering temperature, heating, and cooling rate ($^{o}$C/min) has been systematically varied from 1300-1800 $^{o}$C, 50-125 ($^{o}$C/min), respectively. Also, this work demonstrated that the densification of the $UO_2$-Mo composite fuel could be controlled by the choice of the processing parameters.

# CHAPTER 6

# THERMOPHYSICAL PROPERTIES OF $UO_2$ AND $UO_2$-Mo COMPOSITES

## 6.1 Brief introduction

The improvements in thermophysical properties of $UO_2$ has been an active area of exploration after the Fukushima disaster, the critical parameter in the reactor design and safety of $UO_2$ fuel is thermal conductivity that governs the transformation of heat produced from the fission to electricity [22]. In the $UO_2$ fuel, the thermal conductivity degrades with increases in temperature, which creates the risk of fuel melting. The composite fuel research is focused on improving the thermophysical properties of $UO_2$, with special additions to improve the thermal conductivity [3,28,30,114]. In composite fuels, the excellent thermal properties, control of fissile material density, good irradiation performance, and superior mechanical properties are possible depending on the concentration of metal added [31,33].

The Molybdenum (Mo) was considered a primary candidate due to its high thermal conductivity, high melting, high boiling point, and low thermal neutron absorption cross-section [35]. In this case, thermal energy is conducted through a percolation pathway; the thermal energy must pass through high thermal conductivity secondary particles and lower thermal conductivity $UO_2$ matrix. Forming a higher heat conducting percolation pathway allows conducting the heat more efficiently [25]. To obtain the desired properties of the composites, it is also essential to ensure that the pellets have a uniform distribution of heat-conducting materials and high densification. To achieve high density and uniform distribution, the choice of synthesis route is important. Previously, Kim *et al.* [35] attempted to produce $UO_2$-Mo micro-cell pellets through conventional sintering. These studies have shown the common conventional sintering to produce $UO_2$-Mo micro-cell pellets. The sintering by the traditional methods still has limitations such as long processing time and difficulties in the production of the dense and high thermal conductivity $UO_2$-Mo pellets.

In this study, we employed the spark plasma sintering (SPS) method to fabricate $UO_2$-Mo composite fuels containing homogeneously dispersed high thermal conducting Mo particles. Several studies have been pursued by many researchers on non-conventional sintering methods such as microwave sintering [36], inductive hot pressing [115], pressureless induction heating [116], and spark plasma sintering (SPS) [117]. Among these sintering methods, SPS has become

the most significant technique for powder consolidation. Ge *et al.* [117] studied the influence of SPS process parameters on the density, microstructure, grain size, and thermal conductivity of $UO_2$. The possibility of SPS sintering for the production of commercial-grade nuclear fuel pellets has been illustrated by Timothy *et al.* [118], but further developments in the die-design configurations and tooling materials are necessary for the large-scale fabrication. Previous studies [119,120] pursued to overcome these limitations. For instance, Papynov *et al.* [119] illustrated the use of the non-standard molybdenum die instead of ordinary graphite die for the fabrication of highly dense $UO_2$ pellets of the necessary quality. Moreover, researchers such as Balice *et al.* [121], Saoudi *et al.* [122], Scott *et al.* [123], and Muta *et al.* [124,125] have prepared the mixed oxides pellets using the SPS route. Further, SPS can sinter the pellets with high density, and by processing conditions, the desired grain size could be controlled without the help of any sintering aid [126]. Therefore, an in-depth investigation of the effect of sintering temperatures and densities of the thermal conductivity of $UO_2$-Mo composite is measured by considering $UO_2$ as a control. However, the high thermal conductivity pellet reduces the fuel temperature during the regular operation, decreases the mobility of the fission gases and short-term accidents [35]. Enhanced thermal conductivity fuel is a highly practical aspect of fuel safety [35,127]. Similarly, our systematic investigations suggest that the $UO_2$-Mo composite pellets showed an enhanced thermal conductivity compared to that of the $UO_2$ pellet.

### 6.2 Methodology

The thermal diffusivity measurements of the pellets carried out using the laser flash technique (TA instruments-DLF-1/EM-1300). In this work, the sintered pellets' density and thickness were measured and remained constant during the whole procedure. The specimens used in this study were disc-shaped and diameters about 12 mm to 12.7 mm in diameter and the thickness in the range of 2 mm to 3 mm. The pellet thickness was evaluated by averaging six values calculated using a calibrated micrometer. Hence, the standard deviation of the average thickness was less than 0.02 mm. The specimen is coated with the graphite spray for better absorption and emissivity of the laser pulse. The measurements were conducted in the argon atmosphere starting from room temperature to 900 $^{o}$C.

### 6.3 Results and discussion

The thermal diffusivity (α), specific heat capacity ($C_p$), and the thermal conductivity (λ) measurement of $UO_2$ and $UO_2$-Mo sintered at different sintering conditions showed in Figure 6.1. The measurements are conducted three times at each temperature, and an average value plotted from room temperature to 900 ºC. The average thermal conductivity values of $UO_2$ are in good agreement with the literature [25,128]. The $UO_2$-Mo composite pellets were considered on three different samples sintered at 1300 ºC, 1500 ºC, and 1800 ºC, respectively, and the measured values of various densities shown in the plot. The $UO_2$-Mo composite fuel pellets have enhanced thermal conductivity than $UO_2$ pellets. Noticeably, the higher the sintering temperature, the higher the measured thermal conductivity. A maximum thermal conductivity improvement was observed in $UO_2$-Mo composite at 1800 ºC, and the increases are 65.7%, 83.4%, 97.2% at 100 ºC, 500 ºC, and 900 ºC, respectively, compared to the $UO_2$ value. The $UO_2$-Mo composite pellets show a similar tendency to $UO_2$, a gradual reduction in conductivity with an increase in temperature. This trend in thermal conductivity measurement is due to the phonon-phonon scattering phenomenon in many ceramic and composite materials [25,129].

It is significant from the results presented in this study that SPS provides denser $UO_2$-Mo composite pellets without any intermetallic products in very shorter sintering time, highly homogeneous composite by reducing the micro-cracks, and above all, significantly enhances thermal conductivity. Previous studies show that a smaller grain size yields a lower thermal conductivity [130,131]. The grain growth is mainly affected by the sintering temperature, the grain size of these pellets sintered at 1300, 1500, and 1800 ºC was 0.9 μm, 2.4 μm, and 5.6 μm. Whereas $UO_2$ pellet sintered at 1300 ºC was 5.5 μm respectively, was observed by electron backscattered diffraction technique (EBSD). The sintering temperature at 1800 ºC of $UO_2$-Mo composite has a similar grain size as $UO_2$ pellet sintered at 1300 ºC, shown in Figure 4.6. The result of the thermal diffusivity and heat capacity measurements for $UO_2$ and $UO_2$-Mo composite pellets obtained with the laser flash analysis (LFA) is shown in Figure 6.1 (a, b). In this technique, the samples were heated in a graphite resistive furnace, and the measurements were carried out under vacuum from 25 ºC to 900 ºC. The laser flash apparatus based on the standard propagation of error results from the nature of the thermal conductivity measurements. The relative error for temperature-dependent specific heat capacity is about 2% and is at about 5% for thermal diffusivity, and 3% for temperature-dependent

density [122]. In this method, by multiplying density ρ with thermal diffusivity (α) and specific heat capacity ($C_p$), the thermal conductivity (λ) was calculated. Examined data was in good agreement with the values for $UO_2$-Mo micro-cell pellet by Kim *et al*. [35]. Still, differences do exist between densification and the processing conditions of the pellet. The data of Kim are slightly lower than in the current work. In this evaluation; pellet density, grain size, and particle size seem to produce $UO_2$-Mo composite pellets with enhanced thermal conductivity.

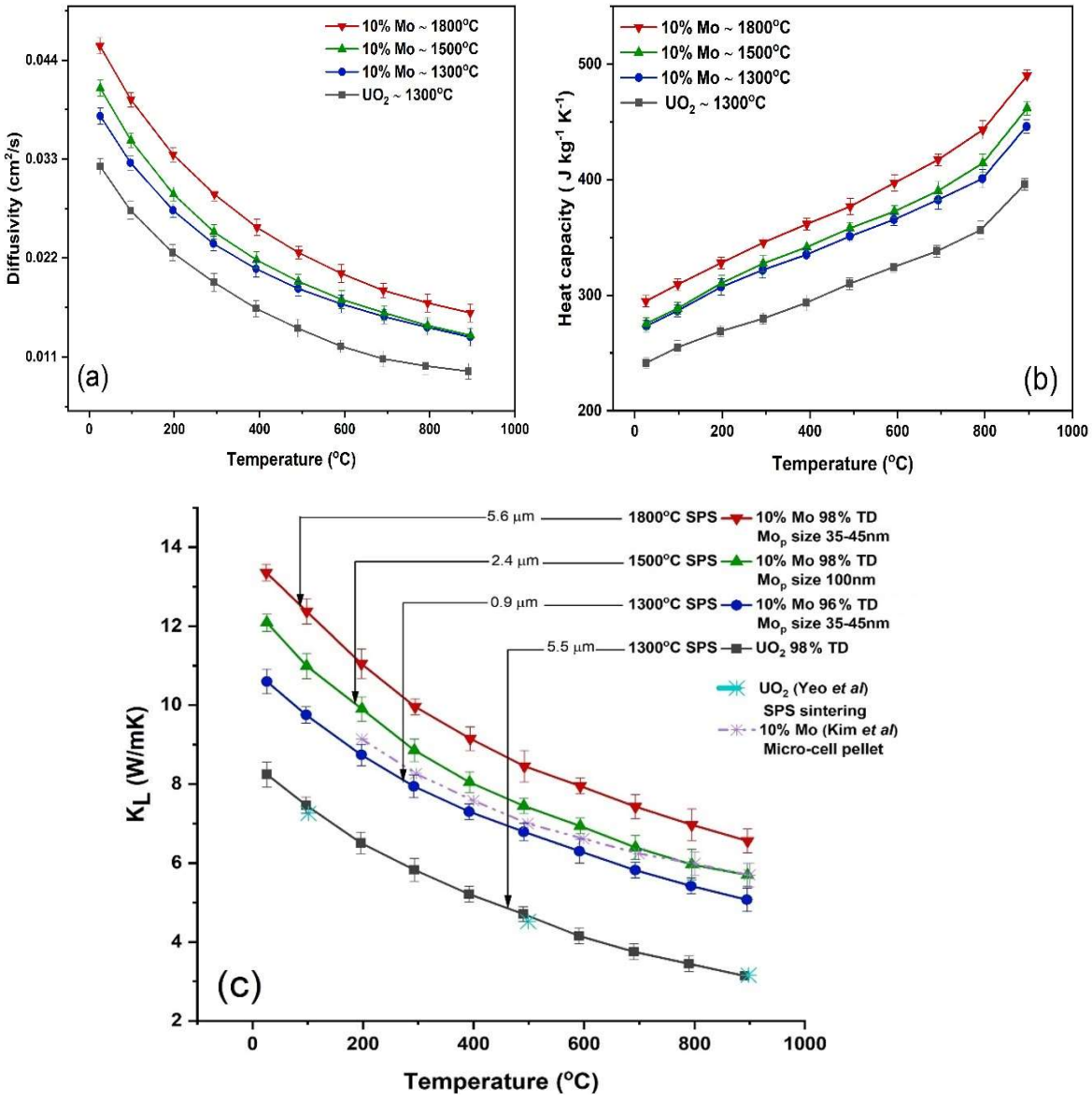


Figure 6.1: (a) thermal diffusivity, (b) heat capacity, and (c) thermal conductivity of $UO_2$ and $UO_2$-Mo as a function of temperature for samples sintered at 1300 °C, 1500 °C, and 1800 °C. The error bars are marked on the graphs.

### 6.4. Summary

Uranium dioxide ($UO_2$)-10 vol% Molybdenum (Mo) composite fuel pellets were prepared at a range of temperatures from 1300–1800 ºC by using SPS. Both Mo micro and nanoparticles were utilized. The thermal conductivity measurement reveals their dependence on the densification, grain size, and particle size of the specimens. Understanding the effect of the processing parameters on the density, grain size, and thermal conductivity enables us to tailor the sintering parameter to fabricate a highly customized fuel with desired properties. Combined experimental investigations demonstrated that the $UO_2$-Mo composite pellet has significantly improved the thermal conductivity of the $UO_2$ pellet.

# CHAPTER 7

# CONCLUSION AND FUTURE WORK

## 7.1 Conclusion

$UO_2$-Mo 10vol% composite produced by SPS revealed high-density pellets without any sintering aid such as magnesium oxide (MgO) and dinitrogen pentoxide ($N_2O_5$). A systematic analysis of the influence of sintering parameters on the density, microstructure, grain size, and thermal conductivity of the $UO_2$-Mo pellets has been presented. The XRD analysis of the $UO_2$-Mo powder and sintered pellets represents that there is no formation of any intermetallic products or concerns of reactions between the two phases during the SPS sintering temperatures from 1300 $^oC$ to 1800 $^oC$ respectively. The $UO_2$-Mo composite pellets were analyzed by electron backscatter diffraction (EBSD) to evaluate the grain size, grain boundary misorientation, and the concentration of low Σ boundaries of Σ3, Σ5, Σ9 boundaries for exceptional mechanical and kinetic properties. The grain boundaries responsible for several material properties that direct fuel performance, such as fission gas release and build up an imperative scenario in accidents by the failure of the fuel rod.

The EBSD analysis quantitatively reveals that the higher sintering temperatures result in larger grain size. By adjusting the sintering conditions, the densification and grain size of the sintered pellets can be control. The orientation maps demonstrated that some texture closed to <111> orientation was observed in the pellets sintered at 1500 $^oC$. The $UO_2$-Mo pellet with the desired density of ~97% TD was obtained at a temperature as low as 1300 $^oC$, this can potentially overcome one of the significant issues in the front end of the fuel cycle when problems related to the industrial processing with the SPS techniques are solved. It has also shown that by varying the Mo particle size, it is possible to tune the microstructural characteristics of $UO_2$-Mo composite fuel. It was observed that the thermal conductivity depends on the densification, grain size, and particle size of the molybdenum powders. Understanding the impact of the sintering conditions on the density, grain size, intergranular pores, and thermal conductivity enables us to tailor the sintering conditions to manufacture a highly customized nuclear fuel with the required properties. Our combined experimental investigations suggest that the $UO_2$-Mo composite pellets are more favorable with a wide array of microstructural features and enhance the thermal conductivity of $UO_2$ fuel.

## 7.2 Future work

The microstructural and thermophysical properties of $UO_2$-Mo composites have been investigated. This research has proved that Mo-doped $UO_2$ fuels with both the Mo micro and nanoparticles allow improving the thermal conductivity of fuel. A systematic investigation of the influence of SPS processing parameters of the density, microstructure, grain size, grain boundary characteristic features, and thermal conductivity of the $UO_2$-Mo pellets has been presented. Future work might consider, other doping elements such as Chromium oxide ($Cr_2O_3$), Aluminum oxide ($Al_2O_3$), and Thorium oxide ($ThO_2$). To enhance the grain size and further improve the microstructural and thermophysical properties.

The characteristics of the oxidation behavior of $UO_2$-Mo composites at temperatures ranging from 25 to 1000 $^oC$ is important. Furthermore, the texture, grain boundaries, phase analysis have to be characterized after oxidation at high temperatures for new composites. The oxidized samples at high temperatures can be characterized by SEM/EBSD and X-ray diffraction (XRD) to develop an understanding of the oxidation processes.

The irradiation behavior of the composite pellets needs to be evaluated for the $UO_2$-Mo under reactor operating conditions. The thermal conductivity of the composite before and after irradiation needs to be evaluated. Also, data on the influence of fission gas release in the composite fuels on the thermal conductivity are important for commercial application.

# REFERENCES


[1] J. Newman, Physics of the Life Sciences., 2008. doi:10.1007/978-0-387-77259-2.

[2] L. Szilard, Improvements in or relating to the transmutation of chemical elements, GB630726, 1936.

[3] X.M. Bai, M.R. Tonks, Y. Zhang, J.D. Hales, Multiscale modeling of thermal conductivity of high burnup structures in UO2 fuels, J. Nucl. Mater. 470 (2016) 208–215. doi:10.1016/j.jnucmat.2015.12.028.

[4] World Nuclear Association, Generation IV Nuclear Reactors, (2015). http://www.world-nuclear.org/information-library/nuclear-fuelcycle/%0Anuclear-power-reactors/generation-iv-nuclear-reactors.aspx (accessed May 17, 2016).

[5] The First Reactor, U.S. Atomic Energy Commission, Division of Technical Information., 1982.

[6] Chicago Pile reactors create enduring research legacy, Argonne's Hist. News Releases. (n.d.). anl.gov.

[7] Experimental Breeder Reactor 1., in: Idaho Natl. Lab. Wayback Mach., n.d.

[8] H. Hernandez, Nuclear Reactor Power Characterization and Simulation Tools, (2016). http://www.nuclear.utah.edu/wp-content/themes/nuclearexpress-%0Atheme/uploads/INPOAdditonalInfo.pdf (accessed May 17, 2016).

[9] W.M. Stacey, Nuclear Reactor Physics: Second Edition, 2007. doi:10.1002/9783527611041.

[10] U. Doe, Nuclear physics and reactor theory, 1993.

[11] World Nuclear Association, Nuclear Power Reactors, (2016). https://www.world-nuclear.org/information-library/nuclear-fuel-cycle/nuclear-power-reactors/nuclear-power-reactors.aspx (accessed May 17, 2016).

[12] E.E. Lewis, Fundamentals of Nuclear Reactor Physics, Elsevier Inc., 2008. doi:10.1016/B978-0-12-370631-7.X0001-0.

[13] S. Glasstone, Nuclear Reactor Engineering: Reactor systems engineering, 2010.

[14] J.C. Courtney, Nuclear Energy Technology: Theory and Practice of Commercial Nuclear Power, Nucl. Technol. (1982). doi:10.13182/nt82-a32965.

[15] G. Choppin, J.O. Liljenzin, J. Rydberg, C. Ekberg, Radiochemistry and Nuclear Chemistry: Fourth Edition, 2013. doi:10.1016/C2011-0-07260-5.

[16] K. Wirtz, Nuclear Fission Reactors, Nucl. Technol. (1984). doi:10.13182/nt84-a33543.

[17] R.E. MacFarlane, Neutron Slowing Down and Thermalization, in: Handb. Nucl. Eng., 2010. doi:10.1007/978-0-387-98149-9_3.

[18] F.C. Olds, NUCLEAR POWER ENGINEERING., Power Eng. (Barrington, Illinois). (1975).

[19] World Nuclear Association, Physics of Uranium and Nuclear Energy, (2018). https://www.world-nuclear.org/information-library/nuclear-fuel-cycle/introduction/physics-of-nuclear-energy.aspx (accessed August 1, 2017).

[20] A. Mark, Physics of Uranium and Nuclear Energy, World Nucl. Assoc. (2014) 1–9.

[21] R. Pywell, Cross Section, Subatomic Physics, Lecture Notes, University of Saskatchewan, 2010.

[22] K. Gofryk, S. Du, C.R. Stanek, J.C. Lashley, X.Y. Liu, R.K. Schulze, J.L. Smith, D.J. Safarik, D.D. Byler, K.J. McClellan, B.P. Uberuaga, B.L. Scott, D.A. Andersson, Anisotropic thermal conductivity in uranium dioxide, Nat. Commun. 5 (2014) 1–7. doi:10.1038/ncomms5551.

[23] M. Lenzen, Current state of development of electricity-generating technologies: A literature review, Energies. 3 (2010) 462–591. doi:10.3390/en3030462.

[24] E.E. Lewis, Fundamentals of Nuclear Reactor Physics, 2008. doi:10.1016/B978-0-12-370631-7.X0001-0.

[25] S. Yeo, E. McKenna, R. Baney, G. Subhash, J. Tulenko, Enhanced thermal conductivity of uranium dioxide-silicon carbide composite fuel pellets prepared by Spark Plasma Sintering (SPS), J. Nucl. Mater. 433 (2013) 66–73. doi:10.1016/j.jnucmat.2012.09.015.

[26] S.C. Finkeldei, J.O. Kiggans, R.D. Hunt, A.T. Nelson, K.A. Terrani, Fabrication of UO 2 - Mo composite fuel with enhanced thermal conductivity from sol-gel feedstock, J. Nucl. Mater. (2019). doi:10.1016/j.jnucmat.2019.04.011.

[27] M. Amaya, M. Hirai, H. Sakurai, K. Ito, M. Sasaki, T. Nomata, K. Kamimura, R. Iwasaki, Thermal conductivities of irradiated UO2 and (U,Gd)O2 pellets, J. Nucl. Mater. 300 (2002) 57–64. doi:10.1016/S0022-3115(01)00704-8.

[28] W.J. Weber, A. Navrotsky, S. Stefanovsky, E.R. Vance, E. Vernaz, M aterials Science of High-Level Immobilization, MRS Bull. 34 (2009) 46–52.

[29] L.J. Ott, K.R. Robb, D. Wang, Preliminary assessment of accident-tolerant fuels on LWR performance during normal operation and under DB and BDB accident conditions, J. Nucl. Mater. (2014). doi:10.1016/j.jnucmat.2013.09.052.

[30] L.H. Ortega, B.J. Blamer, J.A. Evans, S.M. McDeavitt, Development of an accident-tolerant fuel composite from uranium mononitride (UN) and uranium sesquisilicide (U3 Si2) with increased uranium loading, J. Nucl. Mater. 471 (2016) 116–121. doi:10.1016/j.jnucmat.2016.01.014.

[31] R. Newell, Y. Park, A. Mehta, D. Keiser, Y. Sohn, Mechanical properties examined by nanoindentation for selected phases relevant to the development of monolithic uranium-molybdenum metallic fuels, J. Nucl. Mater. 487 (2017) 443–452. doi:10.1016/j.jnucmat.2017.02.018.

[32] S. Hu, A.M. Casella, C.A. Lavender, D.J. Senor, D.E. Burkes, Assessment of effective thermal conductivity in U-Mo metallic fuels with distributed gas bubbles, J. Nucl. Mater. (2015). doi:10.1016/j.jnucmat.2015.03.039.

[33] W.E. Lee, M. Gilbert, S.T. Murphy, R.W. Grimes, Opportunities for advanced ceramics and composites in the nuclear sector, J. Am. Ceram. Soc. 96 (2013) 2005–2030. doi:10.1111/jace.12406.

[34] J.S.T. J. A. Khan, T. W. Knight, S. B. Pakala, W. Jiang, R. Fang, Enhanced Thermal Conductivity for LWR Fuel, Nucl. Technol. 169 (2010) 61–72.

[35] D.J. Kim, Y.W. Rhee, J.H. Kim, K.S. Kim, J.S. Oh, J.H. Yang, Y.H. Koo, K.W. Song, Fabrication of micro-cell UO<inf>2</inf>-Mo pellet with enhanced thermal conductivity, J. Nucl. Mater. 462 (2015) 289–295. doi:10.1016/j.jnucmat.2015.04.003.

[36] J.H. Yang, K.W. Song, Y.W. Lee, J.H. Kim, K.W. Kang, K.S. Kim, Y.H. Jung, Microwave process for sintering of uranium dioxide, J. Nucl. Mater. 325 (2004) 210–216. doi:10.1016/j.jnucmat.2003.12.003.

[37] R.J. McEachern, P. Taylor, A review of the oxidation of uranium dioxide at temperatures below 400°C, J. Nucl. Mater. (1998). doi:10.1016/S0022-3115(97)00343-7.

[38] S. Aronson, R.B. Roof, J. Belle, Kinetic Study of the Oxidation of Uranium Dioxide Kinetic Study of the Oxidation of Uranium Dioxide*, J. Chem. Phys. 27 (1957) 1–9. doi:10.1063/1.1743653.

[39] M.J. Bannister, THE STORAGE BEHAVIOUR OF URANIUM DIOXIDE POWDERS - REVIEW ARTICLE, 26 (1968) 174–184.

[40] D.J.M. Bevan, I.E. Grey, B.T.M. Willis, The Crystal Structure of $\mathrm{beta-U_40_{9-y}}$, J. Solid State Chem. 61 (1986) 1–7.

[41] B.T.M. Willis, Crystallographic studies of anion-excess uranium oxides, J. Chem. Soc. Faraday Trans. 2 Mol. Chem. Phys. 83 (1987) 1073–1081. doi:10.1039/F29878301073.

[42] P.E. Blackburn, J. Weissbart, E.A. Gulbransen, Oxidation of uranium dioxide, J. Phys. Chem. (1958). doi:10.1021/j150566a002.

[43] P.E. Blackburn, Oxygen pressures over fast breeder reactor fuel (I) A model for UO2±x, J.

Nucl. Mater. (1973). doi:10.1016/0022-3115(73)90038-X.

[44] B.J. Lewis, B. Szpunar, F.C. Iglesias, Fuel oxidation and thermal conductivity model for operating defective fuel rods, J. Nucl. Mater. 306 (2002) 30–43. doi:10.1016/S0022-3115(02)01231-X.

[45] D.S. Cox, F.C. Iglesias, C.E.L. Hunt, N.A. Keller, R.D. Barrand, J.R. Mitchell, R.F. O'Connor, Oxidation of $UO_2$ in air and steam with relevance to fission product releases, Proc. Symp. Chem. Phenom. Assoc. with Radioact. Releases Dur. Sev. Nucl. Plant Accid. (1986).

[46] B. Szpunar, Assessment of the models of urania fuel oxidation in steam-rich atmosphere, J. Nucl. Sci. Technol. 49 (2012) 1186–1192. doi:10.1080/00223131.2012.739348.

[47] D.S. Iglesias, F.C. Hunt, C.E.L. Garisto, F. and Cox, Ruthenium release kinetics from uranium oxides, 10016 (1989) 187–196.

[48] M. Amaya, T. Kubo, Y. Korei, Thermal conductivity measurements on UO2+x from 300 to 1,400 K, J. Nucl. Sci. Technol. 33 (1996) 636–640. doi:10.1080/18811248.1996.9731970.

[49] J.K. Watkins, D.P. Butt, B.J. Jaques, Microstructural degradation of UN and UN-UO 2 composites in hydrothermal oxidation conditions, J. Nucl. Mater. 518 (2019) 30–40. doi:10.1016/j.jnucmat.2019.02.027.

[50] X. Wang, Z. Long, H. Huang, R. Bin, Y. Hu, L. Luo, K.Z. Liu, P.C. Zhang, Insight on the oxidation resistance of UOxNy layers: A density functional study, Comput. Mater. Sci. (2016). doi:10.1016/j.commatsci.2016.06.029.

[51] G.A.R. Rao, S.K. Mukerjee, V.N. Vaidya, V. Venugopal, D.D. Sood, Oxidation and hydrolysis kinetic studies on UN, J. Nucl. Mater. (1991). doi:10.1016/0022-3115(91)90340-D.

[52] S. Sunder, N.H. Miller, XPS and XRD studies of corrosion of uranium nitride by water, J. Alloys Compd. (1998). doi:10.1016/S0925-8388(98)00157-1.

[53] K. Johnson, V. Ström, J. Wallenius, D.A. Lopes, Oxidation of accident tolerant fuel candidates, J. Nucl. Sci. Technol. 54 (2017) 280–286. doi:10.1080/00223131.2016.1262297.

[54] V.J. Wheeler, R.M. Dell, E. Wait, Uranium trioxide and the UO3 hydrates, J. Inorg. Nucl. Chem. (1964). doi:10.1016/0022-1902(64)80007-5.

[55] A.A. Solomon, S.T. Revankar, J.K. McCoy, Enhanced Thermal Conductivity Oxide Fuels, DOE Award Number DE-FG07-02SF22613. (2005).

[56] K.H. Kang, S.H. Kim, K.K. Kwak, C.K. Kim, Oxidation behavior of U – 10 wt % Mo alloy in air at 473 – 773 K, J. Nucl. Mater. 304 (2002) 242–245.

[57] J.E. Antill, K.A. Peakall, Oxidation of uranium alloys in carbon dioxide and air, J. Less-Common Met. (1961). doi:10.1016/0022-5088(61)90066-2.

[58] S. Miwa, M. Osaka, T. Nozaki, T. Arima, K. Idemitsu, Oxygen potential of a prototypic Mo-cermet fuel containing plutonium oxide, J. Nucl. Mater. 465 (2015) 840–842. doi:10.1016/j.jnucmat.2015.06.004.

[59] Y.K. Ha, J. Lee, J.G. Kim, J.Y. Kim, Effect of Ce doping on UO2 structure and its oxidation behavior, J. Nucl. Mater. 480 (2016) 429–435. doi:10.1016/j.jnucmat.2016.08.026.

[60] B.G. Santos, H.W. Nesbitt, J.J. Noël, D.W. Shoesmith, X-ray photoelectron spectroscopy study of anodically oxidized SIMFUEL surfaces, Electrochim. Acta. (2004). doi:10.1016/j.electacta.2003.12.016.

[61] J.G. Kim, Y.K. Ha, S.D. Park, K.Y. Jee, W.H. Kim, Effect of a trivalent dopant, Gd3+, on the oxidation of uranium dioxide, J. Nucl. Mater. (2001). doi:10.1016/S0022-3115(01)00639-0.

[62] Y.-K. Ha, J.-G. Kim, W.-H. Kim, Studies on the Air-oxidation Behavior of Uranium Dioxide I. Phase transformation from (U 1-y Gd y )O 2 to (U l-y Gd y ) 3 O S , J. Nucl. Sci. Technol. (2002). doi:10.1080/00223131.2002.10875581.

[63] Y.K. Ha, J.G. Kim, Y.J. Park, W.H. Kim, Effect of a tetravalent dopant, Th4+ on the oxidation of uranium dioxide, Key Eng. Mater. (2005).

[64] Y.K. Ha, J.G. Kim, Y.S. Park, S.D. Park, K. Song, Behaviors of molybdenum in U02 fuel matrix, Nucl. Eng. Technol. 43 (2011) 309–316. doi:10.5516/NET.2011.43.3.309.

[65] J. Cobos, D. Papaioannou, J. Spino, M. Coquerelle, Phase characterisation of simulated high burn-up UO2 fuel, J. Alloys Compd. (1998). doi:10.1016/S0925-8388(98)00170-4.

[66] S. Imoto, Chemical state of fission products in irradiated UO2, J. Nucl. Mater. (1986). doi:10.1016/0022-3115(86)90192-3.

[67] R.S. Dobedoe, G.D. West, M.H. Lewis, Spark plasma sintering of ceramics: Understanding temperature distribution enables more realistic comparison with conventional processing, Adv. Appl. Ceram. (2005). doi:10.1179/174367605X16662.

[68] M. TOKITA, Trends in Advanced SPS Spark Plasma Sintering Systems and Technology. Functionally Gradient Materials and Unique Synthetic Processing Methods from Next Generation of Powder Technology., J. Soc. Powder Technol. Japan. (1993). doi:10.4164/sptj.30.11_790.

[69] U. Anselmi-Tamburini, J.E. Garay, Z.A. Munir, Fundamental investigations on the spark plasma sintering/synthesis process, Mater. Sci. Eng. A. (2005). doi:10.1016/j.msea.2005.06.066.

[70] Z. Chen, G. Subhash, J.S. Tulenko, Master sintering curves for UO2 and UO2-SiC composite processed by spark plasma sintering, J. Nucl. Mater. 454 (2014) 427–433. doi:10.1016/j.jnucmat.2014.08.023.

[71] J. Buckley, J.D. Turner, T.J. Abram, Uranium dioxide - Molybdenum composite fuel pellets with enhanced thermal conductivity manufactured via spark plasma sintering, J. Nucl. Mater. 523 (2019) 360–368. doi:10.1016/j.jnucmat.2019.05.059.

[72] D.M. Hulbert, A. Anders, D. V. Dudina, J. Andersson, D. Jiang, C. Unuvar, U. Anselmi-Tamburini, E.J. Lavernia, A.K. Mukherjee, The absence of plasma in “spark plasma

sintering," J. Appl. Phys. (2008). doi:10.1063/1.2963701.

[73] M. Omori, Sintering, consolidation, reaction and crystal growth by the spark plasma system (SPS), Mater. Sci. Eng. A. (2000).

[74] G.-D. Zhan, J. Kuntz, J. Wan, J. Garay, A.K. Mukherjee, A Novel Processing Route to Develop a Dense Nanocrystalline Alumina Matrix (<100 nm) Nanocomposite Material, J. Am. Ceram. Soc. (2003). doi:10.1111/j.1151-2916.2003.tb03306.x.

[75] N. Chawake, L.D. Pinto, A.K. Srivastav, K. Akkiraju, B.S. Murty, R.S. Kottada, On Joule heating during spark plasma sintering of metal powders, Scr. Mater. (2014). doi:10.1016/j.scriptamat.2014.09.003.

[76] H. Mehrer, Diffusion in solids: fundamentals, methods, materials, diffusion-controlled processes, Springer Ser. Solid-State Sci. (2007). doi:10.1007/978-3-540-71488-0.

[77] A. Prasad R, Spark plasma sintering of cerium dioxide and its composites, (2017). doi:10.14288/1.0355271.

[78] M. Nygren, Z. Shen, On the preparation of bio-, nano- and structural ceramics and composites by spark plasma sintering, Solid State Sci. (2003). doi:10.1016/S1293-2558(02)00086-9.

[79] C. Manière, L. Durand, A. Weibel, C. Estournès, Spark-plasma-sintering and finite element method: From the identification of the sintering parameters of a submicronic α-alumina powder to the development of complex shapes, Acta Mater. (2016). doi:10.1016/j.actamat.2015.09.003.

[80] T. Hungría, J. Galy, A. Castro, Spark plasma sintering as a useful technique to the nanostructuration of piezo-ferroelectric materials, Adv. Eng. Mater. (2009). doi:10.1002/adem.200900052.

[81] R.M. Wilson, Archimedes's principle gets updated, Phys. Today. 65 (2012) 15–17. doi:10.1063/PT.3.1701.

[82] W.J. Parker, R.J. Jenkins, C.P. Butler, G.L. Abbott, Flash method of determining thermal diffusivity, heat capacity, and thermal conductivity, J. Appl. Phys. (1961). doi:10.1063/1.1728417.

[83] T.T. Molla, Modeling Macroscopic Shape Distortions during Sintering of Multi-layers Modeling Macroscopic Shape Distortions during Sintering of Multi-layers By : Tesfaye Tadesse Molla, 2016.

[84] M.F. Ashby, A first report on sintering diagrams, Acta Metall. 22 (1974) 275–289. doi:10.1016/0001-6160(74)90167-9.

[85] L.B. Kong, Y. Huang, W. Que, T. Zhang, S. Li, J. Zhang, Z. Dong, D. Tang, Sintering and Densification (I)---Conventional Sintering Technologies, in: Transparent Ceram., Springer International Publishing, Cham, 2015: pp. 291–394. doi:10.1007/978-3-319-18956-7_5.

[86] J. Hu, A.C. Hayes, W.B. Wilson, Rizwan-Uddin, Fission gas production in reactor fuels including the effects of ternary fission, Nucl. Eng. Des. 240 (2010) 3751–3757. doi:10.1016/j.nucengdes.2010.08.020.

[87] R.I. Todd, B. Derby, Thermal stress induced microcracking in alumina-20% SiCp composites, Acta Mater. 52 (2004) 1621–1629. doi:10.1016/j.actamat.2003.12.007.

[88] B.R. POWELL, G.E. YOUNGBLOOD, D.P.H. HASSELMAN, L.D. BENTSEN, Effect of Thermal Expansion Mismatch on the Thermal Diffusivity of Glass-Ni Composites, J. Am. Ceram. Soc. 63 (1980) 581–586. doi:10.1111/j.1151-2916.1980.tb10769.x.

[89] T.C. Lu, J. Yang, Z. Suo, A.G. Evans, R. Hecht, R. Mehrabian, Matrix cracking in intermetallic composites caused by thermal expansion mismatch, Acta Metall. Mater. 39 (1991) 1883–1890. doi:10.1016/0956-7151(91)90157-V.

[90] S.Y. Fu, X.Q. Feng, B. Lauke, Y.W. Mai, Effects of particle size, particle/matrix interface adhesion and particle loading on mechanical properties of particulate-polymer composites, Compos. Part B Eng. 39 (2008) 933–961. doi:10.1016/j.compositesb.2008.01.002.

[91] B. Burton, G.L. Reynolds, J.P. Barnes, The influence of grain size on the creep of uranium

dioxide, J. Mater. Sci. 8 (1973) 1690–1694. doi:10.1007/BF02403517.

[92] J. Watts, G. Hilmas, W.G. Fahrenholtz, Mechanical characterization of ZrB2-SiC composites with varying SiC particle sizes, J. Am. Ceram. Soc. 94 (2011) 4410–4418. doi:10.1111/j.1551-2916.2011.04885.x.

[93] J.A. Turnbull, The effect of grain size on the swelling and gas release properties of uo2 during irradiation, J. Nucl. Mater. (1974). doi:10.1016/0022-3115(74)90061-0.

[94] X. Wang, F. Fan, J.A. Szpunar, L. Zhang, Influence of grain orientation on the incipient oxidation behavior of Haynes 230 at 900 °c, Mater. Charact. 107 (2015) 33–42. doi:10.1016/j.matchar.2015.06.029.

[95] Y.T. Chen, The effect of interface texture on exchange biasing in Ni 80Fe 20/Ir 20Mn 80 system, Nanoscale Res. Lett. 4 (2009) 90–93. doi:10.1007/s11671-008-9207-4.

[96] P. V. Nerikar, K. Rudman, T.G. Desai, D. Byler, C. Unal, K.J. McClellan, S.R. Phillpot, S.B. Sinnott, P. Peralta, B.P. Uberuaga, C.R. Stanek, Grain boundaries in uranium dioxide: Scanning electron microscopy experiments and atomistic simulations, J. Am. Ceram. Soc. 94 (2011) 1893–1900. doi:10.1111/j.1551-2916.2010.04295.x.

[97] C.B. Thomson, V. Randle, The effects of strain annealing on grain boundaries and secure triple junctions in nickel 200, J. Mater. Sci. 32 (1997) 1909–1914. doi:10.1023/A:1018573327408.

[98] H. Akhiani, M. Nezakat, M. Sanayei, J. Szpunar, The effect of thermo-mechanical processing on grain boundary character distribution in Incoloy 800H/HT, Mater. Sci. Eng. A. 626 (2015) 51–60. doi:10.1016/j.msea.2014.12.046.

[99] T. Watanabe, Part IV Applications : Grain Boundary Engineering and Microstructural Design for Advanced Properties, Microstruct. Des. Adv. Eng. Mater. (2013) 403–446. doi:10.1051/forest.

[100] S. Spigarelli, M. Cabibbo, E. Evangelista, G. Palumbo, Analysis of the creep strength of a low-carbon AISI 304 steel with low-Σ grain boundaries, Mater. Sci. Eng. A. 352 (2003)

93–99. doi:10.1016/S0921-5093(02)00903-6.

[101] V. Randle, Sigma-boundary statistics by length and number, Interface Sci. 10 (2002) 271–277. doi:10.1023/A:1020877528820.

[102] J.J. Kai, F.R. Chen, T.S. Duh, Effects of grain boundary misorientation on radiation-induced solute segregation in proton irradiated 304 stainless steels, Mater. Trans. 45 (2004) 40–50. doi:10.2320/matertrans.45.40.

[103] L. Tan, T.R. Allen, J.T. Busby, Grain boundary engineering for structure materials of nuclear reactors, J. Nucl. Mater. 441 (2013) 661–666. doi:10.1016/j.jnucmat.2013.03.050.

[104] L. Tan, K. Sridharan, T.R. Allen, R.K. Nanstad, D.A. McClintock, Microstructure tailoring for property improvements by grain boundary engineering, J. Nucl. Mater. 374 (2008) 270–280. doi:10.1016/j.jnucmat.2007.08.015.

[105] S. Xia, H. Li, T.G. Liu, B.X. Zhou, Appling grain boundary engineering to Alloy 690 tube for enhancing intergranular corrosion resistance, J. Nucl. Mater. 416 (2011) 303–310. doi:10.1016/j.jnucmat.2011.06.017.

[106] E.A. West, G.S. Was, IGSCC of grain boundary engineered 316L and 690 in supercritical water, J. Nucl. Mater. 392 (2009) 264–271. doi:10.1016/j.jnucmat.2009.03.008.

[107] G. Palumbo, E.M. Lehockey, P. Lin, Applications for grain boundary engineered materials, Jom. 50 (1998) 40–43. doi:10.1007/s11837-998-0248-z.

[108] M. Sekine, N. Sakaguchi, M. Endo, H. Kinoshita, S. Watanabe, H. Kokawa, S. Yamashita, Y. Yano, M. Kawai, Grain boundary engineering of austenitic steel PNC316 for use in nuclear reactors, J. Nucl. Mater. 414 (2011) 232–236. doi:10.1016/j.jnucmat.2011.03.049.

[109] N.T.O. CARY, C. JENNIFER, PERFORMANCE-BASED REGULATION: PROSPECTS AND LIMITATIONS IN HEALTH, SAFETY, AND ENVIRONMENTAL PROTECTION, Lang. Learn. 33 (2003) 107–144. doi:10.1111/j.1944-9720.2000.tb01995.x.

[110] D.K. Smith, S. Gorter, Powder diffraction program information 1990 program list, J. Appl. Crystallogr. 24 (1991) 369–402. doi:10.1107/S0021889891003473.

[111] E.Y. Pikalova, A.A. Murashkina, V.I. Maragou, A.K. Demin, V.N. Strekalovsky, P.E. Tsiakaras, CeO2 based materials doped with lanthanides for applications in intermediate temperature electrochemical devices, Int. J. Hydrogen Energy. 36 (2011) 6175–6183. doi:10.1016/j.ijhydene.2011.01.132.

[112] S.I. Ahmad, P. Koteshwar Rao, I.A. Syed, Sintering temperature effect on density, structural and morphological properties of Mg- and Sr-doped ceria, J. Taibah Univ. Sci. 10 (2016) 381–385. doi:10.1016/j.jtusci.2015.04.003.

[113] J.T. White, A.W. Travis, J.T. Dunwoody, A.T. Nelson, Fabrication and thermophysical property characterization of UN/U3Si2 composite fuel forms, J. Nucl. Mater. 495 (2017) 463–474. doi:10.1016/j.jnucmat.2017.08.041.

[114] L.J. Ott, K.R. Robb, D. Wang, Preliminary assessment of accident-tolerant fuels on LWR performance during normal operation and under DB and BDB accident conditions, J. Nucl. Mater. 448 (2014) 520–533. doi:10.1016/j.jnucmat.2013.09.052.

[115] I. Amato, R.L. Colombo, A.M.P. Balzari, Hot-pressing of uranium dioxide, J. Nucl. Mater. 20 (1966) 210–214. doi:10.1016/0022-3115(66)90009-2.

[116] J.H. Yang, Y.W. Kim, J.H. Kim, D.J. Kim, K.W. Kang, Y.W. Rhee, K.S. Kim, K.W. Song, Pressureless rapid sintering of UO2assisted by high-frequency induction heating process, J. Am. Ceram. Soc. 91 (2008) 3202–3206. doi:10.1111/j.1551-2916.2008.02615.x.

[117] L. Ge, G. Subhash, R.H. Baney, J.S. Tulenko, E. McKenna, Densification of uranium dioxide fuel pellets prepared by spark plasma sintering (SPS), J. Nucl. Mater. 435 (2013) 1–9. doi:10.1016/j.jnucmat.2012.12.010.

[118] T. Ironman, J. Tulenko, G. Subhash, Exploration of viability of spark plasma sintering for commercial fabrication of nuclear fuel pellets, Nucl. Technol. 200 (2017) 144–158. doi:10.1080/00295450.2017.1360714.

[119] E.K. Papynov, O.O. Shichalin, A. Yu Mironenko, I.G. Tananaev, V.A. Avramenko, V.I. Sergienko, UO2 fuel pellets fabrication via Spark Plasma Sintering using non-standard molybdenum die, IOP Conf. Ser. Mater. Sci. Eng. 307 (2018). doi:10.1088/1757-899X/307/1/012029.

[120] E.A. Olevsky, W.L. Bradbury, C.D. Haines, D.G. Martin, D. Kapoor, Fundamental aspects of spark plasma sintering: I. Experimental analysis of scalability, J. Am. Ceram. Soc. 95 (2012) 2406–2413. doi:10.1111/j.1551-2916.2012.05203.x.

[121] L. Balice, D. Bouëxière, M. Cologna, A. Cambriani, J.F. Vigier, E. De Bona, G.D. Sorarù, C. Kübel, O. Walter, K. Popa, Nano and micro U1-xThxO2 solid solutions: From powders to pellets, J. Nucl. Mater. 498 (2018) 307–313. doi:10.1016/j.jnucmat.2017.10.042.

[122] M. Saoudi, D. Staicu, J. Mouris, A. Bergeron, H. Hamilton, M. Naji, D. Freis, M. Cologna, Thermal diffusivity and conductivity of thorium- uranium mixed oxides, J. Nucl. Mater. 500 (2018) 381–388. doi:10.1016/j.jnucmat.2018.01.014.

[123] S.M. Scott, T. Yao, F. Lu, G. Xin, W. Zhu, J. Lian, Fabrication of lanthanum-doped thorium dioxide by high-energy ball milling and spark plasma sintering, J. Nucl. Mater. 485 (2017) 207–215. doi:10.1016/j.jnucmat.2017.01.005.

[124] H. Muta, H. Kado, Y. Ohishi, K. Kurosaki, S. Yamanaka, Effect of oxygen defects on thermal conductivity of thorium-cerium dioxide solid solutions, J. Nucl. Mater. 483 (2017) 192–198. doi:10.1016/j.jnucmat.2016.10.043.

[125] H. Muta, Y. Murakami, M. Uno, K. Kurosaki, S. Yamanaka, Thermophysical properties of Th1-xUxO2 pellets prepared by spark plasma sintering technique, J. Nucl. Sci. Technol. 50 (2013) 181–187. doi:10.1080/00223131.2013.757468.

[126] V. Tyrpekl, M. Cologna, J.F. Vigier, A. Cambriani, W. De Weerd, J. Somers, Preparation of bulk-nanostructured UO2 pellets using high-pressure spark plasma sintering for LWR fuel safety assessment, J. Am. Ceram. Soc. 100 (2017) 1269–1274. doi:10.1111/jace.14647.

[127] A.F. Williams, B.W. Leitch, N. Wang, A microstructural model of the thermal

conductivity of dispersion type fuels with a fuel matrix interaction layer, Nucl. Eng. Technol. 45 (2013) 839–846. doi:10.5516/NET.07.2013.714.

[128] J.K. Fink, Thermophysical properties of uranium dioxide, J. Nucl. Mater. 279 (2000) 1–18. doi:10.1016/S0022-3115(99)00273-1.

[129] N. Mingo, Anharmonic phonon flow through molecular-sized junctions, Phys. Rev. B - Condens. Matter Mater. Phys. 74 (2006) 1–13. doi:10.1103/PhysRevB.74.125402.

[130] C. V. Ramana, M. Noor-A-Alam, J.J. Gengler, J.G. Jones, Growth, structure, and thermal conductivity of yttria-stabilized hafnia thin films, ACS Appl. Mater. Interfaces. 4 (2012) 200–204. doi:10.1021/am2012596.

[131] G. Soyez, J.A. Eastman, L.J. Thompson, G.R. Bai, P.M. Baldo, A.W. McCormick, R.J. DiMelfi, A.A. Elmustafa, M.F. Tambwe, D.S. Stone, Grain-size-dependent thermal conductivity of nanocrystalline yttria-stabilized zirconia films grown by metal-organic chemical vapor deposition, Appl. Phys. Lett. 77 (2000) 1155–1157. doi:10.1063/1.1289803.

# APPENDIX

# COPYRIGHT PERMISSIONS

For the images, graphs or tables used that form a part of a thesis, written permission from the publisher (copyright holder) is required by the College of Graduate Studies and Research (CGSR). This appendix includes the copyright permissions from the publisher for the images, graphs, and tables that were published or are under review and used in this thesis.

Copyright Permissions for Table 1.1

This Agreement between Mr. Murali Krishna Tummalapalli ("You") and Elsevier("Elsevier") consists of your license details and the terms and conditions provided by Elsevier and Copyright Clearance Center.

| | |
|---|---|
| License Number | 4937940880927 |
| License date | Oct 28, 2020 |
| Licensed Content Publisher | Elsevier |
| Licensed Content Publication | Elsevier Books |
| Licensed Content Title | Radiochemistry and Nuclear Chemistry |
| Licensed Content Author | Gregory Choppin, Jan-Olov Liljenzin, Jan Rydberg, Christian Ekberg |
| Licensed Content Date | Jan 1, 2013 |
| Licensed Content Pages | 59 |
| Start Page | 595 |
| End Page | 653 |
| Type of Use | reuse in a thesis/dissertation |
| Portion | figures/tables/illustrations |
| Number of figures/tables/illustrations | 1 |
| Format | both print and electronic |

| | |
|---|---|
| Are you the author of this Elsevier chapter? | No |
| Will you be translating? | No |
| Title | MICROSTRUCTURAL AND THERMOPHYSICALPROPERTIES OF $UO_2$-Mo COMPOSITE REACTOR FUELS |
| Institution name | University of Saskatchewan |
| Expected presentation date | Oct 2020 |
| Portions | Table 19.3 |
| Requestor Location | Mr. Murali Krishna Tummalapalli 208-1020 Matheson Dr Saskatoon, SK S7L5TL Canada |
| Attn: | Mr. Murali Krishna Tummalapalli |
| Publisher Tax ID | GB 494 6272 12 |
| Total | 0.00 USD |

Terms and Conditions

INTRODUCTION

1. The publisher for this copyrighted material is Elsevier. By clicking "accept" in connection with completing this licensing transaction, you agree that the following terms and conditions apply to this transaction (along with the Billing and Payment terms and conditions established by Copyright Clearance Center, Inc. ("CCC"), at the time that you opened your Rights link account and that are available at any time at http://myaccount.copyright.com).

GENERAL TERMS

2. Elsevier hereby grants you permission to reproduce the a forementioned material subject to the terms and conditions indicated.

3. Acknowledgement: If any part of the material to be used (for example, figures) has appeared in our publication with credit or acknowledgement to another source, permission must also be sought from that source. If such permission is not obtained, then that material may not be included in your publication/copies. Suitable acknowledgement to the source must be made, either as a footnote or in a reference list at the end of your publication, as follows:

"Reprinted from Publication title, Vol /edition number, Author(s), Title of article / title of chapter, Pages No., Copyright (Year), with permission from Elsevier [OR APPLICABLESOCIETY

COPYRIGHT OWNER]." Also Lancet special credit - "Reprinted from The Lancet, Vol. number, Author(s), Title of article, Pages No., Copyright (Year), with permission from Elsevier."

4. Reproduction of this material is confined to the purpose and/or media for which permission is hereby given.

5. Altering/Modifying Material: Not Permitted. However figures and illustrations may be altered/adapted minimally to serve your work. Any other abbreviations, additions, deletions and/or any other alterations shall be made only with prior written authorization of Elsevier Ltd. (Please contact Elsevier's permissions helpdesk here). No modifications can be made to any Lancet figures/tables and they must be reproduced in full.

6. If the permission fee for the requested use of our material is waived in this instance, please be advised that your future requests for Elsevier materials may attract a fee.

7. Reservation of Rights: Publisher reserves all rights not specifically granted in the combination of (i) the license details provided by you and accepted in the course of this licensing transaction, (ii) these terms and conditions and (iii) CCC's Billing and Payment terms and conditions.

8. License Contingent Upon Payment: While you may exercise the rights licensed immediately upon issuance of the license at the end of the licensing process for the transaction, provided that you have disclosed complete and accurate details of your proposed use, no license is finally effective unless and until full payment is received from you (either by publisher or by CCC) as provided in CCC's Billing and Payment terms and conditions. If full payment is not received on a timely basis, then any license preliminarily granted shall be deemed automatically revoked and shall be void as if never granted. Further, in the event that you breach any of these terms and conditions or any of CCC's Billing and Payment terms and conditions, the license is automatically revoked and shall be void as if never granted. Use of materials as described in a revoked license, as well as any use of the materials beyond the scope of an unrevoked license, may constitute copyright infringement and publisher reserves the right to take any and all action to protect its copyright in the materials.

9. Warranties: Publisher makes no representations or warranties with respect to the licensed material.

10. Indemnity: You hereby indemnify and agree to hold harmless publisher and CCC, and their respective officers, directors, employees and agents, from and against any and all claims arising out of your use of the licensed material other than as specifically authorized pursuant to this license.

11. No Transfer of License: This license is personal to you and may not be sublicensed, assigned, or transferred by you to any other person without publisher's written permission.

12. No Amendment Except in Writing: This license may not be amended except in a writing signed by both parties (or, in the case of publisher, by CCC on publisher's behalf).

13. Objection to Contrary Terms: Publisher hereby objects to any terms contained in any purchase order, acknowledgment, check endorsement or other writing prepared by you, which terms are inconsistent with these terms and conditions or CCC's Billing and Payment terms and conditions. These terms and conditions, together with CCC's Billing and Payment terms and conditions (which are incorporated herein), comprise the entire agreement between you and publisher (and CCC) concerning this licensing transaction. In the event of any conflict between your obligations established by these terms and conditions and those established by CCC's Billing and Payment terms and conditions, these terms and conditions shall control.

14. Revocation: Elsevier or Copyright Clearance Center may deny the permissions described in this License at their sole discretion, for any reason or no reason, with a full refund payable to you. Notice of such denial will be made using the contact information provided by you. Failure to receive such notice will not alter or invalidate the denial. In no event will Elsevier or Copyright Clearance Center be responsible or liable for any costs, expenses or damage incurred by you as a result of a denial of your permission request, other than a refund of the amount(s) paid by you to Elsevier and/or Copyright Clearance Center for denied permissions.

LIMITED LICENSE

The following terms and conditions apply only to specific license types:

15. Translation: This permission is granted for non-exclusive world English rights only unless your license was granted for translation rights. If you licensed translation rights you may only translate this content into the languages you requested. A professional translator must perform all translations and reproduce the content word for word preserving the integrity of the article.

16. Posting licensed content on any Website: The following terms and conditions apply as follows: Licensing material from an Elsevier journal: All content posted to the web site must maintain the copyright information line on the bottom of each image; A hyper-text must be included to the Homepage of the journal from which you are licensing at http://www.sciencedirect.com/science/journal/xxxxx or the Elsevier homepage for books athttp://www.elsevier.com; Central Storage: This license does not include permission for as canned version of the material to be stored in a central repository such as that provided by Heron/XanEdu.

Licensing material from an Elsevier book: A hyper-text link must be included to the Elsevier homepage at http://www.elsevier.com . All content posted to the web site must maintain the copyright information line on the bottom of each image.

Posting licensed content on Electronic reserve: In addition to the above the following clauses are applicable: The web site must be password-protected and made available only to bonafide students registered on a relevant course. This permission is granted for 1 year only. You may obtain a new license for future website posting.

17. For journal authors: the following clauses are applicable in addition to the above:

Preprints:

A preprint is an author's own write-up of research results and analysis, it has not been peer-reviewed, nor has it had any other value added to it by a publisher (such as formatting, copyright, technical enhancement etc.).

Authors can share their preprints anywhere at any time. Preprints should not be added to or enhanced in any way in order to appear more like, or to substitute for, the final versions of articles however authors can update their preprints on arXiv or RePEc with their Accepted Author Manuscript (see below).

If accepted for publication, we encourage authors to link from the preprint to their formal publication via its DOI. Millions of researchers have access to the formal publications on ScienceDirect, and so links will help users to find, access, cite and use the best available version. Please note that Cell Press, The Lancet and some society-owned have different preprint policies. Information on these policies is available on the journal homepage.

Accepted Author Manuscripts: An accepted author manuscript is the manuscript of an article that has been accepted for publication and which typically includes author-incorporated changes suggested during submission, peer review and editor-author communications.

Authors can share their accepted author manuscript:

Immediate lyvia their non-commercial person homepage or blog by updating a preprint in arXiv or RePEc with the accepted manuscript via their research institute or institutional repository for internal institutional uses or as part of an invitation-only research collaboration work-group directly by providing copies to their students or to research collaborators for their personal use

for private scholarly sharing as part of an invitation-only work group on commercial sites with which Elsevier has an agreement. After the embargo period via non-commercial hosting platforms such as their institutional repository via commercial sites with which Elsevier has an agreement

In all cases accepted manuscripts should:

link to the formal publication via its DOI bear a CC-BY-NC-ND license - this is easy to do if aggregated with other manuscripts, for example in a repository or other site, be shared in alignment with our hosting policy not be added to or enhanced in any way to appear more like, or to substitute for, the published journal article.

Published journal article (JPA): A published journal article (PJA) is the definitive final record of published research that appears or will appear in the journal and embodies all value-adding publishing activities including peer review co-ordination, copy-editing, formatting, (if relevant) pagination and online enrichment.

Policies for sharing publishing journal articles differ for subscription and gold open access articles:

Subscription Articles: If you are an author, please share a link to your article rather than the full-text. Millions of researchers have access to the formal publications on ScienceDirect, and so links will help your users to find, access, cite, and use the best available version.

Theses and dissertations which contain embedded PJAs as part of the formal submission can be posted publicly by the awarding institution with DOI links back to the formal publications on ScienceDirect.

If you are affiliated with a library that subscribes to ScienceDirect you have additional private sharing rights for others' research accessed under that agreement. This includes use for classroom teaching and internal training at the institution (including use in course packs and courseware programs), and inclusion of the article for grant funding purposes.
Gold Open Access Articles: May be shared according to the author-selected end-user license and should contain a Cross Mark logo, the end user license, and a DOI link to the formal publication on ScienceDirect.

Please refer to Elsevier's posting policy for further information.

18. For book authors the following clauses are applicable in addition to the above: Authors are permitted to place a brief summary of their work online only. You are not allowed to download and post the published electronic version of your chapter, nor may you scan the printed edition to create an electronic version. Posting to a repository: Authors are permitted to post a summary of their chapter only in their institution's repository.

19. Thesis/Dissertation: If your license is for use in a thesis/dissertation your thesis may be submitted to your institution in either print or electronic form. Should your thesis be published commercially, please reapply for permission. These requirements include permission for the Library and Archives of Canada to supply single copies, on demand, of the complete thesis and include permission for Proquest/UMI to supply single copies, on demand, of the complete thesis. Should your thesis be published commercially, please reapply for permission. Theses and dissertations which contain embedded PJAs as part of the formal submission can be posted publicly by the awarding institution with DOI links back to the formal publications on ScienceDirect.

Elsevier Open Access Terms and Conditions

You can publish open access with Elsevier in hundreds of open access journals or in nearly2000 established subscription journals that support open access publishing. Permitted third party re-use of these open access articles is defined by the author's choice of Creative Commons user license. See our open access license policy for more information.

Terms & Conditions applicable to all Open Access articles published with Elsevier:

Copyright Permission for Figure 2.1 and Figure 2.2

This Agreement between Mr. Murali Krishna Tummalapalli ("You") and Elsevier("Elsevier") consists of your license details and the terms and conditions provided by Elsevier and Copyright Clearance Center.

| | |
|---|---|
| License Number | 4937950991470 |
| License date | Oct 28, 2020 |
| Licensed Content Publisher | Elsevier |
| Licensed Content Publication | Journal of Nuclear Materials |
| Licensed Content Title | Microstructural degradation of UN and UN-$UO_2$ composites in hydrothermal oxidation conditions |
| Licensed Content Author | Jennifer K. Watkins, Darryl P. Butt, Brian J. Jaques |
| Licensed Content Date | May 1, 2019 |
| Licensed Content Volume | 518 |
| Licensed Content Issue | n/a |
| Licensed Content Pages | 11 |
| Start Page | 30 |
| End Page | 40 |
| Type of Use | reuse in a thesis/dissertation |
| Portion | figures/tables/illustrations |
| Number of figures/tables/illustrations | 2 |
| Format | both print and electronic |
| Are you the author of this Elsevier article? | No |
| Will you be translating? | No |
| Title | MICROSTRUCTURAL AND THERMOPHYSICAL PROPERTIES OF |

| | |
|---|---|
| | $UO_2$-Mo COMPOSITE REACTOR FUELS |
| Institution name | University of Saskatchewan |
| Expected presentation | Date Oct 2020 |
| Portions | Figures 9 and 10 on page 38 |
| Requestor Location | Mr. Murali Krishna Tummalapalli 208-1020 Matheson Dr Saskatoon, SK S7L5TL Canada |

INTRODUCTION

1. The publisher for this copyrighted material is Elsevier. By clicking "accept" in connection with completing this licensing transaction, you agree that the following terms and conditions apply to this transaction (along with the Billing and Payment terms and conditions established by Copyright Clearance Center, Inc. ("CCC"), at the time that you opened your Rights link account and that are available at any time at http://myaccount.copyright.com).

GENERAL TERMS

2. Elsevier hereby grants you permission to reproduce the afore mentioned material subject to the terms and conditions indicated.

3. Acknowledgement: If any part of the material to be used (for example, figures) has appeared in our publication with credit or acknowledgement to another source, permission must also be sought from that source. If such permission is not obtained then that material may not be included in your publication/copies. Suitable acknowledgement to the source must be made, either as a footnote or in a reference list at the end of your publication, as follows:

"Reprinted from Publication title, Vol /edition number, Author(s), Title of article / title of chapter, Pages No., Copyright (Year), with permission from Elsevier [OR APPLICABLESOCIETY COPYRIGHT OWNER]." Also Lancet special credit - "Reprinted from The Lancet, Vol. number, Author(s), Title of article, Pages No., Copyright (Year), with permission from Elsevier."

4. Reproduction of this material is confined to the purpose and/or media for which permission is hereby given.

5. Altering/Modifying Material: Not Permitted. However figures and illustrations may be altered/adapted minimally to serve your work. Any other abbreviations, additions, deletions and/or

any other alterations shall be made only with prior written authorization of Elsevier Ltd. (Please contact Elsevier's permissions helpdesk here). No modifications can be made to any Lancet figures/tables and they must be reproduced in full.

6. If the permission fee for the requested use of our material is waived in this instance, please be advised that your future requests for Elsevier materials may attract a fee.

7. Reservation of Rights: Publisher reserves all rights not specifically granted in the combination of (i) the license details provided by you and accepted in the course of this licensing transaction, (ii) these terms and conditions and (iii) CCC's Billing and Payment terms and conditions.

8. License Contingent Upon Payment: While you may exercise the rights licensed immediately upon issuance of the license at the end of the licensing process for the transaction, provided that you have disclosed complete and accurate details of your proposed use, no license is finally effective unless and until full payment is received from you (either by publisher or by CCC) as provided in CCC's Billing and Payment terms and conditions. If full payment is not received on a timely basis, then any license preliminarily granted shall be deemed automatically revoked and shall be void as if never granted. Further, in the event that you breach any of these terms and conditions or any of CCC's Billing and Payment terms and conditions, the license is automatically revoked and shall be void as if never granted. Use of materials as described in a revoked license, as well as any use of the materials beyond the scope of an unrevoked license, may constitute copyright infringement and publisher reserves the right to take any and all action to protect its copyright in the materials.

9. Warranties: Publisher makes no representations or warranties with respect to the licensed material.

10. Indemnity: You hereby indemnify and agree to hold harmless publisher and CCC, and their respective officers, directors, employees and agents, from and against any and all claims arising out of your use of the licensed material other than as specifically authorized pursuant to this license.

11. No Transfer of License: This license is personal to you and may not be sublicensed, assigned, or transferred by you to any other person without publisher's written permission.

12. No Amendment Except in Writing: This license may not be amended except in a writing signed by both parties (or, in the case of publisher, by CCC on publisher's behalf).

13. Objection to Contrary Terms: Publisher hereby objects to any terms contained in any purchase order, acknowledgment, check endorsement or other writing prepared by you, which terms are inconsistent with these terms and conditions or CCC's Billing and Payment terms and conditions. These terms and conditions, together with CCC's Billing and Payment terms and conditions (which

are incorporated herein), comprise the entire agreement between you and publisher (and CCC) concerning this licensing transaction. In the event of any conflict between your obligations established by these terms and conditions and those established by CCC's Billing and Payment terms and conditions, these terms and conditions shall control.

14. Revocation: Elsevier or Copyright Clearance Center may deny the permissions described in this License at their sole discretion, for any reason or no reason, with a full refund payable to you. Notice of such denial will be made using the contact information provided by you. Failure to receive such notice will not alter or invalidate the denial. In no event will Elsevier or Copyright Clearance Center be responsible or liable for any costs, expenses or damage incurred by you as a result of a denial of your permission request, other than a refund of the amount(s) paid by you to Elsevier and/or Copyright Clearance Center for denied permissions.

LIMITED LICENSE

The following terms and conditions apply only to specific license types:

15. Translation: This permission is granted for non-exclusive world English rights only unless your license was granted for translation rights. If you licensed translation rights you may only translate this content into the languages you requested. A professional translator must perform all translations and reproduce the content word for word preserving the integrity of the article.

16. Posting licensed content on any Website: The following terms and conditions apply as follows: Licensing material from an Elsevier journal: All content posted to the web site must maintain the copyright information line on the bottom of each image; A hyper-text must be included to the Homepage of the journal from which you are licensing at http://www.sciencedirect.com/science/journal/xxxxx or the Elsevier homepage for books athttp://www.elsevier.com; Central Storage: This license does not include permission for a scanned version of the material to be stored in a central repository such as that provided by Heron/XanEdu.

Licensing material from an Elsevier book: A hyper-text link must be included to the Elsevier homepage at http://www.elsevier.com. All content posted to the web site must maintain the copyright information line on the bottom of each image. Posting licensed content on Electronic reserve: In addition to the above the following clauses are applicable: The web site must be password-protected and made available only tobona fide students registered on a relevant course. This permission is granted for 1 year only. You may obtain a new license for future website posting.

17. For journal authors: the following clauses are applicable in addition to the above:

Preprints:

A preprint is an author's own write-up of research results and analysis, it has not been peer-reviewed, nor has it had any other value added to it by a publisher (such as formatting, copyright, technical enhancement etc.).

Authors can share their preprints anywhere at any time. Preprints should not be added to or enhanced in any way in order to appear more like, or to substitute for, the final versions of articles however authors can update their preprints on arXiv or RePEc with their Accepted Author Manuscript (see below).

If accepted for publication, we encourage authors to link from the preprint to their formal publication via its DOI. Millions of researchers have access to the formal publications on ScienceDirect, and so links will help users to find, access, cite and use the best available version. Please note that Cell Press, The Lancet and some society-owned have different preprint policies. Information on these policies is available on the journal homepage.

Accepted Author Manuscripts: An accepted author manuscript is the manuscript of an article that has been accepted for publication and which typically includes author-incorporated changes suggested during submission, peer review and editor-author communications.

Authors can share their accepted author manuscript:

Immediate lyvia their non-commercial person homepage or blog by updating a preprint in arXiv or RePEc with the accepted manuscript via their research institute or institutional repository for internal institutional uses or as part of an invitation-only research collaboration work-group directly by providing copies to their students or to research collaborators for their personal use for private scholarly sharing as part of an invitation-only work group on commercial sites with which Elsevier has an agreement After the embargo period via non-commercial hosting platforms such as their institutional repository via commercial sites with which Elsevier has an agreement

In all cases accepted manuscripts should:

link to the formal publication via its DOI bear a CC-BY-NC-ND license - this is easy to do if aggregated with other manuscripts, for example in a repository or other site, be shared in alignment with our hosting policy not be added to or enhanced in any way to appear more like, or to substitute for, the published journal article.

Published journal article (JPA): A published journal article (PJA) is the definitive final record of published research that appears or will appear in the journal and embodies all value-adding publishing activities including peer review co-ordination, copy-editing, formatting, (if relevant) pagination and online enrichment.

Policies for sharing publishing journal articles differ for subscription and gold open access articles:

Subscription Articles: If you are an author, please share a link to your article rather than the full-text. Millions of researchers have access to the formal publications on ScienceDirect, and so links will help your users to find, access, cite, and use the best available version.

Theses and dissertations which contain embedded PJAs as part of the formal submission can be posted publicly by the awarding institution with DOI links back to the formal publications on ScienceDirect.

If you are affiliated with a library that subscribes to ScienceDirect you have additional private sharing rights for others' research accessed under that agreement. This includes use for classroom teaching and internal training at the institution (including use in course packs and courseware programs), and inclusion of the article for grant funding purposes.

Gold Open Access Articles: May be shared according to the author-selected end-user license and should contain a Cross Mark logo, the end user license, and a DOI link to the formal publication on ScienceDirect.

Please refer to Elsevier's posting policy for further information.

18. For book authors the following clauses are applicable in addition to the above: Authors are permitted to place a brief summary of their work online only. You are not allowed to download and post the published electronic version of your chapter, nor may you scan the printed edition to create an electronic version. Posting to a repository: Authors are permitted to post a summary of their chapter only in their institution's repository.

19. Thesis/Dissertation: If your license is for use in a thesis/dissertation your thesis may be submitted to your institution in either print or electronic form. Should your thesis be published commercially, please reapply for permission. These requirements include permission for the Library and Archives of Canada to supply single copies, on demand, of the complete thesis and include permission for Proquest/UMI to supply single copies, on demand, of the complete thesis. Should your thesis be published commercially, please reapply for permission. Theses and dissertations which contain

Copyright Permission for Figure 2.4

This Agreement between Mr. Murali Krishna Tummalapalli ("You") and Elsevier ("Elsevier") consists of your license details and the terms and conditions provided by Elsevier and Copyright Clearance Center.

| | |
|---|---|
| License Number | 4937961027775 |
| License date | Oct 28, 2020 |
| Licensed Content Publisher | Elsevier |
| Licensed Content Publication | Journal of Nuclear Materials |
| Licensed Content Title | Oxidation behavior of U–10 wt% Mo alloy in air at 473–773 K |
| Licensed Content Author | Kweon Ho Kang, Si Hyung Kim, Kyung Kil Kwak, Chang Kyu Kim |
| Licensed Content Date | Aug 1, 2002 |
| Licensed Content Volume | 304 |
| Licensed Content Issue | 2-3 |
| Licensed Content Pages | 4 |
| Start Page | 242 |
| End Page | 245 |
| Type of Use | reuse in a thesis/dissertation |
| Portion | figures/tables/illustrations |
| Number of figures/tables/illustrations | 2 |
| Format | both print and electronic |
| Are you the author of this Elsevier article? | No |
| Will you be translating? | No |

| | |
|---|---|
| Title | MICROSTRUCTURAL AND THERMOPHYSICAL PROPERTIES OF $UO_2$-Mo COMPOSITE REACTOR FUELS |
| Institution name | University of Saskatchewan |
| Expected presentation date | Oct 2020 |
| Portions | Figure 2 on page 243 and Figure 3 on Page 244 |
| Requestor Location | Mr. Murali Krishna Tummalapalli 208-1020 Matheson Dr Saskatoon, SK S7L5TL Canada |
| Attn: | Mr. Murali Krishna Tummalapalli |
| Publisher Tax ID | GB 494 6272 12 |
| Total | 0.00 USD |
| Terms and Conditions | |

INTRODUCTION

1. The publisher for this copyrighted material is Elsevier. By clicking "accept" in connection with completing this licensing transaction, you agree that the following terms and conditions apply to this transaction (along with the Billing and Payment terms and conditions established by Copyright Clearance Center, Inc. ("CCC"), at the time that you opened your Rights link account and that are available at any time at http://myaccount.copyright.com).

GENERAL TERMS

2. Elsevier hereby grants you permission to reproduce the aforementioned material subject to the terms and conditions indicated.3. Acknowledgement: If any part of the material to be used (for example, figures) has appeared in our publication with credit or acknowledgement to another source, permission must also be sought from that source. If such permission is not obtained then that material may not be included in your publication/copies.

Suitable acknowledgement to the source must be made, either as a footnote or in a reference list at the end of your publication, as follows:

"Reprinted from Publication title, Vol /edition number, Author(s), Title of article / title of

chapter, Pages No., Copyright (Year), with permission from Elsevier [OR APPLICABLE SOCIETY COPYRIGHT OWNER]." Also Lancet special credit - "Reprinted from The Lancet, Vol. number, Author(s), Title of article, Pages No., Copyright (Year), with permission from Elsevier."

4. Reproduction of this material is confined to the purpose and/or media for which permission is hereby given.5. Altering/Modifying Material: Not Permitted. However figures and illustrations may be altered/adapted minimally to serve your work. Any other abbreviations, additions, deletions and/or any other alterations shall be made only with prior written authorization of Elsevier Ltd. (Please contact Elsevier's permissions helpdesk here). No modifications can be made to any Lancet figures/tables and they must be reproduced in full.

If the permission fee for the requested use of our material is waived in this instance, please be advised that your future requests for Elsevier materials may attract a fee.7. Reservation of Rights: Publisher reserves all rights not specifically granted in the combination of (i) the license details provided by you and accepted in the course of this licensing transaction, (ii) these terms and conditions and (iii) CCC's Billing and Payment terms and conditions.

8. License Contingent Upon Payment: While you may exercise the rights licensed immediately upon issuance of the license at the end of the licensing process for the transaction, provided that you have disclosed complete and accurate details of your proposed use, no license is finally effective unless and until full payment is received from you (either by publisher or by CCC) as provided in CCC's Billing and Payment terms and conditions. If full payment is not received on a timely basis, then any license preliminarily granted shall be deemed automatically revoked and shall be void as if never granted. Further, in the event that you breach any of these terms and conditions or any of CCC's Billing and Payment terms and conditions, the license is automatically revoked and shall be void as if Never granted. Use of materials as described in a revoked license, as well as any use of the materials beyond the scope of an unrevoked license, may constitute copyright infringement and publisher reserves the right to take any and all action to protect its copyright in the materials.

9. Warranties: Publisher makes no representations or warranties with respect to the licensed material.

10. Indemnity: You hereby indemnify and agree to hold harmless publisher and CCC, and

their respective officers, directors, employees and agents, from and against any and all claims arising out of your use of the licensed material other than as specifically authorized pursuant to this license.11. No Transfer of License: This license is personal to you and may not be sublicensed, assigned, or transferred by you to any other person without publisher's written permission.12. No Amendment Except in Writing: This license may not be amended except in a writing signed by both parties (or, in the case of publisher, by CCC on publisher's behalf).13. Objection to Contrary Terms: Publisher hereby objects to any terms contained in any purchase
order, acknowledgment, check endorsement or other writing prepared by you, which terms are inconsistent with these terms and conditions or CCC's Billing and Payment terms and conditions. These terms and conditions, together with CCC's Billing and Payment terms and conditions (which are incorporated herein), comprise the entire agreement between you and publisher (and CCC) concerning this licensing transaction. In the event of any conflict between your obligations established by these terms and conditions and those established by CCC's Billing and Payment terms and conditions, these terms and conditions shall control.
14. Revocation: Elsevier or Copyright Clearance Center may deny the permissions described in this License at their sole discretion, for any reason or no reason, with a full refund payable to you. Notice of such denial will be made using the contact information provided by you. Failure to receive such notice will not alter or invalidate the denial. In no event will Elsevier or Copyright Clearance Center be responsible or liable for any costs, expenses or damage incurred by you as a result of a denial of your permission request, other than a refund of the amount(s) paid by you to Elsevier and/or Copyright Clearance Center for denied permissions. LIMITED LICENSE The following terms and conditions apply only to specific license types:15. Translation: This permission is granted for non-exclusive world English rights only unless your license was granted for translation rights. If you licensed translation rights you may only translate this content into the languages you requested. A professional translator must perform all translations and reproduce the content word for word preserving the integrity of the article.16. Posting licensed content on any Website: The following terms and conditions apply as follows: Licensing material from an Elsevier journal All content posted to the web site must maintain the copyright information line on the bottom

Of each image; A hyper-text must be included to the Homepage of the journal from which you are licensing athttp://www.sciencedirect.com/science/journal/xxxxx or the Elsevier homepage for books at http scanned version of the material to be stored in a central repository such as that provided by Heron/XanEdu. Licensing material from an Elsevier book: A hyper-text link
must be included to the Elsevier homepage at http://www.elsevier.com. All content posted to the web site must maintain the copyright information line on the bottom of each image. Posting licensed content on Electronic reserve: In addition to the above the following clauses are applicable: The web site must be password-protected and made available only to bona fide students registered on a relevant course. This permission is granted for 1 year only. You may obtain a new license for future website posting.
17. For journal authors: the following clauses are applicable in addition to the above:
Preprints: A preprint is an author's own write-up of research results and analysis, it has not been peer-reviewed, nor has it had any other value added to it by a publisher (such as formatting, copyright, technical enhancement etc.).
Authors can share their preprints anywhere at any time. Preprints should not be added to or enhanced in any way in order to appear more like, or to substitute for, the final versions of articles however authors can update their preprints on arXiv or RePEc with their Accepted Author Manuscript (see below). If accepted for publication, we encourage authors to link from the preprint to their formal publication via its DOI. Millions of researchers have access to the formal publications on ScienceDirect, and so links will help users to find, access, cite and use the best available version. Please note that Cell Press, The Lancet and some society-owned have different preprint policies. Information on these policies is available on the journal homepage. Accepted Author Manuscripts: An accepted author manuscript is the manuscript of an article that has been accepted for publication and which typically includes author-incorporated changes suggested during submission, peer review and editor-author communications. Authors can share their accepted author manuscript: immediately via their non-commercial person homepage or blog by updating a preprint in arXiv or RePEc with the accepted manuscript via their research institute or institutional repository for internal institutional uses or as part of an invitation-only research collaboration work-group directly by providing copies to their students or to research collaborators for their personal

use for private scholarly sharing as part of an invitation-only work group on commercial sites with which Elsevier has an agreement

After the embargo period via non-commercial hosting platforms such as their institutional repository via commercial sites with which Elsevier has an agreement In all cases accepted manuscripts should: link to the formal publication via its DOI bear a CC-BY-NC -ND license - this is easy to do if aggregated with other manuscripts, for example in a repository or other site, be shared in alignment with our hosting policy not be added to or enhanced in any way to appear more like, or to substitute for, the published journal article.

Published journal article (JPA): A published journal article (PJA) is the definitive final record of published research that appears or will appear in the journal and embodies all value-adding publishing activities including peer review co-ordination, copy-editing, formatting, (if relevant) pagination and online enrichment. Policies for sharing publishing journal articles differ for subscription and gold open access articles:

Subscription Articles: If you are an author, please share a link to your article rather than the full-text. Millions of researchers have access to the formal publications on ScienceDirect, and so links will help your users to find, access, cite, and use the best available version.

Theses and dissertations which contain embedded PJAs as part of the formal submission can be posted publicly by the awarding institution with DOI links back to the formal publications on ScienceDirect. If you are affiliated with a library that subscribes to Science Direct you have additional private sharing rights for others' research accessed under that agreement. This includes use for classroom teaching and internal training at the institution (including use in course packs and courseware programs), and inclusion of the article for grant funding purposes.

Gold Open Access Articles:

May be shared according to the author-selected end-user license and should contain a Cross Mark logo, the end user license, and a DOI link to the formal publication on ScienceDirect.

Please refer to Elsevier's posting policy for further information.18. For book authors the following clauses are applicable in addition to the above:

Authors are permitted to place a brief summary of their work online only. You are not allowed to download and post the published electronic version of your chapter, nor may you scan the printed edition to create an electronic version. Posting to a repository: Authors are

permitted to post a summary of their chapter only in their institution's repository.19. Thesis/Dissertation: If your license is for use in a thesis/dissertation your thesis may be submitted to your institution in either print or electronic form. Should your thesis be published commercially, please reapply for permission. These requirements include permission for the Library and Archives of Canada to supply single copies, on demand, of the complete thesis and include permission for Proquest/UMI to supply single copies, on demand, of the complete thesis. Should your thesis be published commercially, please reapply for permission. Theses and dissertations which contain embedded PJAs as part of the formal submission can be posted publicly by the awarding institution with DOI links back to the formal publications on ScienceDirect. Elsevier Open Access Terms and Conditions You can publish open access with Elsevier in hundreds of open access journals or in nearly 2000 established subscription journals that support open access publishing. Permitted third party re-use of these open access articles is defined by the author's choice of Creative Commons user license. See our  open access license policy for more information. Terms & Conditions applicable to all Open Access articles published with Elsevier: Any reuse of the article must not represent the author as endorsing the adaptation of the article nor should the article be modified in such a way as to damage the author's honour or reputation. If any changes have been made, such changes must be clearly indicated. The author(s) must be appropriately credited and we ask that you include the end user license and a DOI link to the formal publication on ScienceDirect. If any part of the material to be used (for example, figures) has appeared in our publication the credit or acknowledgement to another source it is the responsibility of the user to ensure their reuse complies with the terms and conditions determined by the rights holder. Additional Terms & Conditions applicable to each Creative Commons user license: CC BY: The CC-BY license allows users to copy, to create extracts, abstracts and new works from the Article, to alter and revise the Article and to make commercial use of the Article (including reuse and/or resale of the Article by commercial entities), provided the user gives appropriate credit (with a link to the formal publication through the relevant DOI), provides a link to the license, indicates if changes were made and the licensor is not represented as endorsing the use made of the work. The full details of the license are available at http://creativecommons.org/licenses/by/4.0.CC BY NC SA: The CC BY-NC-SA

Copyright Permission for Figure 2.5

This Agreement between Mr. Murali Krishna Tummalapalli ("You") and Elsevier ("Elsevier") consists of your license details and the terms and conditions provided by Elsevier and Copyright Clearance Center.

| | |
|---|---|
| License Number | 4937961301631 |
| License date | Oct 28, 2020 |
| Licensed Content Publisher | Elsevier |
| Licensed Content Publication | Journal of Nuclear Materials |
| Licensed Content Title | Oxygen potential of a prototypic Mo-cermet fuel containing plutonium oxide |
| Licensed Content Author | Shuhei Miwa, Masahiko Osaka, Takahiro Nozaki, Tatsumi Arima, Kazuya Idemitsu |
| Licensed Content Date | Oct 1, 2015 |
| Licensed Content Volume | 465 |
| Licensed Content Issue | n/a |
| Licensed Content Pages | 3 |
| Start Page | 840 |
| End Page | 842 |
| Type of Use | reuse in a thesis/dissertation |
| Portion | figures/tables/illustrations |
| Number of figures/tables/illustrations | 2 |
| Format | both print and electronic |
| Are you the author of this Elsevier article? | No |
| Will you be translating? | No |
| Title | MICROSTRUCTURAL AND THERMOPHYSICALPROPERTIES OF $UO_2$-Mo COMPOSITE REACTOR |

| | |
|---|---|
| | FUELS |
| Institution name | University of Saskatchewan |
| Expected presentation date | Oct 2020 |
| Portions | Figure 1 and 2 on page 841 |
| Requestor Location | Mr. Murali Krishna Tummalapalli<br>208-1020 Matheson Dr Saskatoon,<br>SK S7L5TL Canada |
| Attn: | Mr. Murali Krishna Tummalapalli |
| Publisher Tax ID | GB 494 6272 12 |
| Total | 0.00 USD |

Terms and Conditions

INTRODUCTION

1. The publisher for this copyrighted material is Elsevier. By clicking "accept" in Connection with completing this licensing transaction, you agree that the following terms and conditions apply to this transaction (along with the Billing and Payment terms and conditions established by Copyright Clearance Center, Inc. ("CCC"), at the time that you opened your Rights link account and that are available at any time at http://myaccount.copyright.com.

GENERAL TERMS

2. Elsevier hereby grants you permission to reproduce the aforementioned material subject To the terms and conditions indicated.

3. Acknowledgement: If any part of the material to be used (for example, figures) has appeared in our publication with credit or acknowledgement to another source, permission must also be sought from that source. If such permission is not obtained then that material may not be included in your publication/copies. Suitable acknowledgement to the source must be made, either as a footnote or in a reference list at the end of your publication, as follows:

"Reprinted from Publication title, Vol /edition number, Author(s), Title of article / title of chapter, Pages No., Copyright (Year), with permission from Elsevier [OR APPLICABLESOCIETY COPYRIGHT OWNER]." Also Lancet special credit - "Reprinted from The Lancet, Vol. number, Author(s), Title of article, Pages No., Copyright (Year), with

permission from Elsevier."

4. Reproduction of this material is confined to the purpose and/or media for which permission is hereby given.

5. Altering/Modifying Material: Not Permitted. However figures and illustrations may be altered/adapted minimally to serve your work. Any other abbreviations, additions, deletion sand/or any other alterations shall be made only with prior written authorization of Elsevier Ltd. (Please contact Elsevier's permissions helpdesk here). No modifications can be made to any Lancet figures/tables and they must be reproduced in full.

6. If the permission fee for the requested use of our material is waived in this instance, please be advised that your future requests for Elsevier materials may attract a fee.

7. Reservation of Rights: Publisher reserves all rights not specifically granted in the combination of (i) the license details provided by you and accepted in the course of this licensing transaction, (ii) these terms and conditions and (iii) CCC's Billing and Payment terms and conditions.

8. License Contingent Upon Payment: While you may exercise the rights licensed immediately upon issuance of the license at the end of the licensing process for the transaction, provided that you have disclosed complete and accurate details of your proposed use, no license is finally effective unless and until full payment is received from you (eitherby publisher or by CCC) as provided in CCC's Billing and Payment terms and conditions. If full payment is not received on a timely basis, then any license preliminarily granted shall be deemed automatically revoked and shall be void as if never granted. Further, in the event that youbreach any of these terms and conditions or any of CCC's Billing and Payment terms and conditions, the license is automatically revoked and shall be void as if never granted. Use of materials as described in a revoked license, as well as any use of the materials beyond the scope of an unrevoked license, may constitute copyright infringement and publisher reserves the right to take any and all action to protect its copyright in the materials.

9. Warranties: Publisher makes no representations or warranties with respect to the licensed material.

10. Indemnity: You hereby indemnify and agree to hold harmless publisher and CCC, and their respective officers, directors, employees and agents, from and against any and all claims arising out of your use of the licensed material other than as specifically authorized

pursuant to this license.
11. No Transfer of License: This license is personal to you and may not be sublicensed, assigned, or transferred by you to any other person without publisher's written permission.
12. No Amendment Except in Writing: This license may not be amended except in a writing signed by both parties (or, in the case of publisher, by CCC on publisher's behalf).
13. Objection to Contrary Terms: Publisher hereby objects to any terms contained in any purchase order, acknowledgment, check endorsement or other writing prepared by you, which terms are inconsistent with these terms and conditions or CCC's Billing and Payment terms and conditions. These terms and conditions, together with CCC's Billing and Payment terms and conditions (which are incorporated herein), comprise the entire agreement between you and publisher (and CCC) concerning this licensing transaction. In the event of any conflict between your obligations established by these terms and conditions and those established by CCC's Billing and Payment terms and conditions, these terms and conditions shall control.
14. Revocation: Elsevier or Copyright Clearance Center may deny the permissions described in this License at their sole discretion, for any reason or no reason, with a full refund payable to you. Notice of such denial will be made using the contact information provided by you. Failure to receive such notice will not alter or invalidate the denial. In no event will Elsevier or Copyright Clearance Center be responsible or liable for any costs, expenses or damage incurred by you as a result of a denial of your permission request, other than a refund of the amount(s) paid by you to Elsevier and/or Copyright Clearance Center for denied permissions.
LIMITED LICENSE
The following terms and conditions apply only to specific license types:
15. Translation: This permission is granted for non-exclusive world English rights only unless your license was granted for translation rights. If you licensed translation rights you may only translate this content into the languages you requested. A professional translator must perform all translations and reproduce the content word for word preserving the integrity of the article.
16. Posting licensed content on any Website: The following terms and conditions apply as follows: Licensing material from an Elsevier journal: All content posted to the web site

must maintain the copyright information line on the bottom of each image; A hyper-text must be included to the Homepage of the journal from which you are licensing at http://www.sciencedirect.com/science/journal/xxxxx or the Elsevier homepage for books athttp://www.elsevier.com; Central Storage: This license does not include permission for a scanned version of the material to be stored in a central repository such as that provided by Heron/XanEdu. Licensing material from an Elsevier book: A hyper-text link must be included to the Elsevier homepage at http://www.elsevier.com . All content posted to the web site must maintain the copyright information line on the bottom of each image. Posting licensed content on Electronic reserve: In addition to the above the following clauses are applicable: The web site must be password-protected and made available only to bona fide students registered on a relevant course. This permission is granted for 1 year only You may obtain a new license for future website posting.

17. For journal authors: the following clauses are applicable in addition to the above: Preprints:

A preprint is an author's own write-up of research results and analysis, it has not been peer-reviewed, nor has it had any other value added to it by a publisher (such as formatting, copyright, technical enhancement etc.).

Authors can share their preprints anywhere at any time. Preprints should not be added to Or enhanced in any way in order to appear more like, or to substitute for, the final versions Of articles however authors can update their preprints on arXiv or RePEc with their Accepted Author Manuscript (see below).

If accepted for publication, we encourage authors to link from the preprint to their formal publication via its DOI. Millions of researchers have access to the formal publications on ScienceDirect, and so links will help users to find, access, cite and use the best available version. Please note that Cell Press, The Lancet and some society-owned have different preprint policies. Information on these policies is available on the journal homepage.

Accepted Author Manuscripts: An accepted author manuscript is the manuscript of an article that has been accepted for publication and which typically includes author-incorporated changes suggested during submission, peer review and editor-author communications. Authors can share their accepted author manuscript:

immediate elyvia their non-commercial person homepage or blog by updating a preprint in

18. For book authors the following clauses are applicable in addition to the above: Authors are permitted to place a brief summary of their work online only. You are not allowed to download and post the published electronic version of your chapter, nor may you scan the printed edition to create an electronic version. Posting to a repository: Authors are permitted to post a summary of their chapter only in their institution's repository.
19. Thesis/Dissertation: If your license is for use in a thesis/dissertation your thesis may be submitted to your institution in either print or electronic form. Should your thesis be published commercially, please reapply for permission. These requirements include permission for the Library and Archives of Canada to supply single copies, on demand, of the complete thesis and include permission for Proquest/UMI to supply single copies, on demand, of the complete thesis. Should your thesis be published commercially, please re apply for permission. Theses and dissertations which contain embedded PJAs as part of the formal submission can be posted publicly by the awarding institution with DOI links back to the formal publications on ScienceDirect.
Elsevier Open Access Terms and Conditions
You can publish open access with Elsevier in hundreds of open access journals or in nearly 2000 established subscription journals that support open access publishing. Permitted third party re-use of these open access articles is defined by the author's choice of Creative Commons user license. See our open access license policy for more information.
Terms & Conditions applicable to all Open Access articles published with Elsevier:
Any reuse of the article must not represent the author as endorsing the adaptation of the article nor should the article be modified in such a way as to damage the author's honour or reputation. If any changes have been made, such changes must be clearly indicated.
The author(s) must be appropriately credited and we ask that you include the end user license and a DOI link to the formal publication on ScienceDirect.
If any part of the material to be used (for example, figures) has appeared in our publication with credit or acknowledgement to another source it is the responsibility of the user to ensure their reuse complies with the terms and conditions determined by the rights holder.
Additional Terms & Conditions applicable to each Creative Commons user license:
CC BY: The CC-BY license allows users to copy, to create extracts, abstracts and new works from the Article, to alter and revise the Article and to make commercial use of the Article

Copyright Permission for Figure 2.6

This Agreement between Mr. Murali Krishna Tummalapalli ("You") and Elsevier ("Elsevier") consists of your license details and the terms and conditions provided by Elsevier and Copyright Clearance Center.

| | |
|---|---|
| License Number | 4937970237315 |
| License date | Oct 28, 2020 |
| Licensed Content Publisher | Elsevier |
| Licensed Content Publication | Journal of Nuclear Materials |
| Licensed Content Title | Effect of Ce doping on $UO_2$ structure and its oxidation behavior |
| Licensed Content Author | Yeong-Keong Ha, Jeongmook Lee, Jong-Goo Kim, Jong-Yun Kim |
| Licensed Content Date | Nov 1, 2016 |
| Licensed Content Volume | 480 |
| Licensed Content Issue | n/a |
| Licensed Content Pages | 7 |
| Start Page | 429 |
| End Page | 435 |
| Type of Use | reuse in a thesis/dissertation |
| Portion | figures/tables/illustrations |
| Number of figures/tables/illustrations | 2 |
| Format | both print and electronic |
| Are you the author of this Elsevier article? | No |
| Will you be translating? | No |
| Title | MICROSTRUCTURAL AND THERMOPHYSICAL PROPERTIES OF $UO_2$-Mo COMPOSITE |

| | |
|---|---|
| | REACTOR FUELS |
| Institution name | University of Saskatchewan |
| Expected presentation date | Oct 2020 |
| Portions | Figure 3 on page 431 and Figure 4 on page 432 |
| Requestor Location | Mr. Murali Krishna Tummalapalli<br>208-1020 Matheson Dr Saskatoon, SK S7L5TL Canada |
| Attn: | Mr. Murali Krishna Tummalapalli |
| Publisher Tax ID | GB 494 6272 12 |
| Total | 0.00 USD |

Terms and Conditions

INTRODUCTION

1. The publisher for this copyrighted material is Elsevier. By clicking "accept" in connection with completing this licensing transaction, you agree that the following terms and conditions apply to this transaction (along with the Billing and Payment terms and conditions established by Copyright Clearance Center, Inc. ("CCC"), at the time that you opened your Rights link account and that are available at any time at http://myaccount.copyright.com).

GENERAL TERMS

2. Elsevier hereby grants you permission to reproduce the aforementioned material subject to the terms and conditions indicated.

3. Acknowledgement: If any part of the material to be used (for example, figures) has appeared in our publication with credit or acknowledgement to another source, permission must also be sought from that source. If such permission is not obtained then that material may not be included in your publication/copies. Suitable acknowledgement to the source must be made, either as a footnote or in a reference list at the end of your publication, as follows:

"Reprinted from Publication title, Vol /edition number, Author(s), Title of article / title of chapter, Pages No., Copyright (Year), with permission from Elsevier [OR APPLICABLE SOCIETY COPYRIGHT OWNER]." Also Lancet special credit - "Reprinted from The Lancet, Vol. number, Author(s), Title of article, Pages No., Copyright (Year), with

permission from Elsevier."

4. Reproduction of this material is confined to the purpose and/or media for which permission is hereby given.

5. Altering/Modifying Material: Not Permitted. However figures and illustrations may be altered/adapted minimally to serve your work. Any other abbreviations, additions, deletions and/or any other alterations shall be made only with prior written authorization of Elsevier Ltd. (Please contact Elsevier's permissions helpdesk here). No modifications can be made to any Lancet figures/tables and they must be reproduced in full.

6. If the permission fee for the requested use of our material is waived in this instance, please be advised that your future requests for Elsevier materials may attract a fee.

7. Reservation of Rights: Publisher reserves all rights not specifically granted in the combination of (i) the license details provided by you and accepted in the course of this licensing transaction, (ii) these terms and conditions and (iii) CCC's Billing and Payment terms and conditions.

8. License Contingent Upon Payment: While you may exercise the rights licensed immediately upon issuance of the license at the end of the licensing process for the transaction, provided that you have disclosed complete and accurate details of your proposed use, no license is finally effective unless and until full payment is received from you (either by publisher or by CCC) as provided in CCC's Billing and Payment terms and conditions. If full payment is not received on a timely basis, then any license preliminarily granted shall be deemed automatically revoked and shall be void as if never granted. Further, in the event that you breach any of these terms and conditions or any of CCC's Billing and Payment terms and conditions, the license is automatically revoked and shall be void as if never granted. Use of materials as described in a revoked license, as well as any use of the materials beyond the scope of an unrevoked license, may constitute copyright infringement and publisher reserves the right to take any and all action to protect its copyright in the materials.

9. Warranties: Publisher makes no representations or warranties with respect to the licensed material.

10. Indemnity: You hereby indemnify and agree to hold harmless publisher and CCC, and their respective officers, directors, employees and agents, from and against any and all claims arising out of your use of the licensed material other than as specifically authorized

pursuant to this license.
11. No Transfer of License: This license is personal to you and may not be sublicensed, assigned, or transferred by you to any other person without publisher's written permission.
12. No Amendment Except in Writing: This license may not be amended except in a Writing signed by both parties (or, in the case of publisher, by CCC on publisher's behalf).
13. Objection to Contrary Terms: Publisher hereby objects to any terms contained in any purchase order, acknowledgment, check endorsement or other writing prepared by you, which terms are inconsistent with these terms and conditions or CCC's Billing and Payment terms and conditions. These terms and conditions, together with CCC's Billing and Payment terms and conditions (which are incorporated herein), comprise the entire agreement between you and publisher (and CCC) concerning this licensing transaction. In the event of any conflict between your obligations established by these terms and conditions and those established by CCC's Billing and Payment terms and conditions, these terms and conditions shall control.
14. Revocation: Elsevier or Copyright Clearance Center may deny the permissions described in this License at their sole discretion, for any reason or no reason, with a full refund payable to you. Notice of such denial will be made using the contact information provided by you. Failure to receive such notice will not alter or invalidate the denial. In no event will Elsevier or Copyright Clearance Center be responsible or liable for any costs, expenses or damage incurred by you as a result of a denial of your permission request, other than a refund of the amount(s) paid by you to Elsevier and/or Copyright Clearance Center for denied permissions.
LIMITED LICENSE
The following terms and conditions apply only to specific license types:
15. Translation: This permission is granted for non-exclusive world English rights only unless your license was granted for translation rights. If you licensed translation rights you may only translate this content into the languages you requested. A professional translator must perform all translations and reproduce the content word for word preserving the integrity of the article.
16. Posting licensed content on any Website: The following terms and conditions apply as follows: Licensing material from an Elsevier journal: All content posted to the web site must maintain the copyright information line on the bottom of each image; A hyper-text must

be included to the Homepage of the journal from which you
are licensing athttp://www.sciencedirect.com/science/journal/xxxxx or the Elsevier homepage for books athttp://www.elsevier.com; Central Storage: This license does not include permission for a scanned version of the material to be stored in a central repository such as that provided by Heron/XanEdu.
Licensing material from an Elsevier book: A hyper-text link must be included to the Elsevier homepage at http://www.elsevier.com . All content posted to the web site must maintain the copyright information line on the bottom of each image.
Posting licensed content on Electronic reserve: In addition to the above the following clauses are applicable: The web site must be password-protected and made available only tobona fide students registered on a relevant course. This permission is granted for 1 year only. You may obtain a new license for future website posting.
17. For journal authors: the following clauses are applicable in addition to the above:
Preprints:
A preprint is an author's own write-up of research results and analysis, it has not been peer-reviewed, nor has it had any other value added to it by a publisher (such as formatting, copyright technical enhancement etc.).
Authors can share their preprints anywhere at any time. Preprints should not be added to or enhanced in any way in order to appear more like, or to substitute for, the final versions of articles however authors can update their preprints on arXiv or RePEc with their Accepted Author Manuscript (see below).
If accepted for publication, we encourage authors to link from the preprint to their formal publication via its DOI. Millions of researchers have access to the formal publications on ScienceDirect, and so links will help users to find, access, cite and use the best available version. Please note that Cell Press, The Lancet and some society-owned have different preprint policies. Information on these policies is available on the journal homepage.
Accepted Author Manuscripts: An accepted author manuscript is the manuscript of an article that has been accepted for publication and which typically includes author-incorporated changes suggested during submission, peer review and editor-author communications.
Authors can share their accepted author manuscript:
Immediate lyvia their non-commercial person homepage or blog by updating a preprint in

Please refer to Elsevier's posting policy for further information.

18. For book authors the following clauses are applicable in addition to the above: Authors are permitted to place a brief summary of their work online only. You are not allowed to download and post the published electronic version of your chapter, nor may you scan the printed edition to create an electronic version. Posting to a repository: Authors are permitted to post a summary of their chapter only in their institution's repository.

19. Thesis/Dissertation: If your license is for use in a thesis/dissertation your thesis may be submitted to your institution in either print or electronic form. Should your thesis be published commercially, please reapply for permission. These requirements include permission for the Library and Archives of Canada to supply single copies, on demand, of the complete thesis and include permission for Proquest/UMI to supply single copies, on demand, of the complete thesis. Should your thesis be published commercially, please reapply for permission. Theses and dissertations which contain embedded PJAs as part of the formal submission can be posted publicly by the awarding institution with DOI links back to the formal publications on ScienceDirect.

Elsevier Open Access Terms and Conditions

You can publish open access with Elsevier in hundreds of open access journals or in nearly2000 established subscription journals that support open access publishing. Permitted third party re-use of these open access articles is defined by the author's choice of Creative Commons user license. See our open access license policy for more information.

Terms & Conditions applicable to all Open Access articles published with Elsevier:

Any reuse of the article must not represent the author as endorsing the adaptation of the article nor should the article be modified in such a way as to damage the author's honour or reputation. If any changes have been made, such changes must be clearly indicated.

The author(s) must be appropriately credited and we ask that you include the end user license and a DOI link to the formal publication on ScienceDirect.

If any part of the material to be used (for example, figures) has appeared in our publication with credit or acknowledgement to another source it is the responsibility of the user to ensure their reuse complies with the terms and conditions determined by the rights holder.

Additional Terms & Conditions applicable to each Creative Commons user license:

CC BY: The CC-BY license allows users to copy, to create extracts, abstracts and new